DISSERTATION ZUR ERLANGUNG DES DOKTORGRADES

DER FAKULTÄT FÜR BIOLOGIE

DER LUDWIG-MAXIMILIANS-UNIVERSITÄT MÜNCHEN

Molecular mapping of nuclear organization in the mouse preimplantation embryo

MÁTÉ BORSOS

September 2018

Completed at the Helmholtz Center Munich

German Research Center for Environment and Health (GmbH)

Institute of Epigenetics and Stem Cells (IES)

Date of submission:	**24.09.2018.**
First Examiner:	**Prof. Dr. María-Elena Torres-Padilla**
Second Examiner:	**Prof. Dr. Wolfgang Enard**
Date of the oral examination:	**13.12.2018**

dla moja Liska

Eidesstattliche Erklärung

Ich versichere hiermit an Eides statt, dass die vorliegende Dissertation von mir selbstständig und ohne unerlaubte Hilfe angefertigt ist.

Erklärung

Hiermit erkläre ich, dass die Dissertation nicht ganz oder in wesentlichen Teilen einer anderen Prüfungskommission vorgelegt worden ist.

Ich erkläre weiter, dass ich mich anderweitig einer Doktorprüfung ohne Erfolg **nicht** unterzogen habe.

München, im September 2018

Máté Borsos

Máté Borsos

Acknowledgements

I am grateful to the reviewers of my thesis for accepting to take their time and read this work. I hope they will find excitement in the science that kept me motivated and curious over the past years.

Almost four years ago, when I came to Strasbourg and joined María Elena's lab I did not have the vaguest idea how much these coming years will change my life and me both scientifically and personally. I am incredibly grateful to María Elena for taking me to do this PhD journey, you taught me a lot, believed in me and challenged me. These years in your lab immensely shaped me, I am grateful for your commitment and endurance even when it was not easy.

I am also incredibly grateful for my past mentors who guided me on my scientific journey. Without Gergő who took me as a second year BSc student, I probably would not have continued with biology, his patience, vast knowledge and devotion to explain truly propelled me into pursuing a PhD. Kikuë introduced me to the beauty of working with mouse oocytes and early preimplantation embryos which then grew in me into a passion. I am very grateful for her continuous support over the BSc and MSc and for letting me do all the "cowboy" experiments that fueled my excitement. Déborah got me totally into epigenetics and was generously supportive, I am very happy I could spend time in your lab – even though it was short.

Jop is a great collaborator and fun person, his positivity helped me a lot – regardless that unfortunately we met only a few times. Your hard work with the DamID samples definitely payed off. Sara did a fantastic job with the DamID analysis and we became a very good team during these years, it was great time, I am very grateful for that! Kim, I'm happy that we had such great chats.

I am grateful to Tobias for letting me work on their cluster and for his help with stats. I am particularly thankful to Tamás for his help with the HiC analysis and for teaching me and having the patience to explain bioinformatics to a previously only experimental biologist.

I am thankful to the past and present lab members of the labo Torres. Diego for being Diego; Takashi for shaping my thinking; André for joking even in the midst of hard times; Adam the best British; Camille who keeps this lab running; Emily for being lovely; Ane who has an endless amount of "wise" sentences; Tsune the king of snakes; Manuel, our foci boy; Ken a great Japanese teacher.

Members of my previous labs had a great influence on me and I am very grateful for their support towards me. Sabrina taught scientific rigor and precision with experiments; Joan for encouraging to think outside of the box; Max, a prime example that one can do science and have an awesome family at the same time; Marius assured me that it is actually possible to write a thesis.

I am grateful for my TAC committee Wendy Bickmore, Evi Soutoglou and Peter Meister for the helpful and critical comments, without them this work would not be what it is now. Irina guided me with great devotion in science and she truly is a role model for me in how she thinks and does science, I am very grateful for knowing her.

I thank Strasbourg for being such a beautiful and amazing city in which I spent so much happy times, I wish I will return there one day maybe even to settle. I am also

grateful to the Vosges, the Jura, the south of France, London, the Himalayas, Joniec, the Alps and the lakes around Munich for helping my mind get away from science and fueling me up with energy.

My flat mates, Jenny, Elektra and Elena for creating a place which is good to return to in the evening. My Pasing neighbors are just simply the best, I am so happy that we got to know each other. Thank you very so much for all the garden and balcony beers, dinners and chats. Especially Dijana and Laurin for being such an amazing couple. And for all “our” kids for cheering me up with playing and laughing under my window.

A biomókus kis barátaim nélkül nem lettek volna ilyen szuperek az egyetemi évek es legjobban annak örülök, hogy ezek a barátságok még mindig kitartanak (habár én vagyok a gyengébb láncszem aki csak kevésszer jelenik meg – örülök hogy mindig hívtok). Erik, egy igaz barát, nagyon sokat jelent, hogy ennyire kitartasz mellettem.

Anya, Apa, Luca és Bence, köszönöm, hogy közöttetek nőttem fel, nélkületek nem lennék az aki. Nagyon sokat számít nekem, hogy elfogadtok és támogattok annak ellenére, hogy évek óta csak keveset látjuk egymást. Anama, Julcsi mama es Jóska papa, amikor rátok gondolok, emlékeztet, hogy mennyire szerencsés vagyok amiért a azt csinálhatom amit szeretek és ennyit utazhatok.

Joaska, moim najlepszym przyjacielem, moją miłością. Dziękuję, że jesteś tym, kim jesteś.

Abstract

Upon fertilization the two parental genomes are extensively reprogrammed to give rise to a totipotent state. In the mammalian embryo, this epigenetic reprogramming involves an extensive three dimensional (3D) rearrangement of nuclear organization which only recently have been started to be investigated on a genome-wide scale. The positioning of loci relative to the nuclear periphery has been shown to change during differentiation, potentially regulating gene expression and chromatin. Therefore, it is of question whether the nuclear reorganization in early embryonic cells correlates with or even regulates genome function and embryo development.

During my PhD work, we have created maps of lamina associated domains (LADs) from mouse preimplantation embryos and oocytes at the single cell level. LADs are genomic regions that reside at the nuclear periphery and represent a lowly transcribed, gene-poor fraction of the genome originally identified in somatic cells. We have found that LADs are absent in oocytes but become established already in zygotes and are dynamically rearranged during the 2- and 8-cell stages with little heterogeneity between individual cells. We obtained LAD data from hybrid embryos to distinguish the parental genomes by single nucleotide polymorphisms (SNPs) in sequencing. Our analysis unravelled differences in genome organization between the two parental alleles that likely reflect their different germline history. Moreover, we find that LAD formation precedes the maturation of topologically associated domains (TADs) in a DNA replication independent manner. Additionally, we observed that only the X chromosome contacts the lamina in oocytes, potentially through an interaction with the Lamin B Receptor (LBR) protein.

Eventually, we identified an epigenetic asymmetry of H3K4 methylation on LADs between the paternal and maternal genomes in zygotes. We found that the experimental reduction of the H3K4me3 histone mark by the overexpression of the lysine demethylase Kdm5b results in a loss of LAD structure, specifically in the paternal zygotic genome.

In conclusion, we have uncovered a novel mechanism of allele specific LAD formation through histone methylation. Additionally, this work provides genome wide information on mouse preimplantation nuclear organization contributing a resource for further epigenetic studies of early embryos.

Table of Contents

List of figures

Abbreviations

3D	three dimensional
5hmC	5-hydroxymethylcytosine
5mC	5-methylcytosine
AID-tag	auxin inducible degron tag
ATAC-seq	Assay for Transposase-Accessible Chromatin using sequencing
BAF1	Barrier-to-autointegration factor protein
C. elegans	*Caenorhabditis elegans*
CAST	*Mus musculus castaneus*
Cdx2	Caudal-Type Homeobox Protein 2
CF	Contact Frequency
ChIP-seq	chromatin immunoprecipitation followed by sequencing
CHX	cycloheximide
cLAD	constant LAD
CTCF	CCCTC-binding factor protein
CV	Coefficient of Variation
Dam	*E. coli* DNA adenine methyltransferase protein
DamID	DNA adenine methyltransferase identification
DAPI	4,6-diamidino-2-phenylindole
DD	destabilization domain
DHS	DNase hypersensitive site
disLAD	disappearing LAD
DNA-FISH	DNA-Fluorescent in situ hybridization
DpnI	restriction enzyme that cleaves G^{m6}ATC but not GATC motif
Dppa3	Developmental Pluripotency Associated 3 protein
DRB	5,6-Dichloro-1-β-D-ribofuranosylbenzimidazole
dsRNA	double stranded RNA
E 5.5	embryonic day 5.5
EGFP	enhanced green fluorescent protein
ES cell	Embryonic Stem cell
EU	5-ethynyl uridine
H3	histone 3
H4K20me	methylation on the 20th amino acid of the H4 histone tail

H3K27ac	acetylation on the 27th amino acid of the H3 histone tail
H3K27me3	trimethylation on the 27th amino acid of the H3 histone tail
H3K4me3	trimethylation on the 4th amino acid of the H3 histone tail
H3K9me2	dimethylation on the 9th amino acid of the H3 histone tail
H3K9me3	trimethylation on the 9th amino acid of the H3 histone tail
HMM	Hidden Markov Model
HMT	histone methyltransferase
HP1	heterochromatin protein 1
IAA	indole-3-acetic acid (auxin)
ICM	Inner cell mass
IF	immuno-fluorescent staining
iLAD	inter Lamina Associated Domain
Kb	kilobase
Kdm4d	Lysine Demethylase 4D protein
Kdm5b	Lysine Demethylase 5B protein
Kmt2d	Lysine Methyltransferase 2D
LAD	Lamina Associated Domain
LBR	Lamin B Receptor protein
LINE1	type 1 long interspersed nuclear elements
LmnA/C	Lamin A/C protein
LmnB1	Lamin B1 protein
^{m6}A	adenine-6-methylation
Mb	megabase
MUT	mutant
mRNA	messenger RNA
NE	Nuclear Envelope
newLAD	newly appearing LAD
NGS	next generation sequencing
NL	Nuclear Lamina
NPB	Nucleolar precursor body
Npm2	Nucleophosmin 2 protein
Oct4	POU Class 5 Homeobox 1 protein
OE	Observed over Expected score

PGC	Primordial germ cell
PN	pronucleus
Pol II	RNA Polymerase II
Pol III	RNA Polymerase II
Prdm14	PR/SET Domain 14 protein
RPKM	Reads Per Kilobase of transcript, per Million mapped reads
Scc1	Sister Chromatid Cohesion 1 protein
Setdb1	SET Domain Bifurcated 1 protein
siRNA	small interfering RNA
SNP	Single nucleotide polymorphism
TAD	Topologically Associated Domain
TE	Trophoectoderm
Tet3	Tet Methylcytosine Dioxygenase 3 protein
TES	transcriptional end site
TIR1	Transport Inhibitor Response 1 protein
TS cell	Trophoblast Stem cell
TSS	transcriptional start site
WT	wild-type
ZF	zinc finger protein
ZGA	Zygotic Genome Activation

Aims

The role of nuclear organization – the three-dimensional (3D) positioning of genomic loci relative to one another and to subcompartments of the nucleus – in transcriptional and cell state control is becoming increasingly well-established. Highly dynamic changes in nuclear architecture are known to occur during early mammalian embryogenesis, however these changes have not been systematically characterized, nor have they been probed for functionality. Also, it is unknown whether genome organization is inherited from the germline and the mechanism of LAD formation is unclear.

Therefore, the aims of my PhD work were to:

1) provide a genome-wide map of nuclear organization in the mouse preimplantation embryo at the single cell level
2) determine the allelic differences in genome organization in embryos
3) test if there is a preexisting LAD pattern in gametes that could be inherited through fertilization
4) uncover potential epigenetic mechanisms that could regulate genome organization in these early embryonic nuclei

Introduction

Previously, I have written a review article on nuclear organization in early embryos (Borsos and Torres-Padilla, 2016). In the following introduction I will:

1) introduce mouse preimplantation embryo development

2) highlight our current understanding of genome organization and its connection to gene expression

3) describe the current knowledge on genome organization in preimplantation nuclei

Mouse preimplantation development

Life starts with fertilization, the fusion of two highly differentiated cells: an egg and a sperm. The oocyte is one of the largest cells of the body with a spherical diameter of 60-70 μm in the mouse. Therefore, oocytes are able to store a large cytoplasmic content, an essential supply of proteins and RNA for the early embryo (Susor et al., 2016). Contrarily, the sperm carries barely any cytoplasm, its genome is tightly packaged around protamines instead of histones (Rodman et al., 1984). The sperm head is supported by its neck packed with mitochondria and its tail for rapid movement. These two germ cells acquire very different characteristics during oogenesis and spermatogenesis making them specialized to very different tasks; yet both are essential to support further development of a new organism under natural conditions.

Upon ovulation, the oocyte undergoes nuclear envelope breakdown and executes the first meiotic division halving its DNA content from 4n to 2n by extruding the first polar body (Li and Albertini, 2013). The ovulated egg is surrounded by a protective glycoprotein shell called the zona pellucida. Several layers of somatic cumulus cells are attached to the zona pellucida surrounding the egg. Upon expulsion from the ovary, the egg reaches the oviduct and slowly travels towards the uterus in the oviductal fluid. The ovulated egg(s) are met by the spermatozoa in an enlarged section of the oviduct called the ampulla, where fertilization happens (Eddy and Pauerstein, 1980). Upon penetration of the zona pellucida the sperm head fuses with the plasma membrane of the egg enabling the entry of the paternal genome into the egg's cytoplasm. This fusion induces Ca^{2+} oscillations upon which the egg completes the second meiotic division by extruding the second polar body (Miyazaki and Ito, 2006).

From the fusion of the gametes a zygote emerges bearing the two parental genomes initially at the two opposite sides of the zygote. Both genomes rapidly assemble into two separate nuclei referred to as “pronuclei” (PN): the maternal meiotic chromosomes decondense into interphase and histones are incorporated into the compact sperm genome exchanging its original protamines. During the approximately twelve hours long zygotic cell cycle the two pronuclei gradually migrate towards each other and meet in the center just before the first mitosis begins. The developmental time of a zygote is usually categorized into “pronuclear stages” based on the distance between the two pronuclei (Adenot et al., 1997).

Before the first mitosis, the two separate pronuclei undergo nuclear envelope breakdown and the paternal and maternal chromosomes converge onto a single metaphase plate followed by the division of the zygote into a 2-cell stage embryo. Both zygotes and 2-cell embryos are considered totipotent in mice because each of the single cells of these embryos can give rise to an entire mouse including both extraembryonic and embryonic tissues (**Figure 1**) (Mulnard, 1965; Tarkowski, 1959; Tarkowski and Wroblewska, 1967). The 2-cell embryo divides further and these divisions are referred to as “cleavages” because with each round the cells approximately halve their size. After the 16-cell stage the embryo starts to cavitate creating a fluid cavity between the internal and external cells achieving a ball like structure called the blastocyst (Pratt, 1989). By this stage the embryo already reaches the uterus where the blastocyst hatches from the protective zona pellucida and attaches to the uterine wall and initiates implantation.

Zygotic transcription and the first cell fate decisions

Most transcripts in the zygote are inherited from the oocyte, therefore, are termed “maternal transcripts”. Upon fertilization, the translation form these transcripts is either activated or the majority of these RNAs are actively degraded. The zygote carries out very little ongoing transcription termed minor zygotic genome activation (ZGA). Minor ZGA is primarily executed by RNA Polymerase II (Pol II) on intergenic regions and by RNA Polymerase III (Pol III) on rDNA clusters and is essential for further development (Abe et al., 2018; Lin et al., 2014). It is only by the 2-cell stage when the levels of active transcription by Pol II of genes and also of repetitive elements surges, this process is termed major ZGA (Abe et al., 2015; Schultz, 2002). The major ZGA

not only provides essential transcripts for cell function but is also critical for the remodeling of chromatin (see next chapter).

The early embryonic transcription is peculiar since even though repetitive elements of the genome are usually kept silent in most cell types, in preimplantation stages several classes of repeats are transiently transcribed (Peaston et al., 2004; Rodriguez-Terrones and Torres-Padilla, 2018). For example, the MERV-L type of transposons are highly expressed just preceding major ZGA at the early-2-cell stage (Ishiuchi et al., 2015; Macfarlan et al., 2012; Peaston et al., 2004). Such transcription also gives rise to chimeric transcripts that are likely important for development. Recently, a single transcription factor called Dux was shown to bind these MERV-L elements and also be necessary for the start of major ZGA (De Iaco et al., 2017; Hendrickson et al., 2017; Whiddon et al., 2017). Also, other repeats such as type 1 long interspersed nuclear elements (LINE1) are transiently expressed in early embryos (Fadloun et al., 2013; Jachowicz et al., 2017). The proper timing of this LINE1 expression has been shown to regulate chromatin accessibility and be necessary for embryo development (Jachowicz et al., 2017). These observations suggest that the transient burst of repetitive transcription might play a functional role at these early stages.

The first two distinct cell lineages arise by the blastocyst stage including the pluripotent inner cell mass (ICM) that will constitute the embryo and the more differentiated trophoectoderm (TE) which will constitute the extraembryonic tissues such as the placenta (**Figure 1**). These cell populations are molecularly identified by the expression and kinetics of distinct transcription factors (e.g. Cdx2 for TE, Oct4 for ICM) (Plachta et al., 2011); and are first distinguishable morphologically as an ‘outer’ and an ‘inner’ group of cells at the 16-cell stage morula (Zernicka-Goetz et al., 2009). To what extent cell fate decisions are pre-patterned or arise from random, stochastic processes has been under debate. Recently, considerable epigenetic (e.g. histone arginine methylation) (Torres-Padilla et al., 2007) and gene expression (e.g. *Prdm14, Sox2* expression) (Burton et al., 2013; White et al., 2016) differences have been observed between blastomeres at the 4-cell stage. This suggests that information linked to cell fate might be present at an earlier stage than was previously thought. However, these represent only isolated examples, and information on the genome-wide scale is lacking.

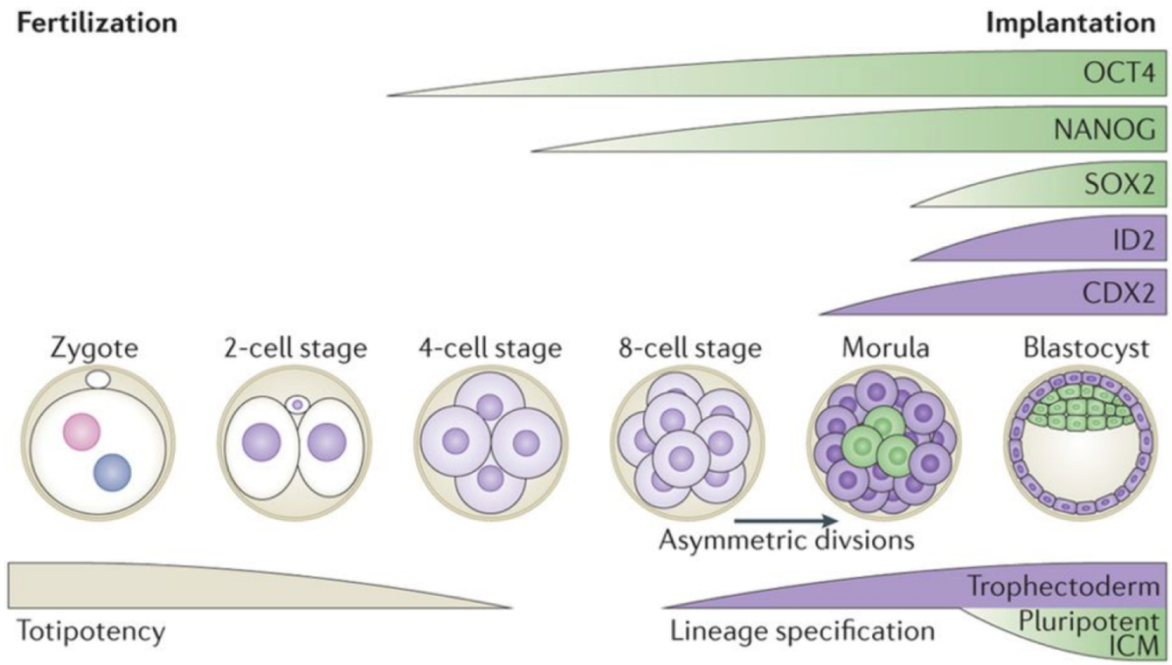

Figure 1. Preimplantation development of the mouse embryo

Mouse development starts with the fertilization of an egg by sperm giving rise to a one-cell zygote. The zygote and 2-cell stage are totipotent and the pluripotent ICM and the differentiated TE lineages emerge by in the morula after the 8-cell stage embryo divides asymmetrically. The two lineages are fully distinguished by the blastocyst stage. The expression pattern of pluripotency and trophoectoderm markers (indicated on top) is distinctive in these two distinct cell lineages. Figure adapted from *Burton et al. 2014*.

Epigenetic reprogramming during preimplantation development

There is an extensive epigenetic reprogramming (the erasure and remodeling of epigenetic marks) occurring in zygotes and 2-cell stage embryos. This processes mainly entail the removal and rewriting of histone marks and DNA modifications. Along with these most studied processes, there might be other yet uncovered features of epigenetic reprogramming taking place such as changes in replication timing, nuclear organization or the remodeling of yet uncharacterized novel histone/DNA modifications.

One of the first epigenetic marks found to be reprogrammed upon fertilization is cytosine methylation of DNA (5mC). Upon fertilization, both genomes carry high levels of 5mC as judged by immuno-fluorescent (IF) staining, however, 5mC from the paternal DNA is rapidly lost (**Figure 2a**). Thus, by the late-zygote stage a clear asymmetry arises, the maternal genome having high and the paternal genome bearing very low

levels of 5mC. One model for this asymmetry proposes that the Dppa3/Stella protein binds to the di-methylated ninth lysine of the H3 histone tail (H3K9me2) in the maternal pronucleus and protects the maternal genome from active demethylation (Nakamura et al., 2007). Yet, the reduction of 5mC in the paternal genome in zygotes involves both active demethylation and passive dilution through replication (Hajkova et al., 2010; Inoue and Zhang, 2011). It has been proposed that the active demethylation takes place by the conversion of 5mC into hydroxymethylcytosine (5hmC) by the Tet3 hydroxylase enzyme (Ladstatter and Tachibana-Konwalski, 2016). Moreover, recently *de novo* methylation activity has also be reported to occur in zygotes which seems to be essential for 5hmC formation (Amouroux et al., 2016). Overall, 5mC levels are unconventionally low during preimplantation development and a more canonical DNA methylation pattern is established only by the blastocyst stage (Smallwood et al., 2014; Smith et al., 2014; Smith et al., 2012).

Posttranslational modifications of histone tails are also extensively remodeled after fertilization (Burton and Torres-Padilla, 2014). Since the sperm chromatin is mainly packaged around protamines, most of the inherited histone modifications are present in the maternal genome. Several of these are erased and rewritten *de novo* as development proceeds. Most of these marks were initially assessed only by IF staining, recently however a few of them were also assessed by genome-wide approaches like ChIP-seq.

One of the most well characterized histone mark in embryos is the tri-methylation on the fourth lysine of the H3 histone tail (H3K4me3). This modification is present in broad, non-canonical domains in the oocyte (**Figure 2b**) (Dahl et al., 2016; Liu et al., 2016; Zhang et al., 2016). Contrarily to its typical correlation of H3K4me3 promoter peaks with active genes, the experimental removal this mark in the oocyte results in incomplete transcriptional silencing – which otherwise would occur by the end of oocyte growth (Zhang et al., 2016). These broad domains of the maternal genome are passed down to the zygote and become remodeled into canonical promoter peaks only upon the zygotic genome activation of gene expression. The function of these broad domains in the zygote and in early-2-cell embryos is unknown. In contrast, the paternal chromatin has lower levels of H3K4me3 at fertilisation and undergoes *de novo* methylation on H3K4 in a more canonical, promoter peak pattern.

The canonical repressive chromatin mark, tri-methylation of H3K9 is also extensively remodeled in embryos. It shows a distinct asymmetry bearing high levels

on the maternal but not on the paternal chromatin of zygotes (**Figure 2a**). Later, H3K9me3 levels are decreased by the middle of preimplantation and are then *de novo* reestablished by the end of implantation. Likely, H3K9me3 acts as a barrier to efficient epigenetic reprogramming, since the use of H3K9me3 depleted donor nuclei in nuclear transfer experiments resulted in a more than twice-fold increase in blastocyst development rate (Matoba et al., 2014). A recent paper employing ChIP-seq and functional experiments have demonstrated that H3K9me3 deposition occurs actively in embryos and contributes to the silencing of repetitive elements through recruiting the DNA methylation machinery (Wang et al., 2018).

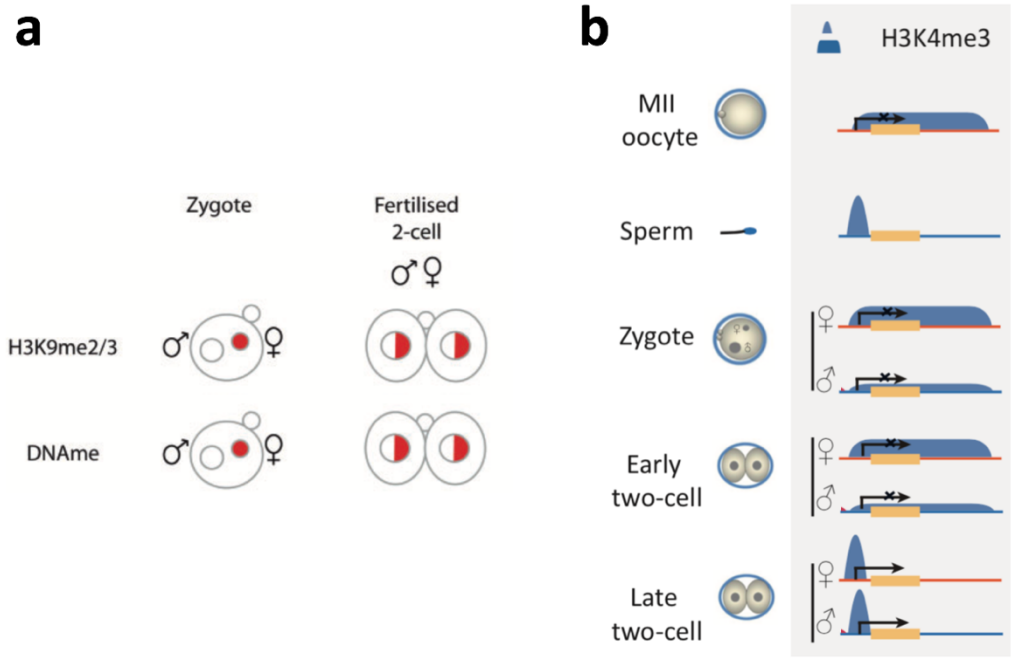

Figure 2. Epigenetic asymmetry of H3K9me and DNA methylation, remodelling of H3K4me3 after fertilization

a) Di- and tri-methylation of H3K9 and DNA methylation shows an asymmetric distribution in zygotes, predominantly covering the maternal genome. This asymmetry is still present at the 2-cell stage as the maternal alleles are higher methylated than the paternal. Gradually, this asymmetry is lost over preimplantation development. Figure adapted from *(Burton and Torres-Padilla, 2010)* © Burton and Torres-Padilla 2010. Published by Oxford University Press. All rights reserved. **b)** H3K4me3 is present in non-canonical broad domain in oocytes and in promoter peaks in the sperm. The sperm H3K4me3 is removed upon fertilization and is de novo re-established. The broad maternal H3K4me3 domains are remodelled only by the late-2-cell stage in a transcription dependent manner. Figure adapted from *(Xu and Xie, 2018)*. © 2017 Elsevier Ltd. All rights reserved. License number: 4514431370475

Another repressive mark, H3K27me3 has also been assessed genome wide using ChIP-seq in embryos (Zheng et al., 2016). This study revealed that sperm

H3K27me3 is completely reset upon fertilization but peaks distal from promoters are inherited from oocytes. H3K27me3 is erased on promoters of developmental genes upon fertilization and is only reestablished around implantation mainly contributing to bivalent promoters (bearing both the activating H3K4me3 mark and the repressive H3K27me3). Moreover, several allele specific H3K27me3 peaks have been identified which contribute to a DNA methylation independent form of imprinting resulting in monoalllelic expression of dozens of genes (Inoue et al., 2017a).

The mouse preimplantation embryo as an experimental model system

Since the mid-1960s, the *in vitro* culture of mouse preimplantation embryos became a reality making this model system accessible for biological studies (Brinster, 1963). Embryos can be obtained after natural matings and the timing of fertilization can be stringently controlled by experimentally inducing ovulation in females with hormonal injections. The developmental program of preimplantation embryos follows a strict timeline of cell divisions, therefore by synchronizing fertilization researchers can determine or manipulate the cell cycle stage precisely.

Due to their large size, transparent nature and synchronized cell cycle, these embryos are applicable to live-cell imaging of several basic cell biological processes such as chromosome segregation (Tachibana-Konwalski et al., 2010). Moreover, mouse preimplantation embryos are fairly easy to micromanipulate. Blastomeres can be fused, individual nuclei can be removed or transplanted, embryos can be aggregated to form chimeras (the experimental fusion of two genetically distinct embryos typically at the 8- or 16-cell stage) as some of the prime examples of classical embryology. Also, the RNAi pathway works very efficiently in embryos (Wianny and Zernicka-Goetz, 2000), therefore siRNA, dsRNA or mRNA microinjections make a wide range of loss-of-function and gain-of-function approaches possible. The disadvantage of these experiments is that each embryo has to be handled manually one-by-one.

The preimplantation embryo is an ideal system to study the very first cell fate decisions in mammals. The small number of cells (1 to 64) makes it possible to track individual cells and their daughters since they can be marked by fluorescent protein coding mRNA injections. Moreover, mouse embryos can be efficiently segregated into single cells and then collected for next generation sequencing (NGS). Therefore, most of the initial single cell RNAseq studies used the preimplantation embryo as a model

system (Deng et al., 2014; Petropoulos et al., 2016; Tang et al., 2010). Regarding either NGS or any biochemistry approaches the disadvantage of preimplantation of embryos lies in the scarcity of material. Realistically, not more than a few thousand embryos/cells can be harvested, which already requires the sacrifice of over a hundred of mice. Additionally, for micromanipulated embryos this number drops with one or two orders of magnitude.

Up until recently, the mouse early embryo culture was limited until the late, hatching blastocyst stage. However, novel *in vitro* methods have been developed to extend the culture periods of mouse embryos up to stages corresponding to implantation around embryonic day 5.5 (E 5.5) (Bedzhov et al., 2014; Bedzhov and Zernicka-Goetz, 2014; Deglincerti et al., 2016). This advancement is particularly valuable since this way embryogenesis could be studied *in vitro* at stages where not only three cell types are present (as in the non-implanted blastocyst) but more, for example even early specifying primordial germ cells (PGCs).

Alternatively to embryos, embryonic stem cells (ES cells) are derived from the ICM of the blastocyst and can be cultured *in vitro* (Evans and Kaufman, 1981). They provide a valuable complementary tool to preimplantation embryos, since the amount of material is not limited. Therefore, most biochemical assays are usually carried out in ES cells instead of embryos.

Nuclear organization and genome function

Pioneering fluorescent in situ hybridization (FISH) studies have revealed that the organization of chromatin within nuclei of differentiated cells is non-random (Bolzer et al., 2005; Cremer et al., 2001). Generally, gene-rich chromosomes tend to be towards the interior, gene-poor ones close to the periphery and gene-rich loci within one chromosome tend to loop out from their territory – presumably because they are within a more accessible chromatin environment (Boyle et al., 2011). The three dimensional (3D) positioning of genomic regions has been associated with their transcriptional status, thus affecting development in multiple cases. For example the HoxB and HoxD cluster is activated upon looping out of its original territory (Chambeyron and Bickmore, 2004; Chambeyron et al., 2005; Eskeland et al., 2010) and the repositioning of genes towards/away from the nuclear envelope is a regulator of B-cell development (Lin et al., 2012). Moreover, the nuclear position of loci seems to be epigenetically heritable throughout several divisions, at least in some cases

(Therizols et al., 2014). Furthermore, several subnuclear compartments (e.g. nucleoli, transcription factories, speckles, polycomb bodies, etc.) have been described to date, many with poorly understood function.

Topologically Associated Domains (TADs)

Chromatin architecture is nowadays widely studied by so called “C” methods (Chromosome Conformation Capture) of which the most commonly used is HiC (Crane et al., 2015; Lieberman-Aiden et al., 2009; Sexton et al., 2012). The purpose of these methods is to unravel physical 3D proximity of neighbouring genomic regions mainly in interphase nuclei. Briefly, it involves the crosslinking the chromatin of intact cells, digestion with restriction enzymes and ligation of these physically proximal fragments. Afterwards, the ligated fragments are purified and sequenced. Based on the identity of the two ligated loci, a matrix of contact frequencies is built computationally on each chromosome (cis contacts) and also between different chromosomes (trans contacts).

The first information HiC contact matrices yielded was the discovery that the genome is partitioned into two main type of compartments that are preferentially interacting with their own type and not the other. Namely, A and B compartments are large, 1-10 Mb sized domains alternating on each chromosome (Lieberman-Aiden et al., 2009; Sexton et al., 2012). The A compartments tend to be rich in genes, they are transcriptionally more active and harbour a more open chromatin state. The B compartments are the opposite, they are gene poor, lowly transcribed and the chromatin is less accessible in these domains.

At a finer resolution, contact matrices show that there are several smaller domains within the same compartment. These tend to self-associate and give rise to the globular organization of interphase chromosomes (**Figure 3**). These domains are in the range of 0.1-1 megabases (Mb) and are called topologically associated domains (TADs) (Dixon et al., 2012; Nora et al., 2012). The general TAD structuring of the genome is evolutionarily conserved and there are little cell type specific differences in TADs within the same species (Dixon et al., 2012; Rao et al., 2014). One method to define TAD boundaries is by calculating insulation scores (Crane et al., 2015). The boundaries exhibit a local minimum of insulation scores between two consecutive TADs. TAD borders are usually bound by architectural insulator proteins like the CCCTC-binding factor (CTCF) and by cohesin rings (Nora et al., 2012; Phillips-Cremins et al., 2013). How TADs are maintained in cells has long been unanswered,

however conditional depletion of CTCF has shown that this boundary protein is not essential for keeping TAD organization in mouse ES cells (Nora et al., 2017). On the other hand, depletion of cohesin subunits or its loaders results in the loss of TAD structuring arguing that TADs are likely formed in a cohesion ring dependent manner (Gassler et al., 2017; Rao et al., 2017; Schwarzer et al., 2017).

Recently the resolution of HiC has been improved to yield contact maps at the resolution of 5 kilobases (Kb) making it possible to distinguish transcriptional units (Bonev et al., 2017). Moreover, HiC is applicable for single cells in which case either haploid or hybrid cells are used to distinguish the two parental alleles based on SNPs (Nagano et al., 2017; Stevens et al., 2017). Additionally, other ligation independent methods like SPRITE revealed a similar chromatin organization confirming the findings of HiC (Quinodoz et al., 2018).

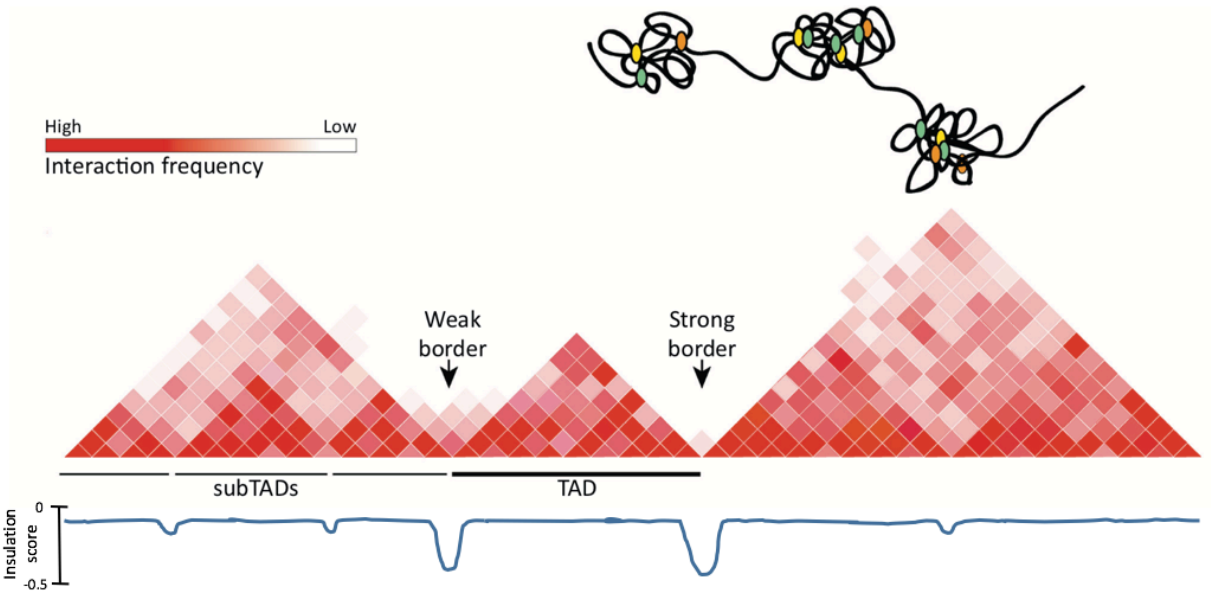

Figure 3. HiC maps of topologically associated domains (TADs)

Chromatin exhibits local preferences of interaction resulting in a globular domain organization of chromosomes. These domains can be determined by crosslinking chromatin and sequencing the crosslinked fragments that are a result of 3D physical proximity. HiC is a form of this crosslinking combined sequencing method that deciphers TAD structures. TADs are visualized as triangles showing higher interaction frequency on the linear scale of a chromosome, TADs represent globular domains of chromatin. TAD borders are visible by a local loss of interaction frequencies illustrated by local minima in the insulation scores. Figure adapted from *(Gomez-Diaz and Corces, 2014)*.

Lamina Associated Domains (LADs)

The nuclear envelope (NE) is a double layered lipid membrane continuous with the endoplasmic reticulum. Underneath the NE a protein meshwork of the nuclear lamina (NL) contributes a scaffold for the interphase nucleus. The NL constitutes of intermediate-type protein filaments, mainly lamin B1, B2 and A/C (Dechat et al., 2010). Either lamin B1 or B2 are present in all cell types, while lamin A/C exhibits a more cell type specific expression pattern having low or undetectable levels in less differentiated cells like ES cells (Constantinescu et al., 2006; Eckersley-Maslin et al., 2013). Moreover, lamin A/C has been suggested to have roles not only at the nuclear periphery but also in the interior (Legartova et al., 2014). Interestingly, mouse embryos lacking lamin B1 and B2 or lamin A/C are able to develop to term but show an early post-natal lethality (Kim et al., 2011; Kim and Zheng, 2013; Sullivan et al., 1999). Also, deletion of these three lamins in ES cells does not perturb differentiation into all neither of the three germ layers *in vitro*, arguing that lamins are not essential for cell differentiation (Kim et al., 2013).

Another typical protein of the nuclear periphery is the lamin B receptor (LBR) that contains seven transmembrane domains and binds to the heterochromatic mark H4K20me and to Heterochromatin Protein 1 (HP1) (Hirano et al., 2012; Ye and Worman, 1996). Moreover, several LEM-domain containing proteins reside at the NL such as Emerin, Man1 or Lap2. These proteins have been also shown to interact with chromatin but mainly indirectly by binding the Barrier-to-autointegration factor (BAF1) (Wilson and Foisner, 2010).

The region directly under the nuclear envelope can also be viewed as a subnuclear compartment. Those parts of the genome that are in close proximity to the nuclear lamina are referred to as lamina associated domains (LADs) (Guelen et al., 2008). These loci contain 1.5-2 fold fewer genes compared to the so-called inter-LADs (iLADs), they tend to be silenced and labelled with heterochromatic marks, such as H3K27me3 and H3K9me2 (Guelen et al., 2008; Peric-Hupkes et al., 2010; Wen et al., 2009). Also, LADs tend to be A/T rich and show a reduced of CpG content (Meuleman et al., 2013). Additionally, LADs seem to overlap with the late replicating domains of the genome which are also generally associated with silenced chromatin (Bickmore and van Steensel, 2013). Moreover, LADs typically coincide with B compartments determined in HiC experiments. The above mentioned details are summarized in (**Table 1**).

It has recently been shown that “mother”-LADs stochastically reshuffle after cell division in the daughter cells and only a sub-fraction of them (32 % based on DNA-FISH) re-associate with the NL (Kind et al., 2013). Furthermore, upon differentiation of ES cell to neuronal progenitors *in vitro*, differences in LAD patterning arise between the two cell types – i.e. some genomic regions are peripherally located only in ES cells or in neurons (Peric-Hupkes et al., 2010). This study also suggested that the cell-type specific rearrangements of LADs coincide with changes in gene expression. Often regions that were actively transcribing in ES cell and became silenced upon transition to the neuronal lineage simultaneously relocated towards the periphery (Peric-Hupkes et al., 2010). However, it remains unclear whether movement towards the NL is necessary for the reduction of transcription or if it is just a consequence of it.

The heterochromatic, more repressive nature of LADs have been demonstrated in several species (Gonzalez-Sandoval et al., 2015; Harr et al., 2015; Towbin et al., 2012). Some of these experiments usually involve the artificial tethering of loci to the NL. This relies on the integration of repetitive arrays of target sites for DNA binding proteins (i.e. LacI/*LacO* system) which are fused to components of the NL, thereby physically linking the periphery with the target region. Often, when loci were artificially relocated towards the NL it resulted in lower transcription of genes from the loci (Finlan et al., 2008; Reddy et al., 2008). However, not all studies have confirmed this phenomenon and it is highly likely that the repressive effect of relocating a locus to the NL is context dependent – both depending on the cell type, and the selected region (Kumaran and Spector, 2008).

Table 1. Typical features of LADs and iLADs

features	LADs	iLADs
Gene density	low	high
Gene expression	low	high
Hi-C compartment	B	A
Replication timing	late	early
Retroelements	LINE	SINE
Sequence A/T content	high	low
Histone marks	H3K9me2, H3K9me3, (H3K27me3)	H3K4me1, H3K4me3, H3K27ac
Nucleolus association	frequent	infrequent

Importantly, the lamin proteins themselves are not required for maintaining LAD structuring of the genome: knock-out of lamin B1 or lamin A/C does not perturb the LAD profile of mouse ES cells (Amendola and van Steensel, 2015). In post mitotic cells such as the rod photoreceptors of the retina, however, it has been genetically demonstrated that peripheral tethering of heterochromatin depends on LBR and on lamin A/C (Solovei et al., 2013).

Because of the potential role of nuclear architecture in regulating gene expression and the epigenetic state of a cell, it is of key importance to determine the nature of LAD establishment in the early embryo, as well as to test their functional role in regulating reprogramming and the developmental program.

The DamID technique to map LADs

The DamID technique was originally developed to map protein-DNA interactions in cells (van Steensel and Henikoff, 2000) and can be efficiently applied to map genome to nuclear lamina interactions (Guelen et al., 2008). It relies on the experimental introduction of a DNA modification, adenine-6-methylation (^{m6}A). This mark is present at barely detectable levels in higher eukaryotes (Wu et al., 2016b) and has not been shown to create background signal in DamID experiments. ^{m6}A can be introduced by the *E. coli* DNA adenine methyltransferase (Dam) enzyme that recognizes GATC motifs in DNA. When a fusion of Dam and lamin B1 is expressed in cells, the methyltransferase activity is sequestered to the lamina, and thus labels only LADs (**Figure 4**). To detect ^{m6}A, genomic DNA from cells expressing Dam-LaminB1 is treated with DpnI, a restriction enzyme that cleaves G^{m6}ATC but not GATC, adaptors are ligated to the fragments which are then the PCR amplified (Vogel et al., 2007). After deep-sequencing, the regions that had been in molecular contact with the NL can be mapped to the reference genome. This method reliably works on single cells with a 100kb window of resolution (Kind et al., 2015). Importantly, the results form lamin B1 DamID experiments are reproducible with orthogonal methods such as ChIP-seq of lamin B1 (Handoko et al., 2011).

Successful methylation of LADs is detectable not only in PCR and sequencing but also visually in the microscope. The ^{m6}A-Tracer is a truncated form of DpnI that cannot cut but can bind methylated GATCs without affecting cell viability and gene expression, fused with the enhanced green fluorescent protein (EGFP) (Kind et al.,

2013). When LADs are methylated a clear fluorescent signal of the ^{m6}A-Tracer is visible at the nuclear periphery (**Figure 4**).

Important controls for Dam-lamin B1 DamID are parallel experiments performed with an unfused Dam protein (Dam-only) that diffuses freely in the nucleus. Methylation by Dam-only is not unbiased but marks open regions of chromatin. Since LADs consist of conventionally more compact heterochromatin, the Dam-only signal usually mirrors LADs in somatic cells (Kind et al., 2015). In experiments on pools of cells, the Dam-lamin B1 signal is usually normalized by the Dam-only signal (Peric-Hupkes et al., 2010), however in single cell experiments this method is not appropriate since variation between the individual cells makes it dubious to pick which cells to normalize with

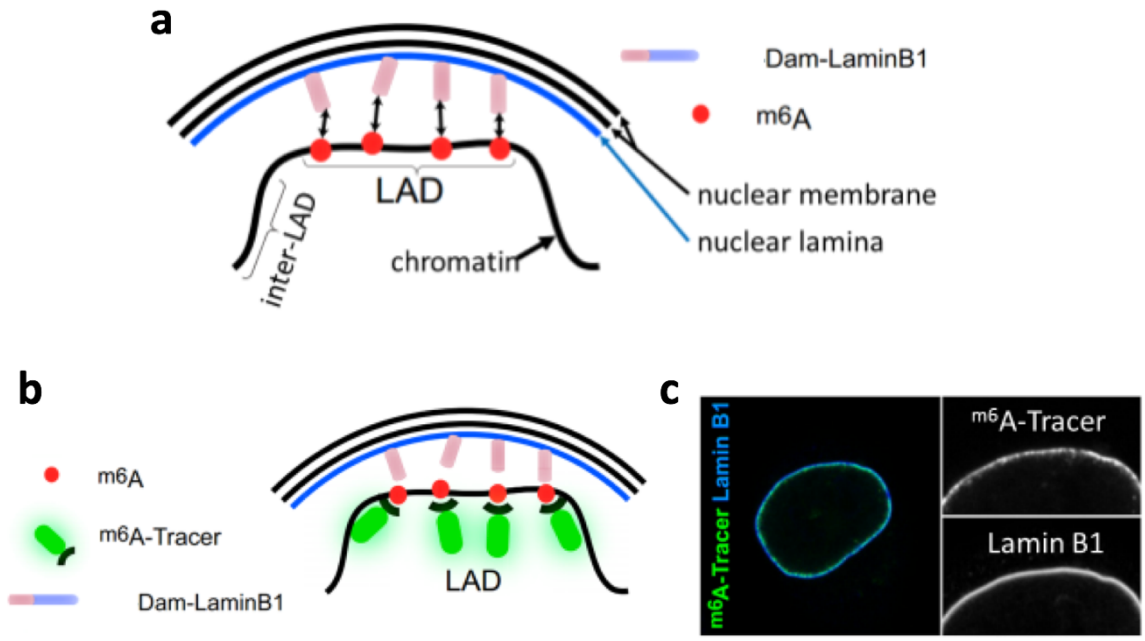

Figure 4. The DamID technique and the visualization of LADs with the ^{m6}A-Tracer

a) The Dam-lamin B1 fusion protein incorporates into the NL, thus tethering the Dam activity to the periphery of the nucleus. Therefore, genomic regions close to the periphery (LADs) are adenine methylated, and central genomic regions (iLADs) are not. **b)** Adenine methylation can be visualized by the ^{m6}A-Tracer (a truncated form of the catalytically inactive DpnI enzyme fused to EGFP). **c)** Exemplary confocal images of lamin B1 immunofluorescence co-localizing with the ^{m6}A-Tracer signal. Figure adapted from *Kind et al. 2013*.

which one. Therefore, single cell DamID usually involves the calculation of observed over expected (OE) scores (Kind et al., 2015). OE scores take into account the total number of GATC motifs within a defined sliding window (usually 100 kb for lamin B1 DamID) as “expected” numbers. The actually methylated GATC numbers “observed”

are divided with the “expected” GATC counts and each cell is also normalized by the total number of GATC reads to account for sequencing variabilities (Kind et al., 2015). Other studies on pools of cells usually do not calculate OE scores but use the read coverage normalized by GATC number per bin. These values are usually normalized with the Dam-only signal. In the case of single cell DamID experiments, however such normalization is not reasonable as one could not assess which single cell from Dam-lamin B1 experiments shall be normalized by which single cell from a Dam-only experiment.

Genome organization in the preimplantation embryo

Along with changes in histone and DNA modifications, another feature of reprogramming is the dramatic global reorganization of nuclear architecture already observable at the microscopic level. Mature oocytes, zygotes and embryos at the 2-cell stage have a peculiar nuclear organization (Burns et al., 2003; Zuccotti et al., 2005). Notably, they contain nucleolar precursor bodies (NPBs) around which the pericentromeric repeats cluster, forming distinctive ring like structures (**Figure 5**). The presence of such structures is known to correlate with efficient reprogramming upon nuclear transfer, but their exact function is still unknown (Martin et al., 2006). By the 4-cell stage, centromeric regions of the genome re-cluster into chromocenters similar to those present in all somatic, differentiated murine nuclei (**Figure 5**). The 3D localization of centromeric repeats around the NPBs in early-2-cell stage and the formation of chromocenters by the late-2-cell stage have been shown to be crucial for proper embryonic development (Casanova et al., 2013; Jachowicz et al., 2013; Probst et al., 2010). Yet, it is unknown why, how and what changes occur to the nuclear architecture genome-wide during this reorganization. Using electron microscopy, electron-dense heterochromatin can be observed at the nuclear periphery in almost all somatic nuclei (Towbin et al., 2013). In zygotic and 2-cell stage nuclei, however, electron dense regions are not visible and gradually become apparent only at later stages (Andre Eid, Torres-Padilla unpublished observations and (Ahmed et al., 2010)). The distinctive genome structure of the totipotent zygotes and 2-cell embryos suggests that the unusual nuclear architecture of the early embryo might be linked to the totipotent state (Borsos and Torres-Padilla, 2016). However, whether changes in nuclear architecture after fertilization are functionally required for reprogramming, cellular plasticity and development is barely explored.

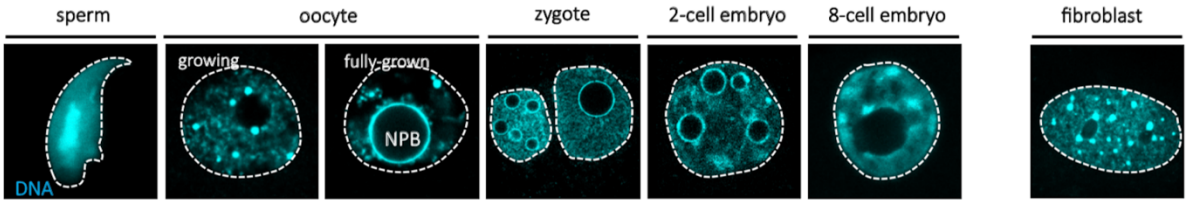

Figure 5. DNA staining of gamete and embryonic nuclei

DNA (DAPI) staining is enriched in A/T dense regions highlighting the pericentromeric repeats of chromosomes. While sperm nuclei show highly condensed chromatin in the center of the sperm head, the growing oocyte nucleus has dispersed chromocenters which re-cluster around the NPB (Nucleolar Precursor Body) by the fully-grown oocyte stage. This ring like arrangement is kept by the mid-2-cell stage. Afterwards, chromocenters are formed again from the pericentric ends of chromosomes. This patchy chromocenters arrangement is typical of the majority of mouse cells, for example in fibroblasts (on the right). Adapted from *Borsos and Torres-Padilla 2016*. © 2016 Borsos and Torres-Padilla; Published by Cold Spring Harbor Laboratory Press.

Chromatin accessibility changes during preimplantation

Accessible chromatin regions usually reflect transcriptionally active loci, whereas compacted chromatin domains are typically lowly transcribed such as LADs. The two most commonly used techniques for mapping chromatin accessibility that are applicable for low-input material (therefore to embryos) are 1) assay for transposase-accessible chromatin coupled with sequencing (ATAC-seq) and 2) DNase hypersensitive site mapping (DHS) (Boyle et al., 2008; Buenrostro et al., 2013; Buenrostro et al., 2015). ATAC-seq relies on a TN5 transposase that incorporates adaptor sequences preferentially to open chromatin regions, subsequently the fragments flanked by the adaptors are amplified and sequenced. The DHS mapping involves the digestion of intact chromatin with DNase I, that has access only to open chromatin regions, followed by the ligation of adapters to the newly created fragments and sequencing.

Recently, two independent groups have used ATAC-seq or DHS mapping to define the accessible chromatin regions of mouse preimplantation embryos (Lu et al., 2016; Wu et al., 2016a). The DHS study found less than 1.000 hypersensitive sites in zygotes, many of which were different between the two pronuclei. By the morula stage the number of DHS gradually increased to 20.000 sites and most of the allelic differences were equalized (Lu et al., 2016). This data argues for a developmentally regulated, gradual establishment of chromatin accessibility landscape during preimplantation (**Figure 6**).

The ATAC-seq study was not performed on zygotes but found higher numbers of accessible regions in the 2-cell and 4-cell stages compared to the DHS study (Lu et al., 2016; Wu et al., 2016a). This discrepancy might result from the differential preference of the TN5 transposase and DNase I. A key finding of the ATAC-seq data is that during ZGA, accessible peaks are found not only at the transcriptional start sites (TSS) of active genes but also at the transcriptional end sites (TES) (Wu et al., 2016a). The authors hypothesize that the openness of the TES might serve as a platform for regulators that could prevent promiscuous transcription.

Moreover, ATAC-seq also identified an embryo specific chromatin accessibility pattern, exhibiting a more relaxed chromatin state particularly at the 2-cell stage (**Figure 5**). The MERV-L transposon is actively transcribed at the onset of ZGA and ATAC-seq identified accessible regions not only at the MERV-L sequences but also several tens of kilobases downstream (Wu et al., 2016a). This data suggests that the activation of repetitive elements can shape the chromatin accessibility landscape of embryos, possibly even contributing to neighboring gene activation. Another repetitive element, LINE1 is also heavily transcribed during early stages of preimplantation development. *In vivo* artificial activation or repression of these endogenous LINE1 elements resulted in persistent opening or premature closing of global chromatin architecture, respectively (Jachowicz et al., 2017). This mechanistic study demonstrates that the timely regulation of chromatin accessibility by repetitive element activation is critical for proper embryo development.

TADs gradually mature during preimplantation

Recently, three independent groups have reported HiC data from mouse preimplantation embryos (Du et al., 2017; Flyamer et al., 2017; Ke et al., 2017).

The first study performed single-cell HiC on fully-grown oocytes and early zygotes. They found that even though TADs are present in interphase oocytes, the compartmentalization is very weak (Flyamer et al., 2017). Oocytes arrested at the metaphase of the second meiotic division show no TAD structure and a complete loss of compartmentalization, suggesting that the chromatin structure is not passed on from the maternal germline to the embryo (Du et al., 2017). Right after fertilization, both pronuclei exhibit very weak TAD structuring in early zygotes (Flyamer et al., 2017). These TADs are not visible on single chromosome contact maps, but only when all contacts are averaged over the known TAD boundaries defined in ES cells.

Interestingly, there is an asymmetry between the paternal and maternal genome in their compartmentalization: the paternal pronucleus exhibits higher compartment strength, whereas compartments in the maternal pronucleus are barely detectable (Flyamer et al., 2017). This asymmetry might arise from the germline history of the two genomes, as the maternal pronucleus is assembled from condensed chromosomes of a metaphase plate. The paternal chromatin, on the other hand, arrives to the egg in a more interphase like conformation that it adopted in the sperm head, making it more likely to inherit some structure.

The second study performed HiC on pools of embryos up to the blastocyst stage. They confirm the very weak signal of TAD boundaries that are again only detectable if averaged over the known boundaries of ES cell TADs (Du et al., 2017). A clear TAD pattern on individual chromosomes is visible only from the 8-cell stage onwards. This data suggests that TADs are either absent in earlier stages or are present only in a primed state with weak insulation at their boundaries which matures only by the 8-cell stage (**Figure 6**). This interpretation is also supported by the third study (Ke et al., 2017).

The authors of the second study also tested if the maturation of TADs from the 2-cell to the 8-cell stage is dependent on active transcription. They inhibited RNA Pol II with alpha-amanitin in 2-cell embryos which caused their arrest at the 2-cell stage. They collected these embryos two days later for HiC – when the untreated control embryos are already in 8-cell stage. Surprisingly, the 2-cell arrested, transcriptionally silent embryos still exhibited TAD maturation and increased insulation at TAD boundaries reminiscent of the transcriptionally active 8-cell stage controls (Du et al., 2017). This data suggests that the maturation of TADs is independent of the transcriptional program.

Whether progression through S-phase is important for TAD maturation was tested in the third study (Ke et al., 2017). Similarly to the alpha-amanitin experiment, 2-cell embryos were treated with aphidicolin to inhibit DNA replication and processed for HiC two days later when the untreated controls reached 8-cell stage. Contrarily to transcription inhibition, the 2-cell embryos could not mature TAD structures without going through S-phase (Ke et al., 2017). Taken together, the consolidation of TADs by the 8-cell stage occurs independently of cell division (alpha-amanitin treated 2-cell embryos do not divide) and transcription; however, progression through the replication cycle is necessary for forming TADs.

The only genetic study to date testing factors necessary for TAD formation in early embryos used a conditional depletion of chromosome cohesion in zygotes (Gassler et al., 2017). The authors demonstrated that TAD establishment depends on the mitotic cohesin subunit Sister Chromatid Cohesion 1 (Scc1). When Scc1 is maternally depleted from oocytes, the fertilized zygotes show a complete lack of the primed TAD insulation (Gassler et al., 2017).

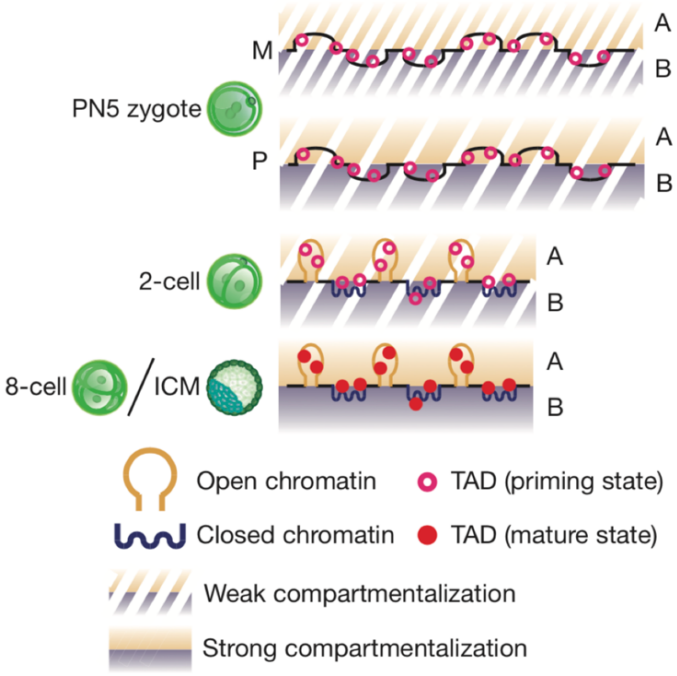

Figure 6. Chromatin accessibility and TAD maturation changes during preimplantation

A/B compartmentalization of the genome is present already in zygotes, however is gradually strengthened during development, becoming strongest by the after the 2-cell stage. TADs are initially in a primed state and not clearly defined, by the 8-cell stage TADs become matured and resemble somatic organization. Chromatin transiently opens up at the 2-cell stage coinciding with ZGA and with the transcription of MERV-L and LINE1. Figure adapted from *Du et al. 2017*.

Results

Establishing conditions for DamID in the mouse preimplantation embryo

There are two possible ways to perform DamID on LADs in preimplantation embryos. The Dam-lamin B1 construct can be expressed from the genome if a knock-in allele is created, however this requires the production of a new transgenic mouse line. This is not only time consuming but also the levels of Dam-lamin B1 cannot be precisely controlled, otherwise several promoters and induction systems (like TET-off or TET-on) need to be tested, each requiring the creation of a different mouse strain. Also, the genomic context of the transgene can affect the level of expression, thus several loci of integration should also be tested making this task even more difficult. The level of Dam-lamin B1 protein is critical since too high or too low expression can result in the oversaturation of the genome or inefficient labelling of LADs. Another method is to physically inject the mRNA coding for Dam-lamin B1 into wild-type embryos. This way, the levels of mRNA and therefore of the Dam-lamin B1 protein can be meticulously titrated. However, injection requires the micromanipulation of each embryo one-by-one in every experiment and there can be a slight variation in the levels of mRNA injected between embryos. Nevertheless, we decided to go for the microinjection approach because of its rapidity, flexibility for testing different conditions and our expertise in the method.

Components of the nuclear lamina dynamically change in embryos

First, we had to select a protein of the nuclear periphery that would be an ideal candidate for performing LAD DamID in embryos. It was important to use an NL protein that is uniformly expressed throughout preimplantation development with similar levels between stages in order to avoid the introduction of artifacts in embryo development. Therefore, we assessed the localization pattern of nuclear periphery proteins (lamin A/C, lamin B1, LBR) with immunofluorescence staining (**Figure 7**). While lamin A/C is only present zygotes and is absent in later stages, LBR is present in all stages but with increasing levels in the blastocyst (**Figure 7**). Therefore, these two proteins are unfavorable for the DamID of LADs. However, lamin B1 shows a clear peripheral staining in all stages with similar intensities, therefore being an ideal candidate to be fused with Dam. We cloned the mouse lamin B1 ORF downstream of Dam in an *in*

vitro mRNA transcription vector, prepared mRNA and went on with injecting it into embryos.

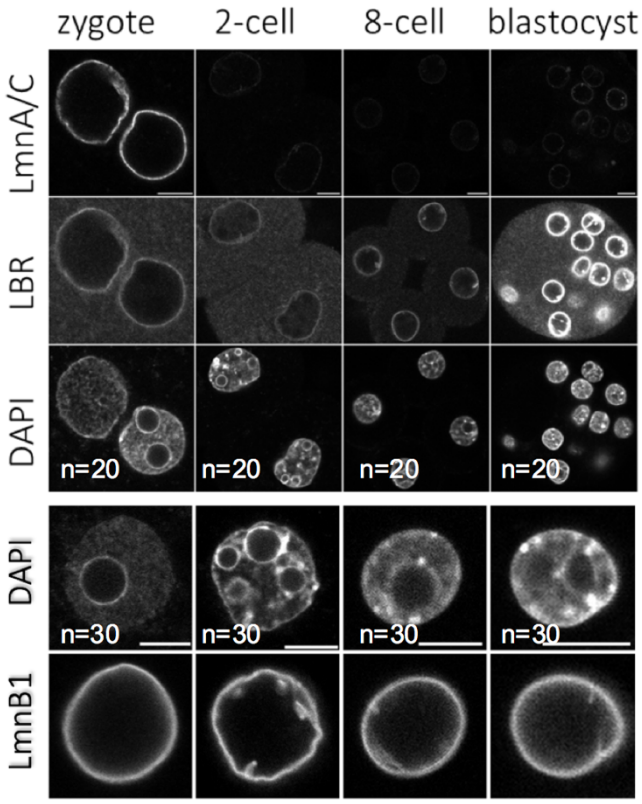

Figure 7. Immunofluorescent staining of endogenous NL components in the mouse embryo

Lamin A/C localizes to the NL in zygotes but is absent from the 2-cell stage onwards. LBR shows also a peripheral staining, however the levels of LBR are much higher in the blastocyst than in earlier embryonic stages. Lamin B1 is present in all stages with similar intensity levels at the nuclear periphery. Scale bars represent 5 μm.

The auxin degron system allows for the temporal control of DamID

Physical injection of preimplantation embryos is hardly feasible after the 2-cell stage because of the small size of the blastomeres. Also, we wanted to ensure having active Dam methylation only in the desired stage we would like to profile and not to carry over Dam methylated DNA from previous stages of development. Therefore, we aimed to temporally restrict the activity of Dam-lamin B1. One can do this by using a degron tag on the Dam-lamin B1 construct that enables turning on/off the protein by driving its proteosomal degradation upon the addition or withdrawal of a small molecule while the mRNA is present continuously.

Initially, we tested a destabilization domain (DD) carrying Dam-LaminB1 construct that is proteosomally degraded by default, unless a synthetic small molecule, Shield1 is bound to its DD (Banaszynski et al., 2006). Ideally, the concentration of Shield1 in the media defines the amount of stable protein in the cell, thus we were hoping that we could further fine tune the Dam-lamin B1 protein concentration by varying Shield1 concentrations. However, in preimplantation embryos the DD-Shield1 system did not give positive results as the DD-Dam-lamin B1 protein was present regardless of incubation with or without Shield1 (**Figure 8**).

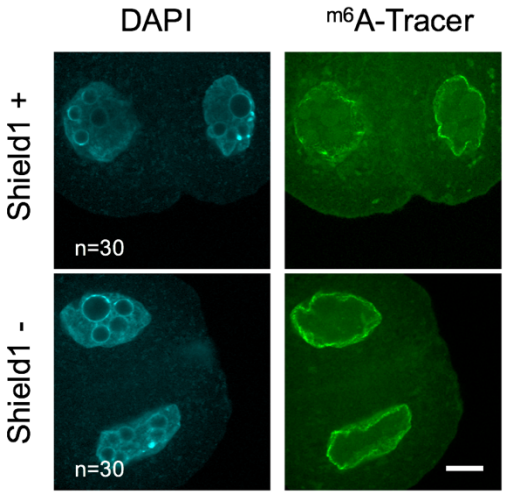

Figure 8. The DD/Shield1 system does not degrade the DD-Dam-lamin B1 fusion

Two-cell stage embryos expressing DD-Dam-lamin B1 show Dam methylation (^{m6}A-Tracer signal) on LADs both with and without Shield1, as opposed to no methylation expected in the without Shield1 condition. Scale bars represent 5 µm.

Therefore, we turned to an alternative approach using the auxin based degron system (Holland et al., 2012; Nishimura et al., 2009). The system relies on the co-expression of the Transport Inhibitor Response 1 protein (TIR1) that couples the auxin inducible degron (AID) tagged protein to the proteosome in the presence of IAA. This tool employs the following logic: when embryos are kept in auxin (IAA), despite mRNA being present the Dam-LaminB1 protein is rapidly degraded, when IAA is washed out, the protein is stabilized and LADs are methylated. Importantly, when injecting the AID-Dam-lamin B1 construct (from hereafter simply referred to as Dam-lamin B1) together with the TIR1 mRNA, this system proved to be successful in embryos yielding Dam methylation only when the embryos were incubated without IAA. This is visible on 1) PCR gels where amplification from ^{m6}A methylated DNA is only detectable from

embryos incubated without IAA; 2) and by microscopy when assessing the ^{m6}A-Tracer signal being absent in embryos cultured in the presence of IAA (**Figure 9**).

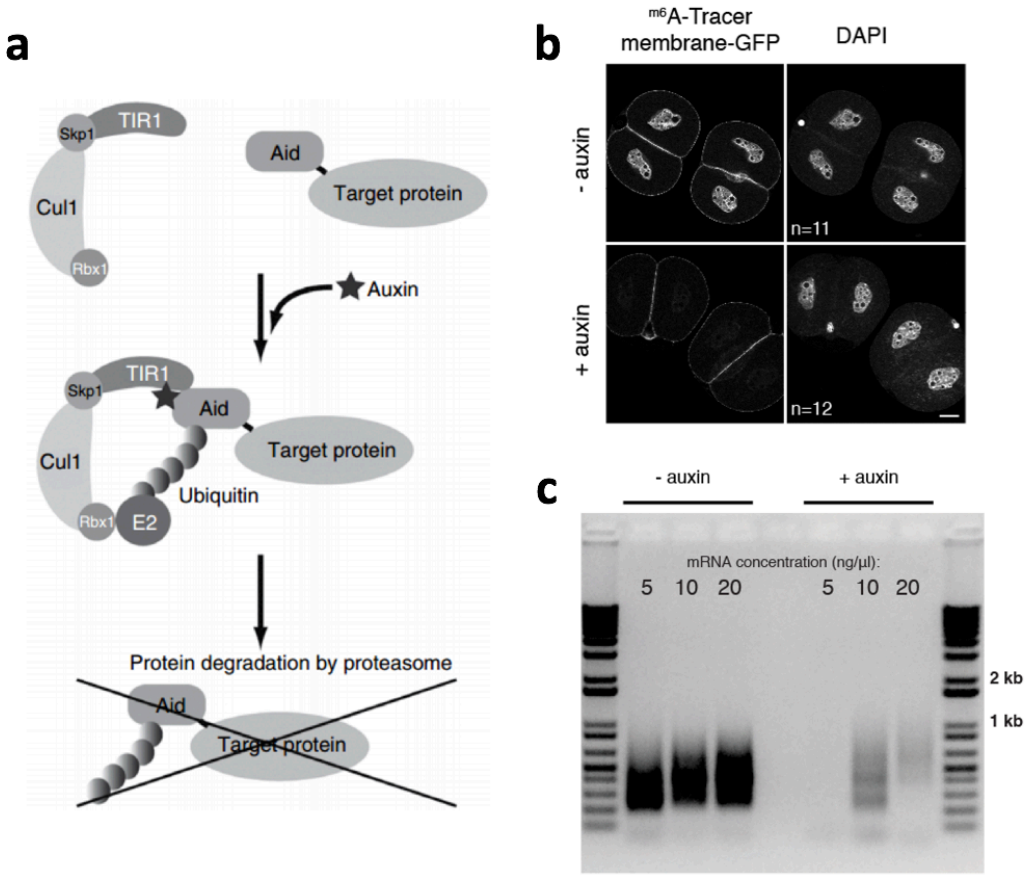

Figure 9. The auxin degron system

a) When TIR1 is co-expressed with the protein of interest fused to the AID-tag in the absence of auxin (IAA) the protein is stably present in the cell. In the presence of IAA, it is proteosomally degraded. Figure adapted from *Nishimura et al. 2009*. © 2009 Nature America, Inc. All rights reserved. License number: 4514410604144 **b)** Two-cell stage embryos show Dam-methylation judged by m6A-Tracer only in the absence of IAA. Scale bars represent 5 µm. **c)** PCR smears from amplification of pools of ten 2-cell stage embryos injected with different AID-Dam-lamin B1 mRNA concentrations show little or no methylation in the presence of IAA.

The established DamID conditions does not perturb preimplantation development

Second, it was critical to find ideal concentrations for Dam-LaminB1 mRNA since too low would yield poor methylation coverage of the LADs, and too high would methylate not only LADs but also regions that were in the nuclear interior. We titrated the mRNA injections using the m6A-Tracer as a readout (**Figure 4 and 10**) to find concentrations at which a clear peripheral ring was visible (**Figure 10**). For each stage a different injection scheme had to be adapted. For profiling zygotes and also 2-cell

embryos, we injected mRNA into either early- or late-zygotes, respectively. Because the Dam-lamin B1 mRNA was not stable enough to persist until the 8-cell stage when injected into zygotes, we had to inject both blastomeres of late 2-cell stage embryos. This way we could obtain 8-cell embryos that still had the injected mRNA present and by washing them out of IAA the Dam-lamin B1 protein could be “turned on”. In controls where Dam was not fused to LaminB1, methylation was everywhere in the nucleus (**Figure 10**). Subsequent DNA sequencing rounds enabled to define the final concentration of mRNA to be used for each stage.

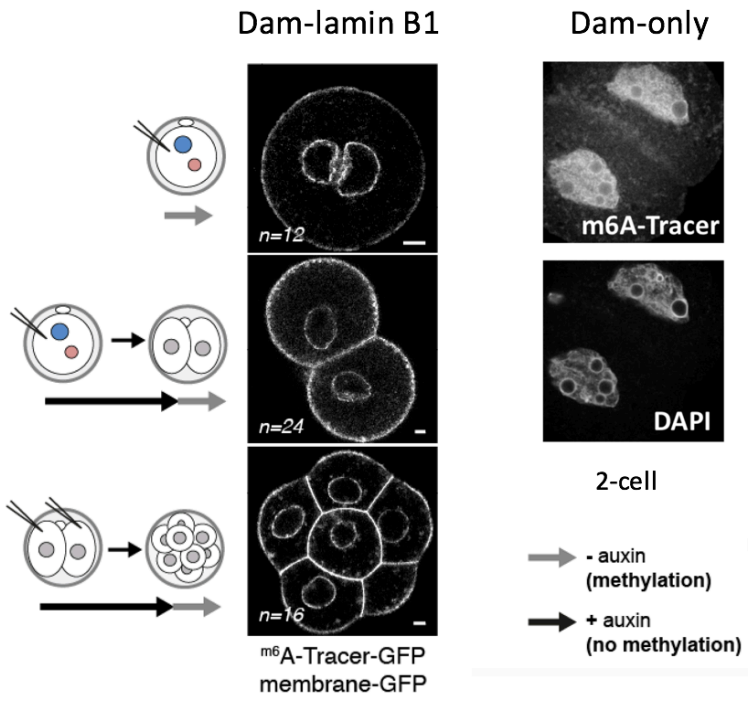

Figure 10. Different experimental injection schemes in zygote, 2-cell and 8-cell embryos

The scheme of experiments and representative images of live embryos injected with ^{m6}A-Tracer, TIR1 and Dam-lamin B1 or Dam-only mRNA are shown. The cell membrane is labelled by a GAP43-EGFP fusion. The Dam-lamin B1 injected embryos show a clear ring-like peripheral signal of the ^{m6}A-Tracer, while the Dam-only injected embryos (2-cell stage shown on the right) show a signal dispersed around in the whole nucleus. Scale bar represents 5 µm.

In addition, we tested whether the auxin based degron system has an effect on normal embryo development. We incubated uninjected embryos in the presence or absence of IAA from zygote to blastocyst stage *in vitro* (**Figure 11**). Scoring of blastocyst rate confirmed that the presence of IAA does not affect embryo development to the blastocyst. Next, we assessed if the designed injection schemes including LAD

methylation and the ^{m6}A-Tracer binding to the genome has an effect on developmental potential. Compared to the uninjected group both Dam-only and Dam-lamin B1 injected embryos developed to the blastocyst stage with normal rate, regardless if they were washed out of IAA to methylate LADs at the 2-cell stage or not (**Figure 11**).

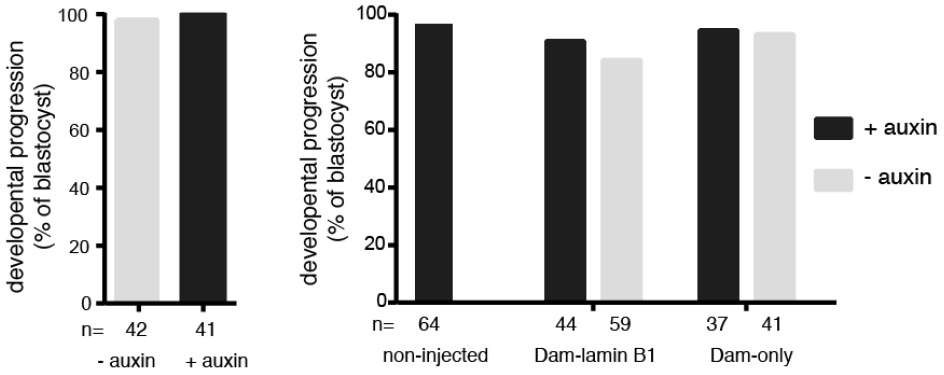

Figure 11. The rate of blastocyst development in vitro is not perturbed by IAA or by the experimental ^{m6}A methylation of DNA

Bar graphs represent the rate of blastocyst development for auxin treated (black) or non-treated (gray) uninjected embryos (left). Similarly, injected embryos with either Dam-only or Dam-lamin B1 mRNA are developing to the blastocyst at normal levels regardless if methylation is allowed by the washout from IAA (right).

Genome wide mapping of LADs post-fertilization

LADs are present already in zygotes and dynamically reshuffle during development

First, we used pools of embryos for sequencing to obtain LAD information. We mapped genome-NL interactions in zygotes, 2- and 8-cell stage embryos using pools of 15, 20, and 24 cells, respectively. The DamID PCRs and library preparations were performed by Jop Kind and the sequencing was done in the facility of the Hubrecht Institute. The raw data was analyzed by a bioinformatician postdoc in Jop Kind's laboratory, Sara Perricone. We sequenced three independent population samples for each stage and Jop Kind's laboratory also performed lamin B1 DamID in mouse ES cell clones expressing Dam and Dam-lamin B1 under the same auxin-inducible conditions as we used in the embryo.

Genomic tracks of OE values for two replicates above each other showed that there is a good correspondence between the population biological replicates (**Figure 12a**). This is further illustrated by a t-distributed neighbour embedding (t-SNE) map

which highlights that the three replicates cluster together based on the stage of embryos used for DamID (**Figure 12b**). The ^{m6}A mark is enriched in broad continuous domains over all autosomes both in zygotes, 2- and 8-cell stage embryos (**Figure 12a**). This pattern is similar to those previously observed in somatic cells with Dam-lamin B1 DamID. The genomic Dam-lamin B1 profiles showed a clearly distinct pattern compared to the Dam-only embryos (**Figure 13a and 13b**). This difference indicates that the detected LAD structure is not a result of biases related to the Dam protein's preference for methylating certain regions but is truly due to specific genome-NL contacts.

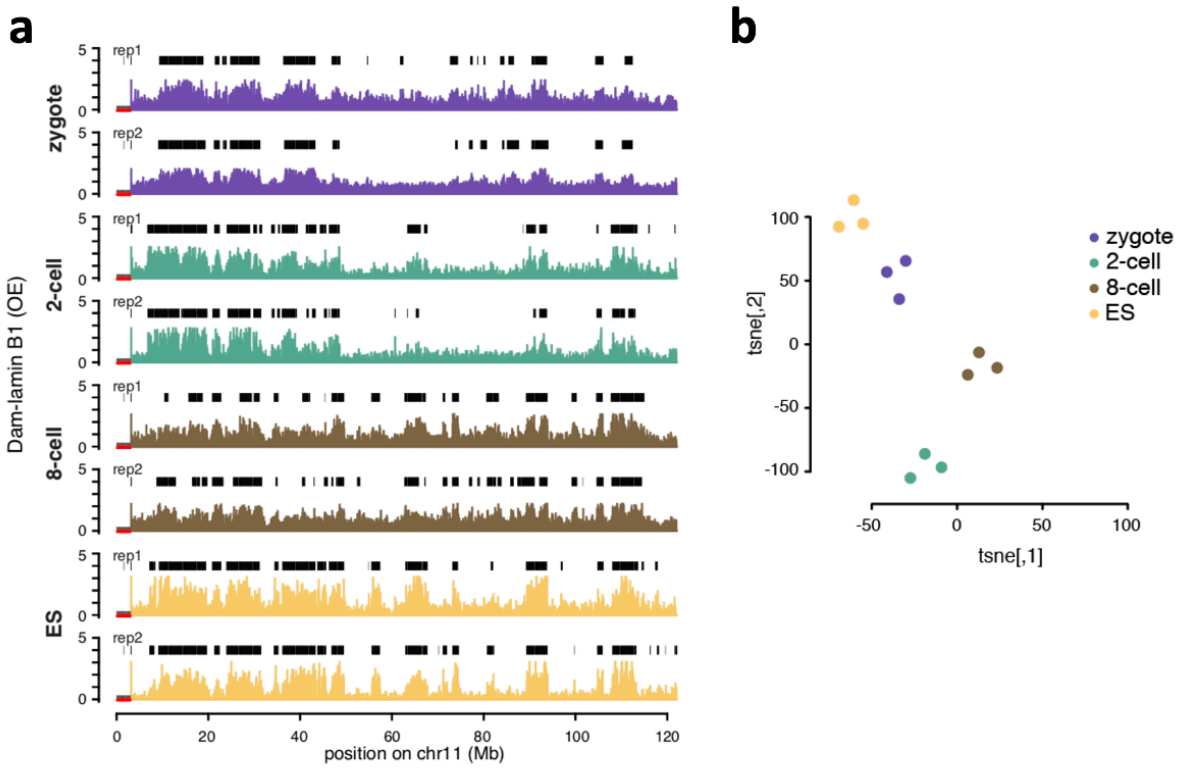

Figure 12. DamID profiles of Dam-lamin B1 injected embryo pools

a) Chromosome plots of two biological replicates for each developmental stage. Peaks represent OE (observed over expected) methylation signal. Black bars above peaks highlight the LAD domains called by Hidden-Markov model (HMM) algorithm. **b)** Clustering of three biological replicates on a t-SNE plot shows clear distinction of samples based on the stage of development.

In order to compare our data to other datasets and between stages we had to binarize the data and divide the genome into categories of LADs and iLADs. We defined LADs using a two-state Hidden-Markov model (HMM) that binarizes the data. As input, we used the average of the three population replicate profiles for each embryonic stage. Genome-NL contacts in preimplantation development occurred in

broad domains with a median size ranging between 1 Mb and 1.9 Mb illustrated by violin plots (**Figure 15b**). Bar plots show that the genomic coverage is rather stable between stages, it ranges between 42% and 62%, reminiscent of LADs of somatic cells (**Figure 15a**). Overall, LADs were present throughout zygotes, 2-cell, 8-cell embryos and ES cells. Interestingly, the 2-cell stage showed more and smaller domains as it is visible on all autosomes in three biological replicates (**Figure 14**).

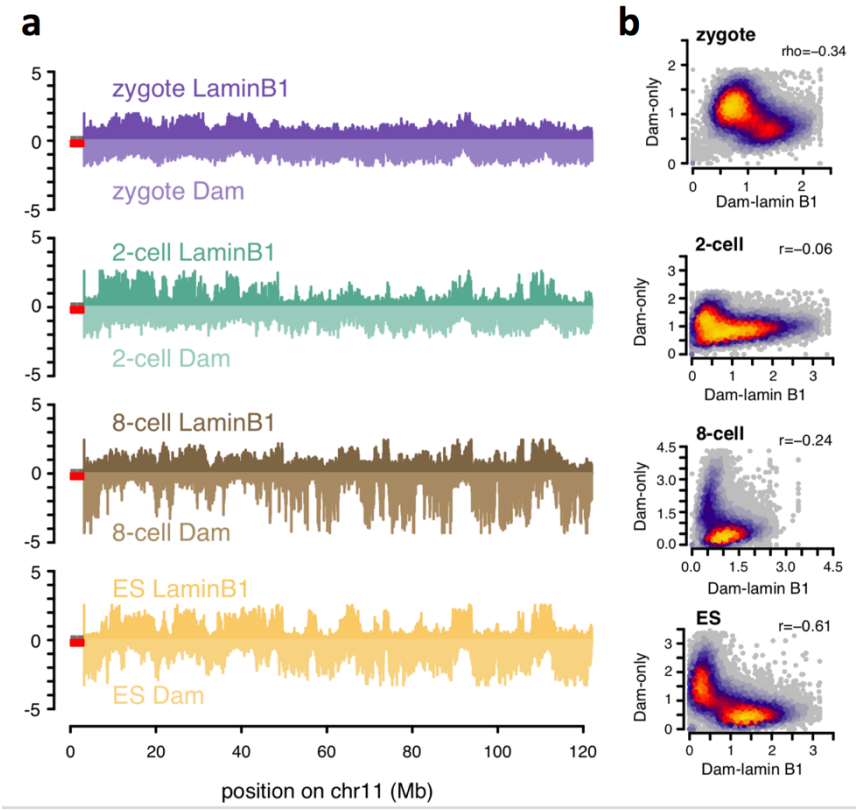

Figure 13. Comparison of Dam-lamin B1 and Dam-only signals in embryos

a) Chromosome plots on top (darker color) show the OE values of Dam-lamin B1 methylation, on the bottom (lighter color) the Dam-only methylation signal is represented. **b)** Scatter plots of OE values from the whole genome show an increasing anti-correlation between Dam-only and Dam-lamin B1 methylated regions as development progresses. Pearson's rho is indicated.

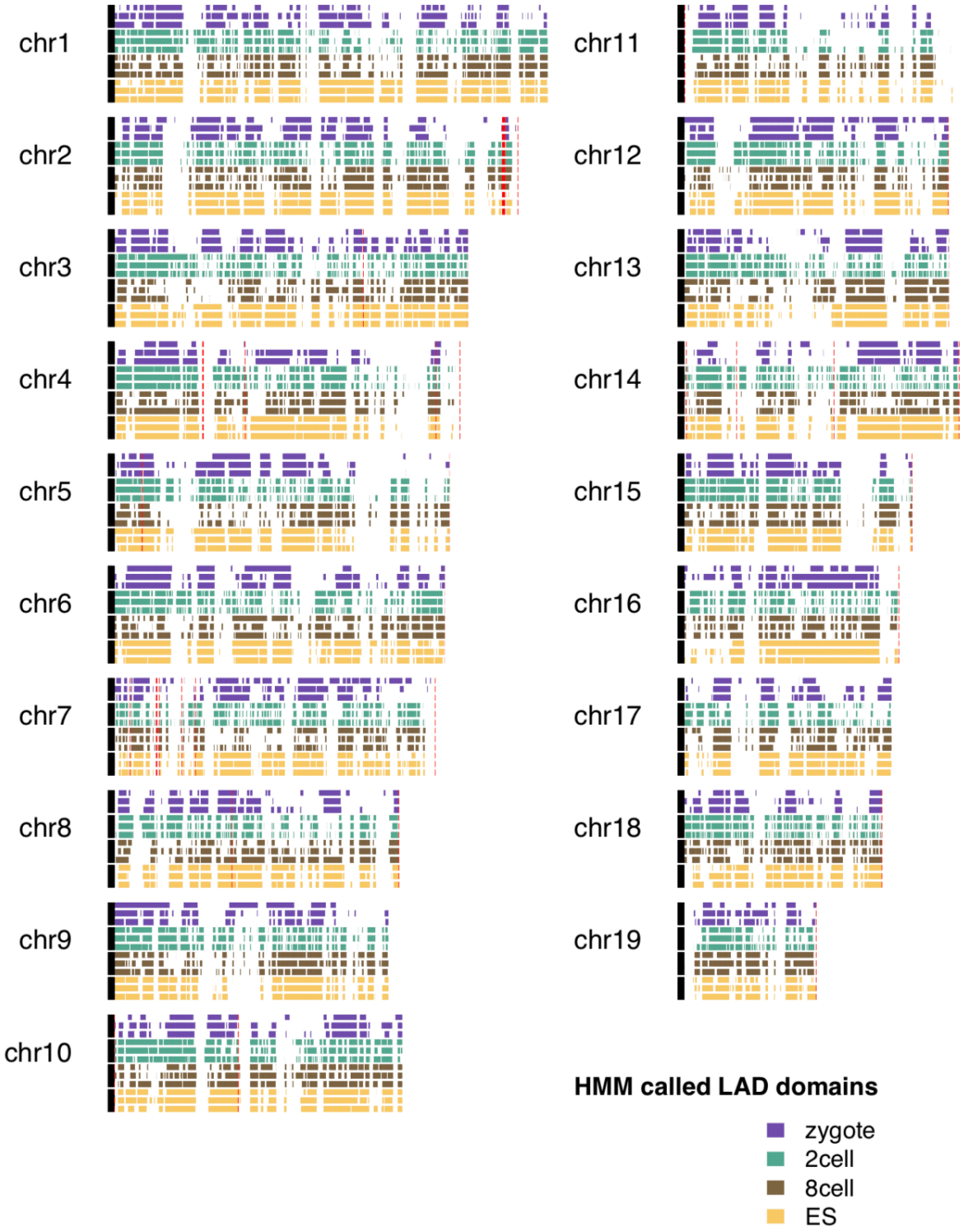

Figure 14. Maps of LADs on all autosomes in three biological replicates

Coloured rectangles represent HMM called LAD domains in three biological replicates in all stages profiled. Black bars on the left indicate centromeres, unmappable regions are highlighted in red color.

Next, we tracked the fate of genomic regions being LADs or iLADs between stages of embryo development. This analysis revealed an extensive reshuffling of regions towards and away from the lamina between stages as shown on an alluvial plot (**Figure 15c**). 42% of the zygotic genome changes NL-positioning at the 2- or 8-cell stage, but 90% of the zygotic LADs that dissociated from the NL in the 2- and 8-cell stages re-associate with the NL in ES cells (**Figure 15c**). The overlap between LADs in zygotes and ES cells is very high (96%), which is further illustrated by the t-SNE map showing close proximity of the zygote data to the ES cell data. This suggests that there is a canonical LAD structure present right after fertilization which is then remodelled at the 2-cell stage and is subsequently consolidated by implantation.

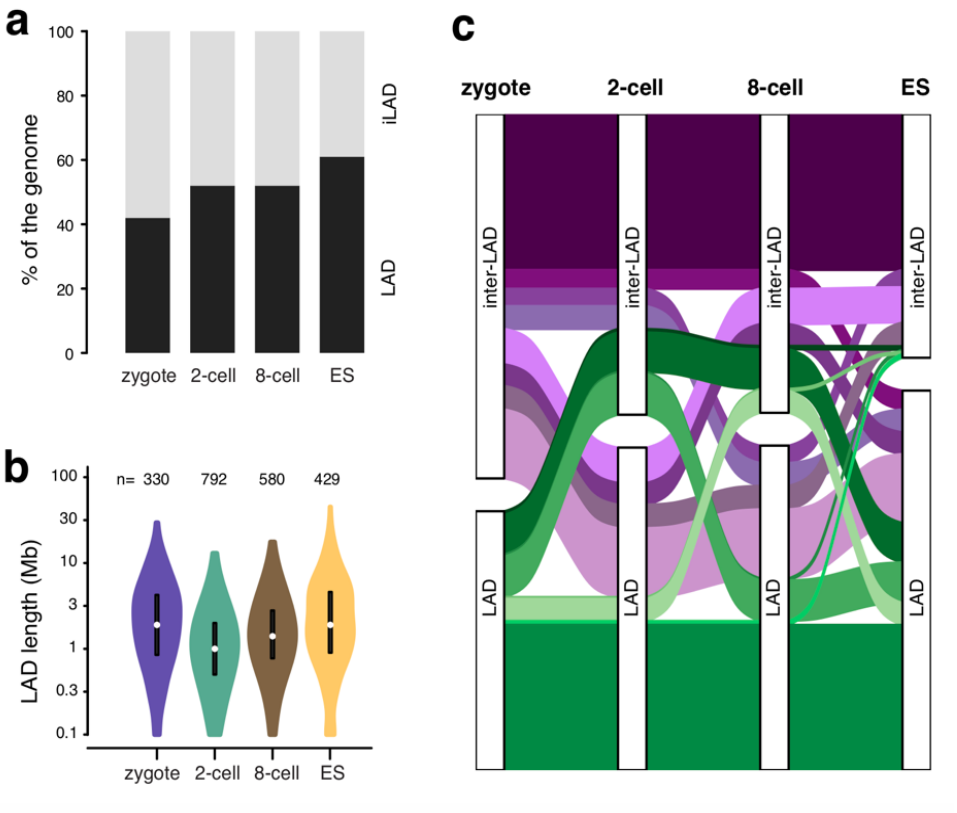

Figure 15. Genomic coverage and rearrangement of LADs in embryos

a) Bar plots showing the percentage of the genome being a LAD (black) across stages. **b)** Violin plots of LAD domain length across the developmental stages profiled, "n=" indicates the number of LADs defined by HMM. **c)** Alluvial plot showing the fate of the entire genome with respect to being on the nuclear periphery (LAD bars) or in the nuclear interior (inter-LAD bars).

Embryonic LADs show similar genomic features to typical LAD

Since genes in LADs are usually lowly transcribed we used public RNAseq data from mouse preimplantation embryos to compare LADs with gene expression (Zhang

et al., 2016) to plot average RPKM values of genes within LADs or within iLADs. This analysis revealed that genes in LADs at the 2- and 8-cell stages are indeed less transcribed compared to genes in iLADs (**Figure 16a**). We did not analyze RNAseq data from zygotes because global transcription is very low at this stage and because the majority of transcripts in zygotes are carried over from the oocyte and thus does not represent active transcription.

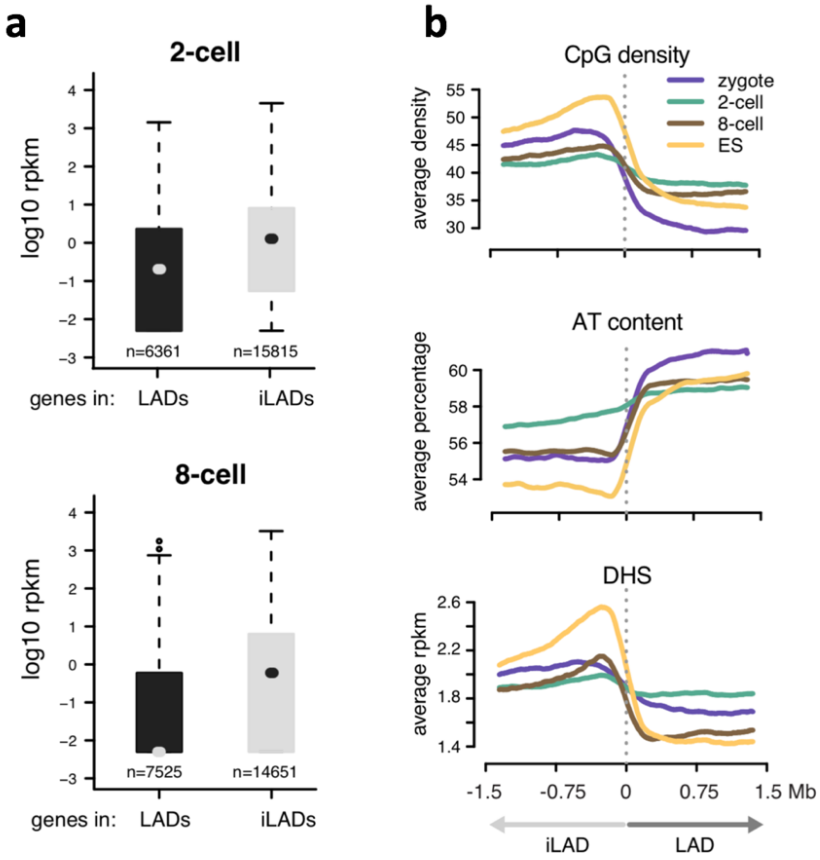

Figure 16. Comparison of RNA expression and genomic features with LADs

a) Boxplots of RNAseq RPKM values (data from *Zhang et al. 2016*) from 2-cell and 8-cell embryos show that genes within LAD regions exhibit lower expression when compared to genes within iLADs. **b)** Cumulative plots over the borders of all LADs (LADs to the left from the center, neighbouring iLADs to the right form the center) show that embryonic LADs exhibit the canonical pattern of low CpG levels and high A/T content. Chromatin accessibility (DHS) is clearly higher outside LADs from the 8-cell stage onwards.

Next, we overlaid genomic features such as CpG density, A/T-content and chromatin accessibility (as determined by DNase hypersensitivity sites – DHS in embryos (Lu et al., 2016)) with our LAD domains. The cumulative plots showed that LADs in the embryo have genomic features comparable to somatic cells, being CpG poor and having an increased A/T-content, although this tendency was less clear at

the 2-cell stage (**Figure 16b**). While 8-cell and ES cell LADs were depleted of open chromatin regions, zygote and 2-cell LADs were more accessible (**Figure 16b**), this is consistent with findings in other papers describing a more open chromatin conformation at the very beginning of development (Lu et al., 2016; Wu et al., 2016a).

Embryonic LADs show low heterogeneity between single cells

There is an increasing intra-embryonic cell-to-cell heterogeneity in mouse preimplantation embryos as development progresses. This heterogeneity in epigenetic states and gene expression levels is linked to cell fate decisions which arise by the blastocyst stage. To address whether genome-NL interactions also display intra-embryonic heterogeneity, we generated Dam-lamin B1 profiles of zygotes, 2- and 8-cell embryos and ES cells at the single-cell level. The population data (15-24 cells) and the average of single-cell Dam-lamin B1 profiles showed a very similar pattern on chromosome plots (**Figure 17a**) which justifies our single cell approach. We used a cut-off score of 1 on the observed over expected (OE) values to generate binary NL-

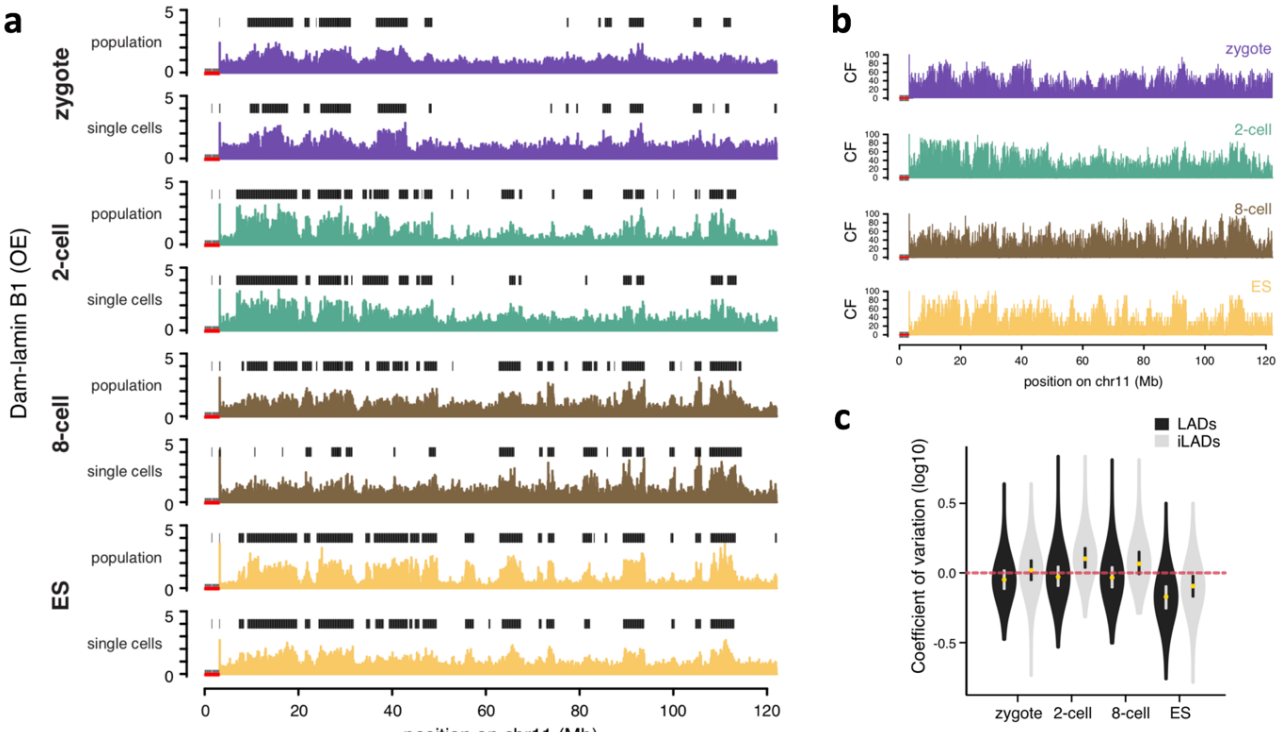

Figure 17. Dam-lamin B1 single cell data correlates well with data from pools of embryos and shows heterogeneity between cells

a) Chromosome plots comparing population and single cell average OE values and HMM called LADs (black boxes) for each developmental stage. **b)** Contact Frequency (CF) scores on an exemplary chromosome for each developmental stage. **c)** Violin plots of coefficient of variation (CV) values for LAD and iLAD regions between stages.

contact maps and calculated contact frequencies (CF). CF values range from zero to 100 and indicate the percentage of single cells showing lamina association for each 100 kb bin. Chromosomal plots of CF values showed that there is a wide range of contact frequencies in genome-NL contacts at all stages (**Figure 17b**). This is indicative of cell-to-cell variability in LADs. However, the comparable coefficients of variation (CV) indicate a similar variability in genome-NL contacts between individual cells of the three embryonic stages (**Figure 17c**). The segmentation of the genome into clear LADs and iLADs was more consistent in the ES cells as indicated by more contrastive chromosome plots of CF values and by the lower CV for LAD and iLADs compared to embryos (**Figure 17b and 17c**).

The orthogonal method of DNA-FISH confirms DamID

To confirm the validity of our findings with a DamID independent method, we turned to 3D mounted DNA fluorescent in situ hybridization (DNA-FISH). Due to the scarce number of embryos available, we optimized the initial protocol used in our laboratory to be able to visualize as many FISH probes simultaneously as possible. Using a white laser confocal microscope and after testing several labelling methods and fluorophores, we could image five different fluorophores from the same embryo.

Additionally, we combined immunofluorescence staining of the nuclear envelope with DNA-FISH enabling to create a reference point of the nuclear periphery. With the help of our image analysis specialist Julien Pontabry, we developed a semi-automated pipeline to analyze the DNA-FISH data. This was challenging, especially for zygotes, where the two pronuclei had to be separated apart, which was done manually. However, it was critical to establish the pipeline, since we performed experiments with more than 25 probes at three different developmental stages acquiring between 50-150 nuclei per stage. Eventually, we measured the 3D distance of DNA-FISH spots to the nuclear periphery (based on the mask of the DAPI signal), normalized by nuclear size.

The 3D distance measurements of the tested LADs and iLADs at the 2- and 8-cell stage indicated that all FISH probes in LADs were in closer proximity to the nuclear periphery than iLADs (**Figure 18a and 18b**). Moreover, for these regions we compared the mean distance of the DNA-FISH signals with the CF scores from single cell DamID. The resulting scatter plots showed a high positive correlation between these two orthogonal methods (**Figure 18c**).

Also, we categorized FISH spots manually as “overlapping” or “not-overlapping” the nuclear lamina based on their co-localization with the nuclear envelope staining (**Figure 19a**). Both of these analysis methods show similar results, confirming a preference of LADs being at the nuclear periphery as opposed to iLADs.

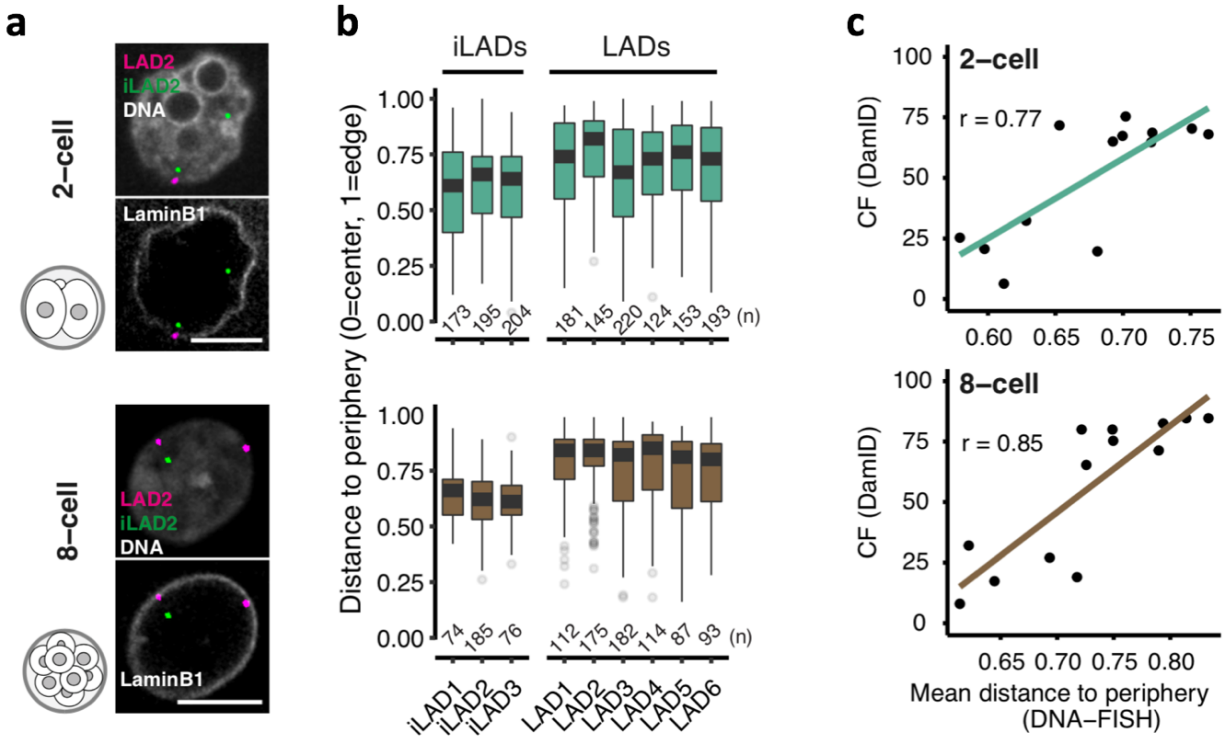

Figure 18. DNA-FISH on LADs and iLADs confirms the validity of our DamID data

a) Exemplary images of 2-cell and 8-cell embryonic nuclei with DNA-FISH spots for a selected LAD and iLAD probe. Upper panels show overlay with DNA (DAPI), lower panels show the overlay with the nuclear envelope (nucleoporin staining). Scale bar represents 5 µm. **b)** Quantification of 3D distance measurements of all tested LAD and iLAD probes normalized with nuclear size. A value of 1 represents complete peripheral localization, 0 represents central positioning. The number of FISH spots quantified are indicated as (n) numbers. **c)** Scatter plots show a clear correlation between the DNA-FISH distance measurements and the CF values obtained from the single cell DamID data, Pearson’s rho is indicated.

In addition, we selected LADs that relocated towards or away from the nuclear periphery while the embryos transit from the 2-cell to the 8-cell stage (“changing LADs”) (**Figure 19b**). We named those regions that dissociate from the lamina from 2- to 8-cell stage “disLADs”, and those that newly move to the lamina from 2- to 8-cell stage “newLADs”. DNA-FISH distance measurements indicated that these selected changing LADs indeed relocate between the 2- and 8-cell stage, as predicted by

DamID (**Figure 19c**). This further reassured the validity of our findings from sequencing data.

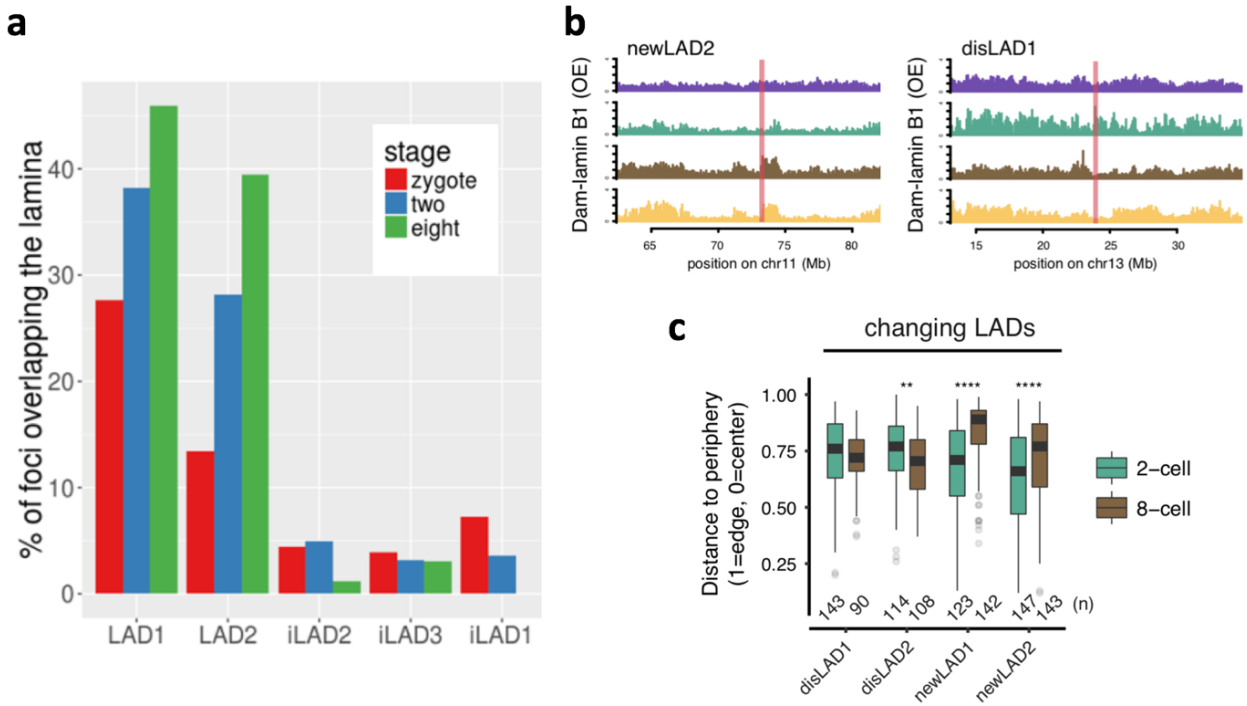

Figure 19. Manual quantification of DNA-FISH and changing LADs

a) Bar plots show the percentage of FISH spots overlapping the nuclear envelope staining as judged by manual scoring (for each stage and each probe between 30 to 50 FISH spots were quantified.. **b)** Exemplary chromosome plots of DamID OE values with the location of changing LAD probes (red bars). **c)** 3D distance quantification of four changing LADs at the 2- and 8-cell stages. “disLADs” move away from the NL by the 8-cell stage, “newLADs” move towards the NL by the 8-cell stage as predicted by DamID.

Extensive differences in LADs exist between the parental alleles

In order to obtain information specifically on maternal versus paternal alleles (particularly important at zygote stage, where the two parental genomes are in distinct pronuclei) we had to perform DamID on embryos from hybrid crosses between CAST (paternal) and CBAxC57Bl6 (maternal) mice. This was a major challenge, since such crosses yielded ~ 25-fold less embryos then normal crosses, thus severely extending the time spent on injections and embryo collection. Nevertheless, we obtained sequencing data and we split the reads based on the single nucleotide polymorphisms (SNPs) and allocated them either to the paternal or maternal alleles.

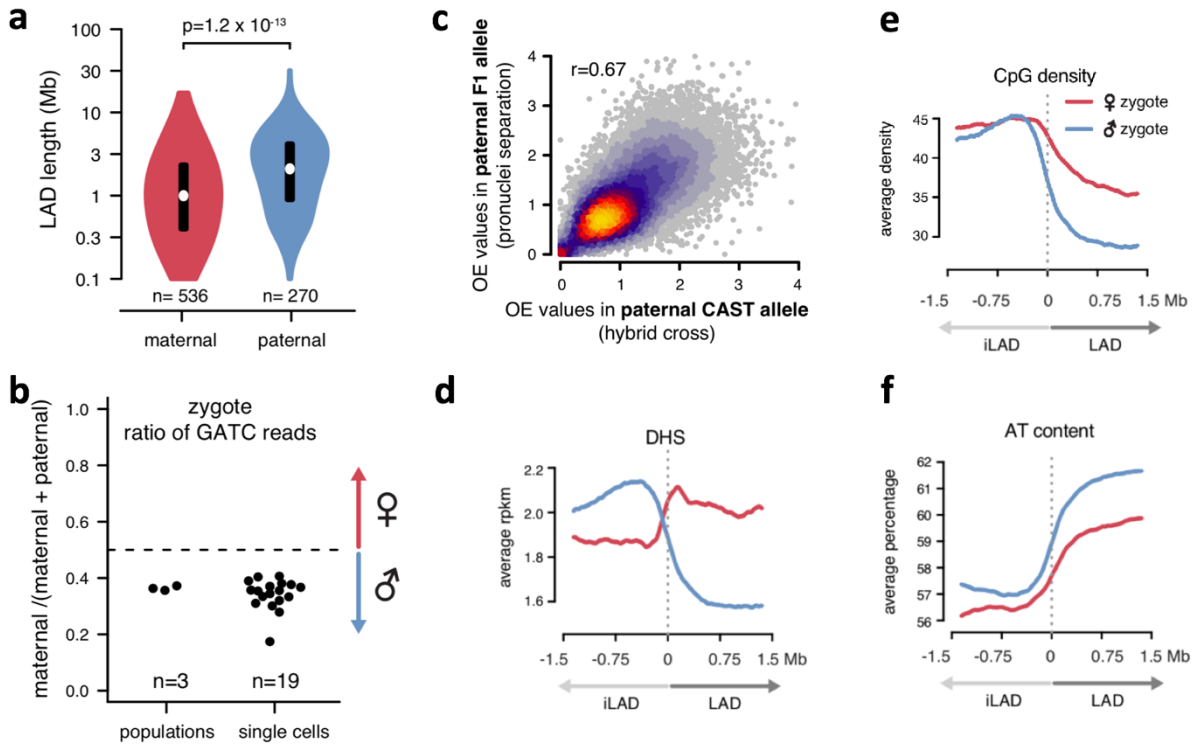

Figure 20. Allelic differences of LAD structure in zygotes

a) Violin plots of LAD domain length in maternal and paternal pronuclei show larger and fewer LADs on the paternal allele. The number of LADs is indicated as (n=). **b)** The ratio of the total number of GATC reads show an allelic bias in zygote population Dam-lamin B1 samples. **c)** Scatter plot of the paternal OE values obtained from hybrid crosses versus from non-hybrid crosses in which the pronuclei were mechanically separated. Pearson's rho is indicated. **d)** Cumulative plot of chromatin accessibility (DHS signal) shows a difference in the maternal versus paternal pronuclei. **e)** Cumulative plot of CpG density shows a reduction of CpG content in LADs on both zygotic alleles, to less extent on the maternal allele. **f)** Cumulative plot of A/T content shows an enrichment of A/T content in LADs on both zygotic alleles, to less extent on the maternal allele.

This analysis revealed that while both parental genomes display specific genome-NL interactions in the zygote, the paternal genome appears to be more defined with fewer and broader domains compared to the more fragmented patterns

observed in the maternal zygotic genome (**Figure 20a**). Moreover, we systematically detected fewer genome-NL contacts in the maternal genome as compared to the paternal genome in the zygote (**Figure 20b**). Whether these differences were due to strain specificity or truly due to the different germline history of the alleles we used physically separated pronuclei from the same strain in a second experiment which confirmed that our results are not due to the strain but they are truly allele specific differences (**Figure 20c**). Despite the less structured appearance of the maternal LAD-organisation, the regions that do contact the NL in both paternal and maternal pronuclei by DamID (not allele specific LADs) are positioned with similar average distances to the nuclear periphery measured by DNA-FISH (**Figure 21**).

The genomic features associated with the paternal and maternal genome-NL regions differed substantially. Paternal zygotic LADs are associated with all the features typical for LADs (CpG poor, A/T rich, compact chromatin), whereas maternal LADs are less enriched for LAD-features and even contain regions with increased

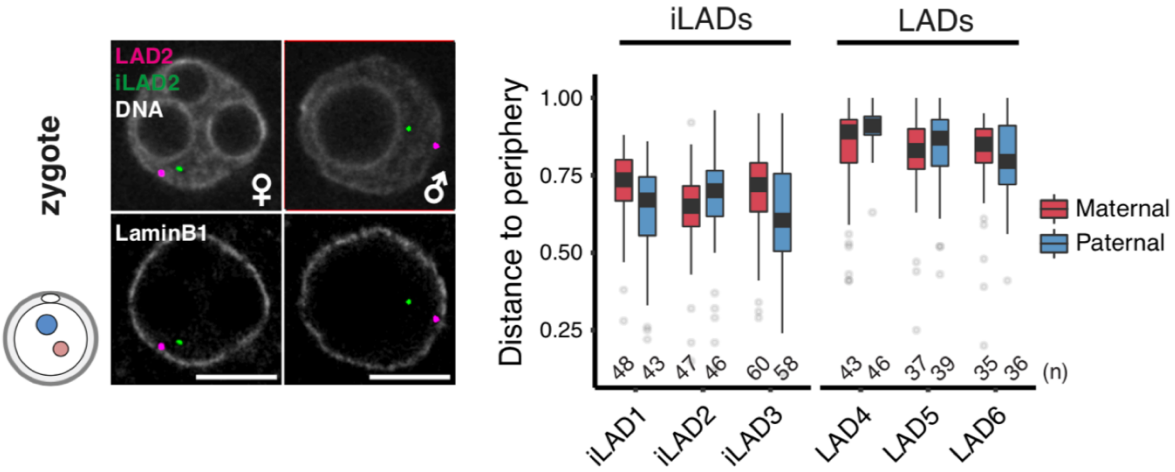

Figure 21. DNA-FISH on zygotes

a) Exemplary images of zygote pronuclei with DNA-FISH spots for a selected LAD and iLAD probe. Upper panels show overlay with DNA (DAPI), lower panels show the overlay with the nuclear envelope (nucleoporin staining). Scale bar represents 5 µm. **b)** Quantification of 3D distance measurements normalized with nuclear size. A value of 1 represents complete peripheral localization, 0 represents central positioning, number of FISH spots quantified are indicated as (n) numbers.

DNaseI hypersensitivity (**Figure 20d, 20e and 20f**). From the 2-cell stage onwards the genomic features are similar and canonical between LADs of both alleles.

At later stages the chromosomal plots still show differences between alleles but these differences are equalized by the ES cell stage (**Figure 22a**). An allele specific t-SNE map confirms that these differences exist at the 2- and 8-cell stages (**Figure 22b**),

albeit to a much less pronounced extent than in the zygote. Again, the results are not due to strain specific differences since our data from embryos derived from reciprocal hybrid crosses (CAST-maternal and CBAxC57Bl6-paternal) at the 2-cell stage positively correlates (Pearson's r=0.64) with data from embryos of "normal" crosses (CAST-paternal and CBAxC57Bl6-maternal) (**Figure 22c**).

LAD establishment precedes TAD maturation

Recent work suggests that TADs are largely absent in zygotes and gradually consolidate to form "mature" TADs only at later cleavage stages around the 8-cell stage (Du et al., 2017; Ke et al., 2017). The interdependence between TADs and LADs has not been addressed neither in embryos nor in somatic cells so far. To investigate the interdependency between spatial genome organisation and the establishment of

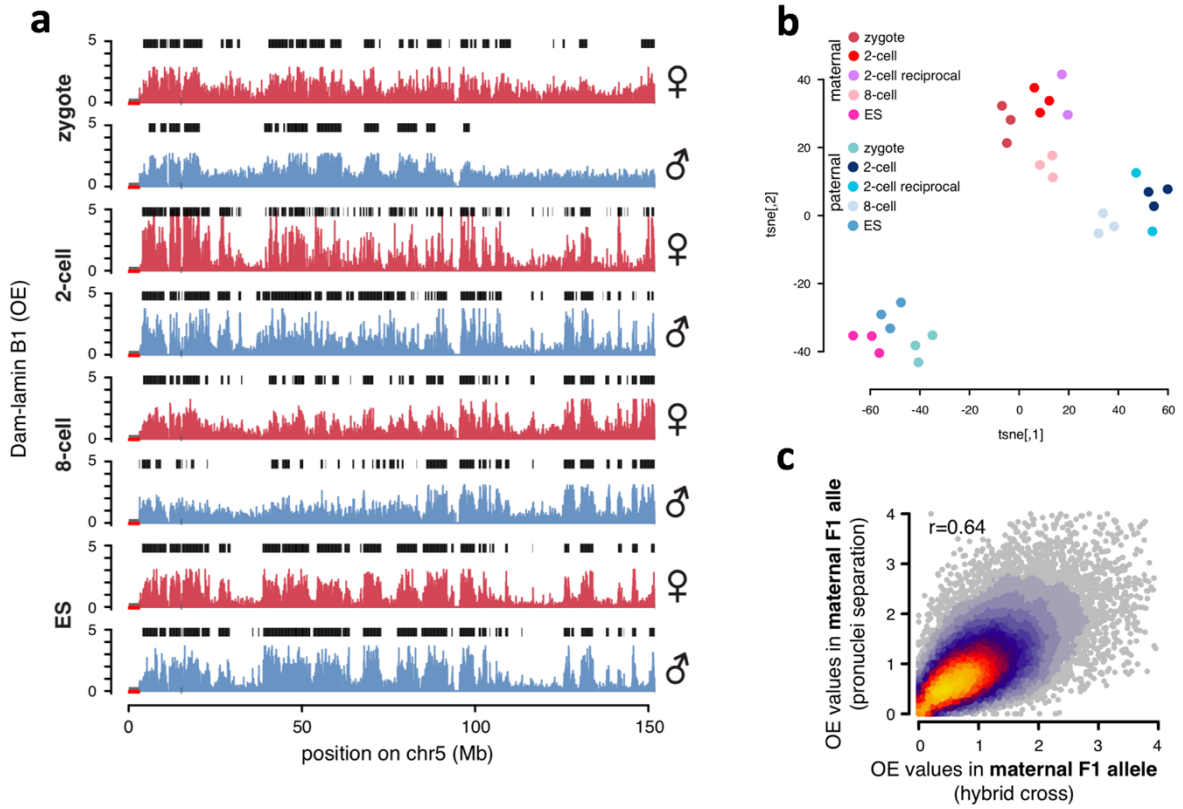

Figure 22. Allelic differences in LADs at all stages

a) Chromosome plots showing maternal and paternal OE values and HMM called LADs (black boxes) for each developmental stage. **b)** Clustering on a t-SNE plot of allelic OE values, including reciprocal crosses from the 2-cell stage. **c)** Scatter plot comparing OE values of the maternal allele in the 2-cell stage from normal (CAST-paternal and CBAxC57Bl6-maternal) and reciprocal (CAST-maternal and CBAxC57Bl6-paternal) crosses.

chromatin topology, we analysed published HiC data (Du et al., 2017). We calculated the insulation scores in the zygote, 2- and 8-cell stages at TAD boundaries defined in ES cells. As shown previously, TAD-boundaries become progressively insulated as development proceeds (**Figure 23a**).

In contrast, when we projected OE values from Dam-lamin B1 DamID on LAD boundaries (defined by HMM domain calling) per stage, we observed that LADs are already clearly defined as early as in zygotes and are stably present throughout all stages (**Figure 23b**). These findings suggest that the presence of LADs may precede the establishment of TADs.

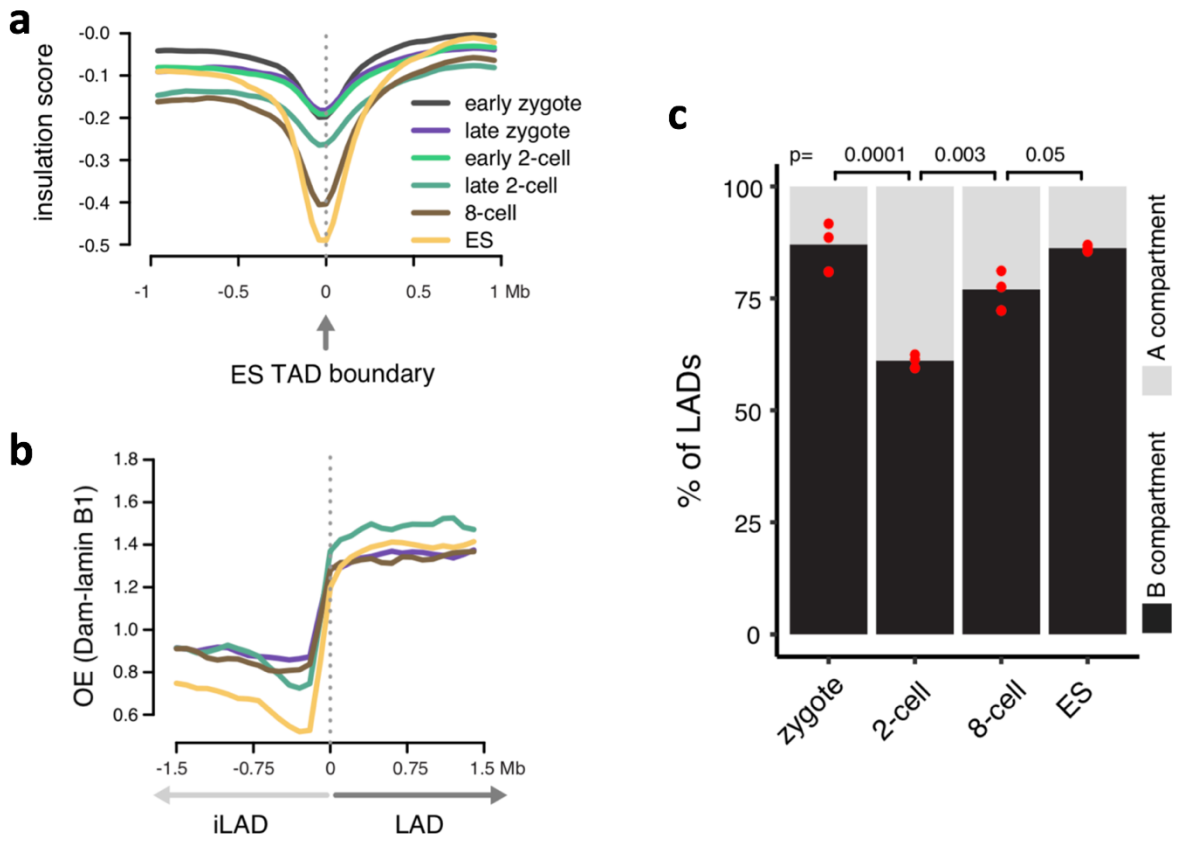

Figure 23. Comparison of TAD and LAD establishment dynamics and the overlap between compartments and LADs

a) Cumulative plot of insulation scores from HiC plotted over ES cell TAD boundaries indicates the gradual maturation of TAD boundaries with development (data form *Du et al. 2017*). **b)** The cumulative plot of OE scores from Dam-lamin B1 DamID plotted over LAD boundaries indicate that LADs are clearly present as early as in zygotes. **c)** Bar plot showing the percentage of LADs overlapping A (grey) or B (black) compartments as determined in embryo HiC datasets (data form *Du et al. 2017*). Bars represent the mean of three biological replicates of DamID experiments each replicated indicated by red dots, p-values were obtained with a post-hoc Tukey-test.

Unlike mature TADs, A and B compartments can be observed as early as the zygotic stage, however with higher compartment strength in the paternal genome (Flyamer et al., 2017). Since LADs are usually coinciding with B compartments in somatic cells (Bickmore and van Steensel, 2013), next we compared embryo LADs with embryo compartments. The majority of LADs overlapped with B compartments in zygotes, 8-cell embryos and ES cells (87%, 77% and 86%, respectively) (**Figure 23c**). Notably, however, there was a significant portion of LADs in the 2-cell embryos, that coincided with A compartments (39%) (**Figure 23c**).

This unexpected change in compartmentalisation at the 2-cell stage prompted us to investigate whether LADs precede B compartments or whether B compartments precede LADs. We determined compartments scores in regions showing different patterns of LAD dynamics. Regions that were iLADs throughout early development were persistently in A compartments, while constant LAD regions were invariably in B compartments (**Figure 24**). This suggests that for approximately half of the genome,

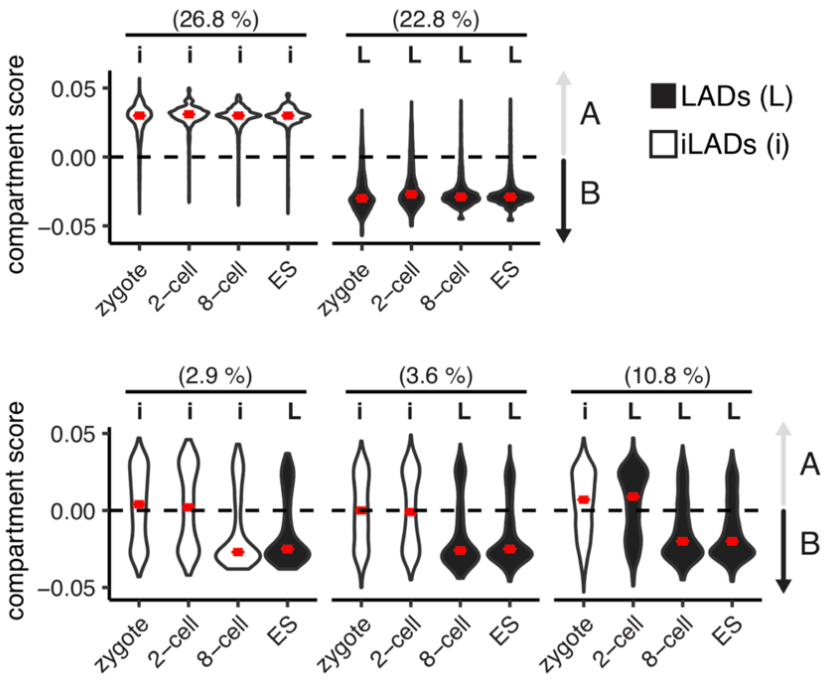

Figure 24. Compartment scores in LADs with different developmental dynamics

Violin plots of compartment scores (negative – B compartment, positive – A compartment). The percentage above LAD categories represent the percentage of the genome these regions occupy. The letters "i" above stages of development indicate iLAD position (white filled violins), "L" indicates LAD position of the regions (black filled violins). The top two panels are constant LADs or iLADs in all stages. The bottom three categories are *de novo* forming LADs at different times of development.

LAD and compartment formation occur simultaneously. In contrast, for LADs that form *de novo* at the 2-cell stage and remain LADs through to the 8-cell stage and in ES cells (10.8% of the genome), LAD formation preceded the establishment of B compartments (**Figure 24**). However, the alternative scenarios also exist: (i) *de novo* LADs at the 8-cell stage coincide with the formation of B compartments (3.6% of the genome) and (ii) iLADs that become LADs in ES cells (2.9% of the genome) are within B compartments already in 8-cell embryos (**Figure 24**).

Inhibiting DNA replication shows no effect on LAD maintenance at the 2-cell stage

Previously, it has been reported that inhibiting replication perturbs LAD formation in somatic cells (Shachar et al., 2015). Also, in embryos TAD consolidation is prevented by blocking DNA replication with aphidicolin (Ke et al., 2017). In the HiC embryo paper reporting the dependence of TAD formation on replication, the authors did not analyze their data to check if A/B compartments are affected by aphidicolin. Thus, we reanalyzed their HiC data and observed that A/B compartments do not change upon the inhibition of replication at the 2-cell stage (**Figure 25a and 25c**). To

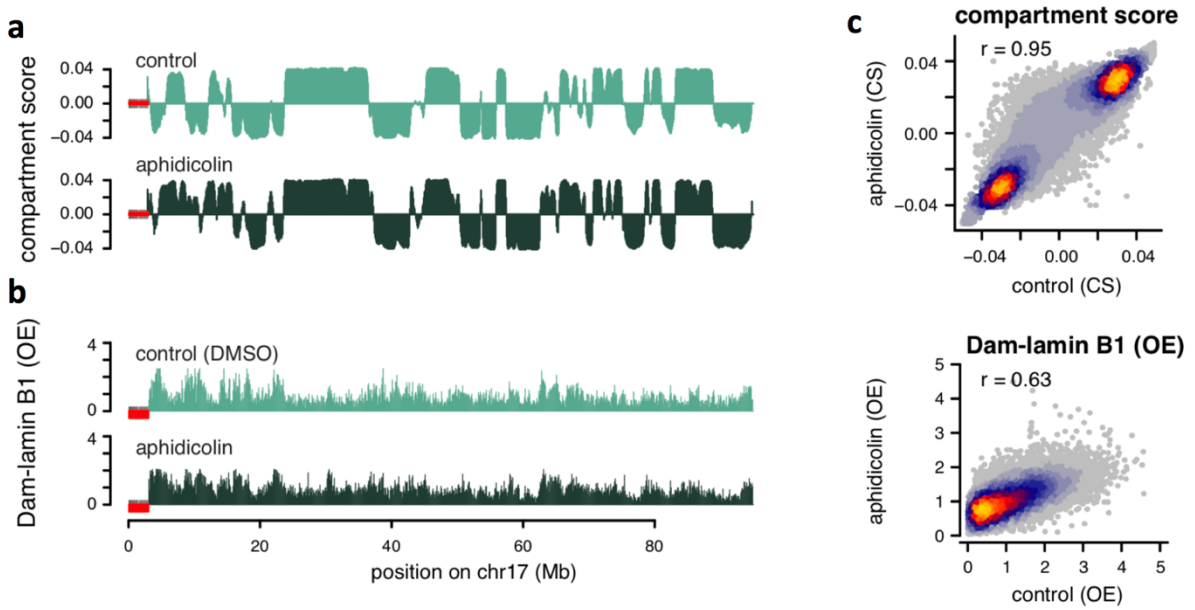

Figure 25. Inhibition of DNA replication at the 2-cell stage neither perturbs compartment formation nor LAD formation

a) Chromosome plots of compartment scores (HiC data from *Ke et al. 2017*) in control and aphidicolin treated 2-cell stage embryos. **b)** Chromosome plots of OE values (lamin B1 DamID data) in control and aphidicolin treated 2-cell stage embryos. **c)** Scatter plots of genome wide compartment scores and OE values comparing control and aphidicolin treated 2-cell stage embryos, Pearson's rho is indicated.

check whether LAD maintenance at the 2-cell stage is also affected by treatment with a DNA polymerase inhibitor, we treated late zygotes undergoing mitosis with aphidicolin or DMSO as control and let them develop to the late 2-cell stage followed by DamID. Similarly to compartments, LADs remained globally unaffected after aphidicolin treatment, although the LAD patterning appeared less distinctive as in controls (**Figure 25b and 25c**).

Reducing H3K4me3 but not H3K9me3 affects paternal LAD establishment in zygotes

We aimed to investigate the role of histone modifications in the potential mechanisms of LAD formation. When we correlated our LAD domains with public ChIP-seq data we found that the levels of H3K4me3 projected on LAD boundaries showed that LADs and iLADs are progressively demarcated by differential H3K4me3 levels (H3K4me3 being on iLADs and excluded from LADs) as development proceeds (**Figure 26a**). Yet, between the maternal and paternal genomes in the zygote, only the paternal genome displayed a clear canonical profile of H3K4me3 being excluded form LADs (**Figure 26b**). On the other hand, the maternal genome showed an uncanonical enrichment of H3K4me3 in LADs of zygotes. No preferred localization of H3K4me3 was observed at the 2-cell stage and the conventional H3K4me3 devoid LAD pattern was apparent only from the 8-cell stage onwards on the maternal allele (**Figure 26c**).

To address directly if H3K4me3 plays a role in LAD establishment, we aimed to experimentally modify the levels of H3K4me3. To do so, we injected mRNA coding for the mouse H3K4me3 demethylase Kdm5b into zygotes. As a negative control, we used the catalytic inactive mutant (H499A) of Kdm5b in our experiments. We tested the effects of overexpression by IF staining of the H3K4me3 mark. Wild-type Kdm5b expression led to a clear reduction of H3K4me3 levels in both pronuclei compared to non-injected embryos or compared to embryos expressing the catalytically inactive Kdm5b mutant (**Figure 26e**). When we quantified the immunofluorescent staining signal, we observed a clear statistically significant reduction of H3K4me3 in both pronuclei upon WT Kdm5b injection (**Figure 26f**).

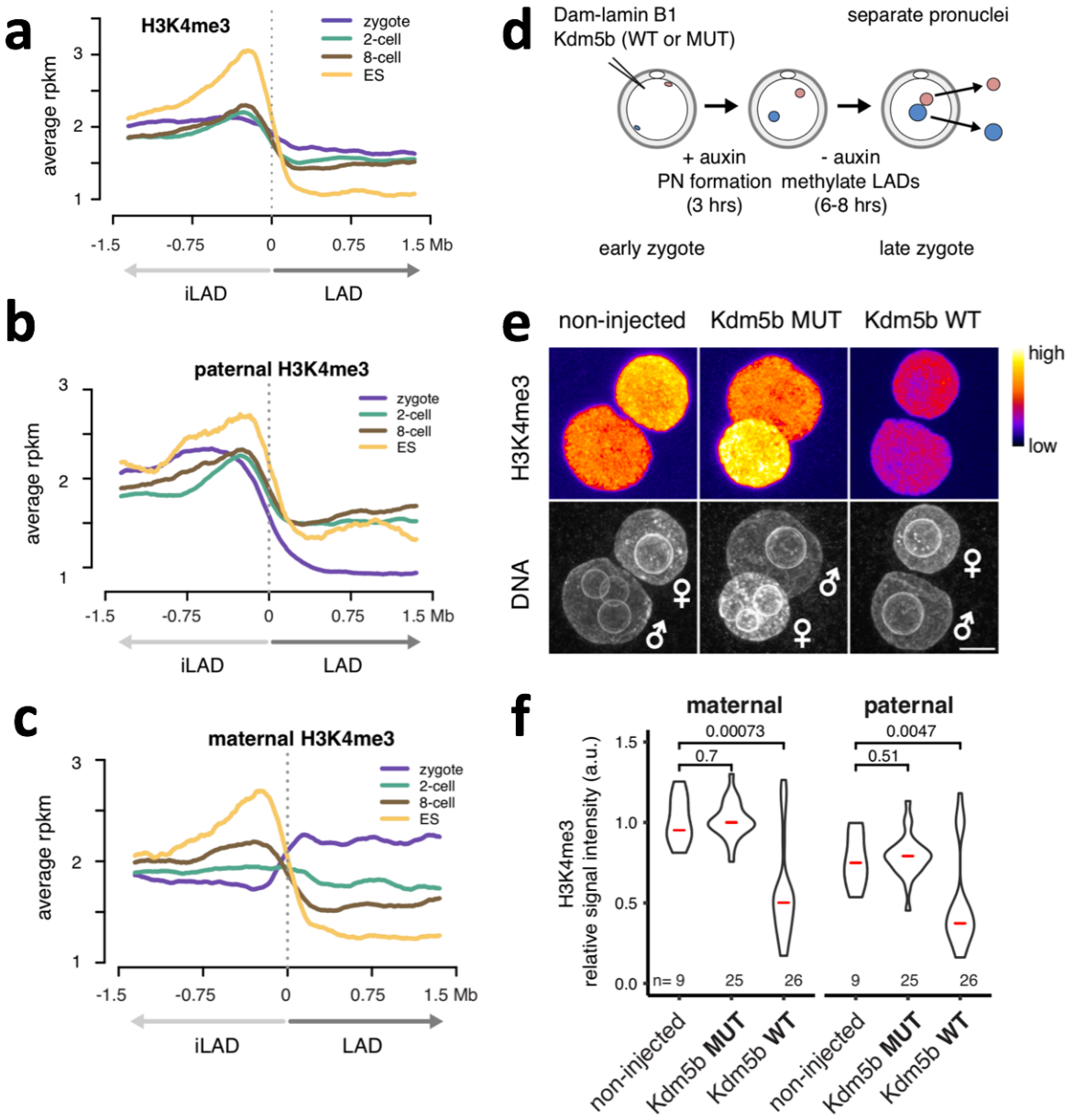

Figure 26. H3K4me3 is mostly reduced in LADs and its levels can be modulated by the overexpression of Kdm5b

a) Cumulative plots showing reduced H3K4me3 levels (ChIP-seq data from *Zhang et al 2016*) in embryonic LADs when the parental alleles are not distinguished. **b)** Cumulative plots of the paternal genome show a reduction in H3K4me3 in LADs at all stages. **c)** Cumulative plots of the maternal genome show a dynamic reorganization of H3K4me3 with respect to LADs as development progresses. **d)** Experimental strategy to reduce H3K4me3 levels and perform DamID on these embryos. **e)** Immunofluorescent staining of H3K4me3 in non-injected, wild-type (WT) or mutant (MUT) Kdm5b injected zygotes. Scale bars represent 10 µm. **f)** Quantification of the immunofluorescent staining from panel e). p-values are a result of a Wilcoxon-test. The number of embryos indicated as (n=).

To test the effect of H3K4me3 reduction on LAD formation, we injected early-zygotes right after fertilization with a mix of WT or MUT Kdm5b and Dam-lamin B1. It was critical to inject early-zygotes to allow enough time for Kdm5b to exert its demethylating effect. However, pronuclei are not yet formed in early zygotes and we wanted to avoid having the Dam-lamin B1 protein present before pronucleus formation to avoid methylation artefacts arising by free Dam-lamin B1 contacting DNA. Therefore, we kept the embryos in IAA until pronucleus formation to have only Dam-lamin B1 mRNA but not protein present along with Kdm5b protein before pronucleus formation. Afterwards, we washed the embryos out of IAA to allow for the presence of the Dam-lamin B1 protein as well (**Figure 26d**). At the late-zygote stage, we physically separated the maternal and paternal pronuclei into different tubes – this was necessary to distinguish the alleles because at that time we had no hybrid embryos available.

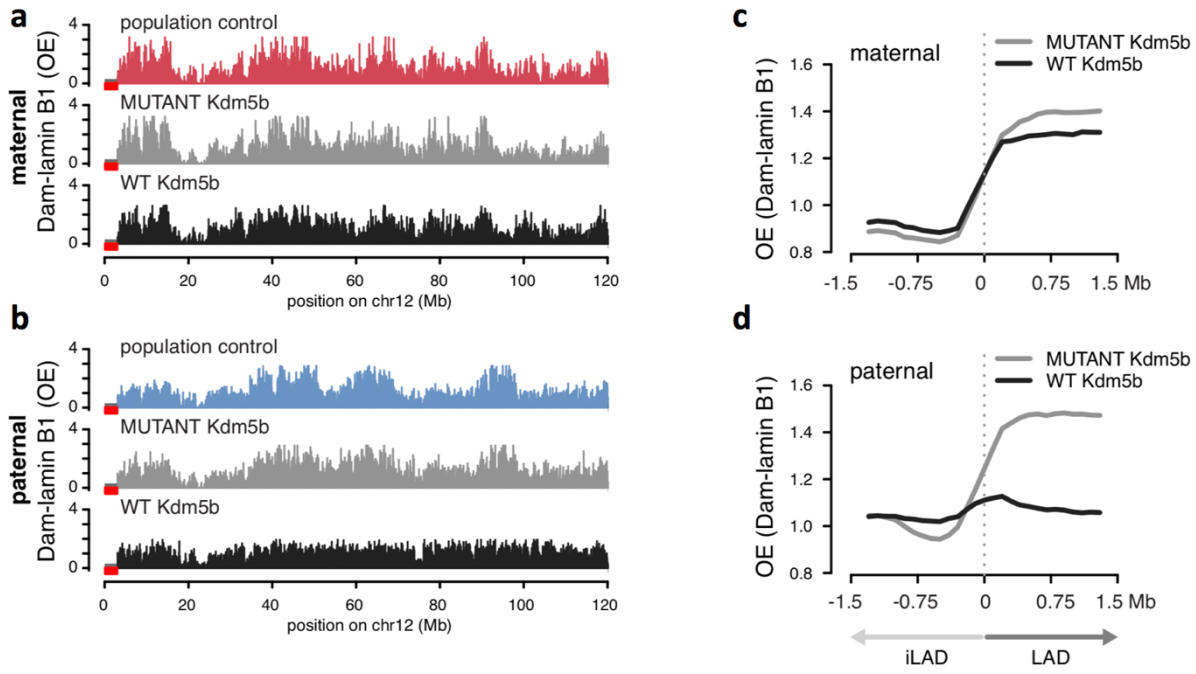

Figure 27. Depletion of H3K4me3 results in paternal specific loss of LAD structure in zygotes

a) Chromosome plot of the maternal pronucleus showing no change in LAD structure in Kdm5b MUT or WT injected embryos. **b)** Chromosome plot of the paternal pronucleus showing a loss of LAD patterning specifically in the Kdm5b WT injected embryos. **c)** Cumulative plots of the maternal OE values over genome-wide LAD borders defined in non-injected embryos showing no change upon Kdm5b injection. **d)** Cumulative plots of the paternal OE values over genome-wide LAD borders defined in non-injected embryos showing a specific change upon WT Kdm5b injection.

Remarkably, the ectopic expression of the wild-type Kdm5b, but not the catalytically inactive mutant, resulted in the complete erasure of LAD structure in the paternal genome, and had little or no effect on the pattern of maternal genome-NL interactions as shown on selected chromosome plots of OE values (**Figure 27a, 27b**). Moreover, using cumulative analysis of the whole autosomal genome has also shown that LAD regions defined in non Kdm5b manipulated zygotes show a loss of OE values (i.e. no NL interaction) in zygotes which have reduced H3K4me3 but only in the paternal allele (**Figure 27c, 27d**). These results suggest that H3K4me3 in the paternal pronucleus underlies the establishment of genome-NL interactions.

Importantly, we checked if the loss of LAD structure upon H3K4me3 reduction is a result a perturbed nuclear lamina formation in zygotes. Immunofluorescent staining of endogenous lamin B1 after mutant or wild-type Kdm5b injection showed proper NL formation and with unaffected protein, thus levels excluding this possibility (**Figure 28a**). Moreover, we were concerned whether the ectopic Kdm5b overexpression also modifies other histone methylation marks. Since H3K9me2 and H3K9me3 are enriched on LADs in somatic cells, we checked by immunofluorescence if the levels of these two repressive heterochromatin marks are perturbed in Kdm5b injected zygotes. The quantification and exemplary images of these experiments show that Kdm5b is specific to H3K4me3, it does not affect the methylation of H3K9 (**Figure 28c and 28d**).

Since H3K4me3 is an activating histone mark involved in transcription, we checked whether upon Kdm5b injection global RNA transcription is perturbed. We incubated mutant or wild-type Kdm5b injected zygotes in 5-ethynyl uridine (EU) and detected the incorporated nucleotides with click-chemistry. Global transcription levels did not change significantly in H3K4me3 reduced zygotes (**Figure 28b**), arguing that the effect of reducing this histone mark might not act upon LAD formation in a transcription dependent manner.

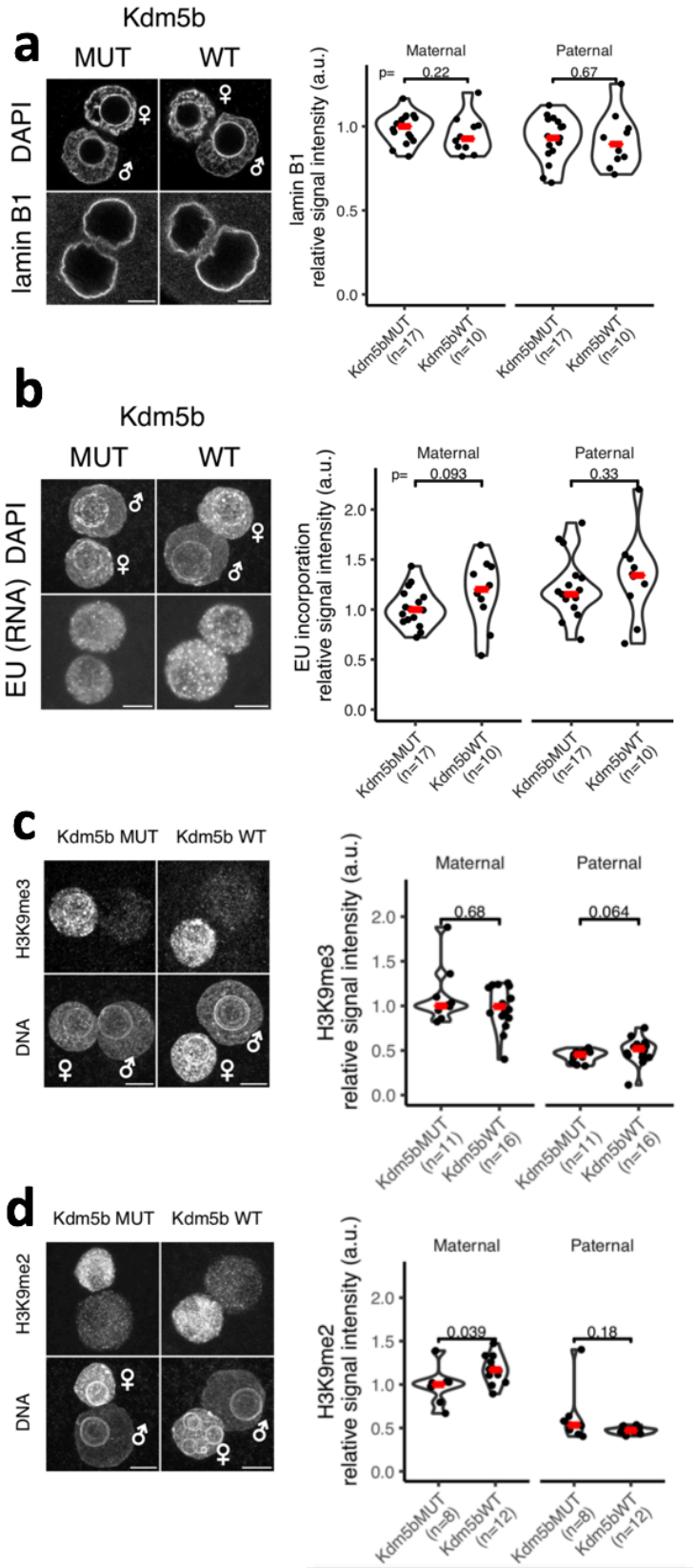

Figure 28. Reduction of H3K4me3 by Kdm5b overexpression does not affect lamin B1 localization, global transcription and neither H3K9me2 nor H3K9me3

a) Immunofluorescent staining of endogenous lamin B1 in MUT and WT Kdm5b injected embryos, violin plots show the quantified levels of lamin B1. **b)** Fluorescent visualization of global transcription after EU pulse in MUT and WT Kdm5b injected embryos, violin plots show the quantified levels of total RNA incorporation. **c)** Immunofluorescent staining of H3K9me2 in MUT and WT Kdm5b injected embryos, violin plots show the quantified levels of H3K9me2. **d)** Immunofluorescent staining of H3K9me3 in MUT and WT Kdm5b injected embryos, violin plots show the quantified levels of H3K9me3. Scale bar represents 10 µm.

It remained a question whether the H3K4 methylation responsible for paternal LAD formation is inherited already from the sperm or is established *de novo* upon fertilization. To this end, we analyzed public ChIP-seq data of H3K4me3 from sperm, early- and late-zygotes (Zhang et al., 2016). Both chromosome plots and a cumulative analysis of the entire autosomal genome revealed that regions that become LADs in the paternal pronucleus by the late zygote stage do are not demarcated by H3K4me3 in the sperm but become flanked by H3K4me3 in the early zygote (**Figure 29**). This data argues that it is *de novo* H3K4me3 deposition upon fertilization that is important for paternal LAD formation in the zygote.

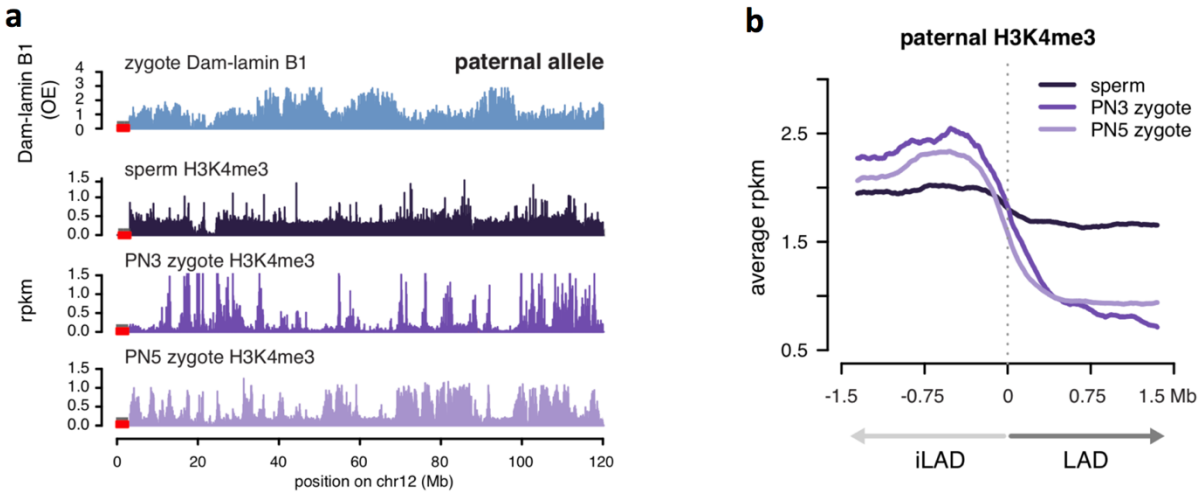

Figure 29. Paternal H3K4me3 is established de novo outside of LADs upon fertilization

a) Chromosome plot of paternal OE values from Dam-lamin B1 DamID (top in blue) and the paternal H3K4me3 ChIP-seq signal in sperm, early-zygotes and late-zygotes (shades of purple). **b)** Cumulative plots of the paternal H3K4me3 ChIP-seq signal over genome-wide LAD borders on the paternal allele. (ChIP-seq data from *Zhang et al 2016*)

To test the potential contribution of H3K9me3 to LAD formation in the zygote, we performed the overexpression of an H3K9me3 specific demethylase (Kdm4d) in a with the same experimental design as done for H3K4me3 with Kdm5b. Immunofluorescence staining of H3K9me3 in WT and MUT Kdm4d injected zygotes revealed that H3K9me3 is significantly depleted in both pronuclei upon WT but not upon MUT Kdm4d overexpression (**Figure 30**). When we performed DamID on zygotes injected with Kdm4d, we observed no change in genome-wide LAD patterning neither in MUT nor in WT injected zygotes. Therefore, it occurs that the heterochromatic H3K9me3 mark does not play a role in zygotic LAD formation contrary to H3K4me3.

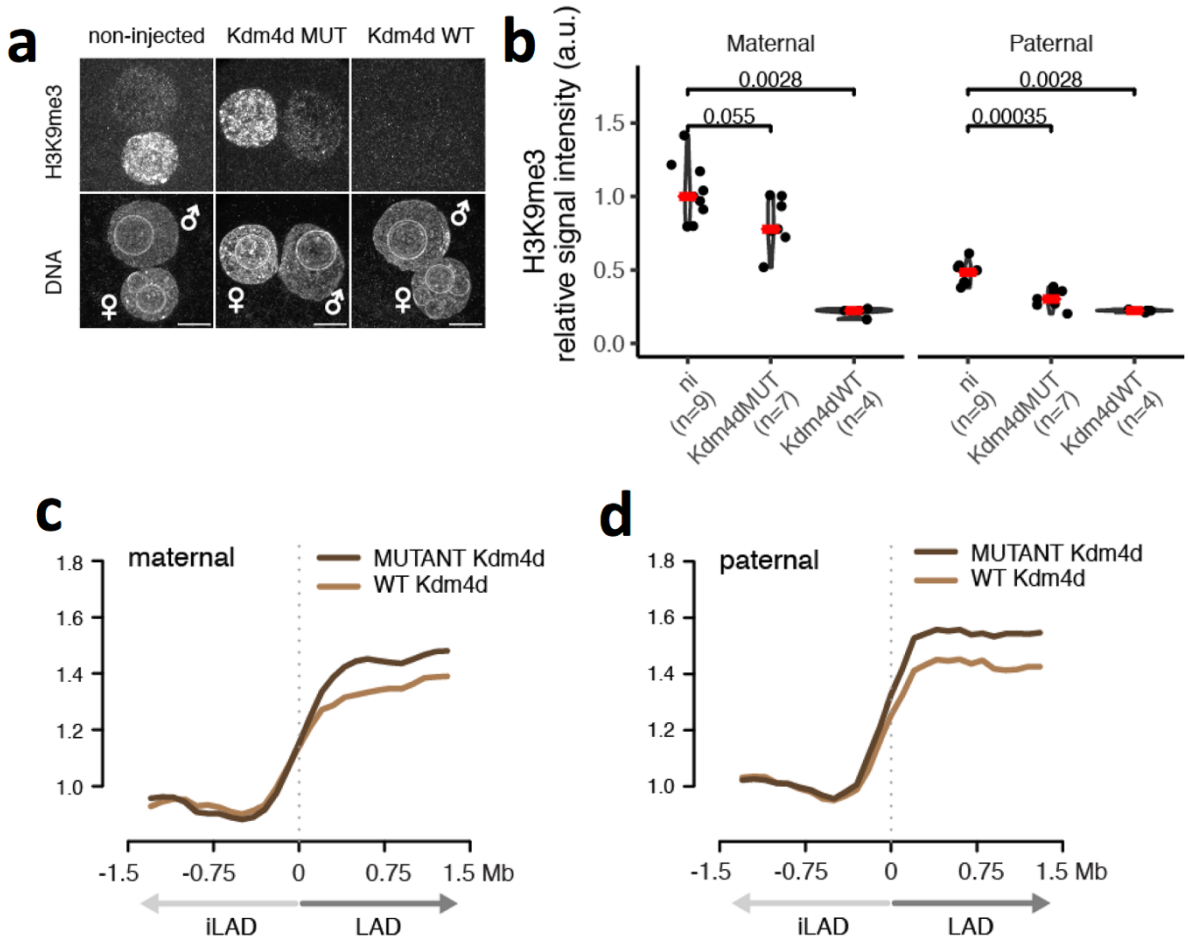

Figure 30. Kdm4d overexpression depletes H3K9me3 but does not perturb LADs in zygotes

a) Immuno-fluorescent staining of H3K9me3 in MUT and WT Kdm4d injected embryos. Scale bar represents 10 µm. **b)** Violin plot quantifications of immunofluorescence staining show a clear reduction of H3K9me3 upon WT Kdm4d overexpression. **c)** Chromosome plot of the maternal pronucleus showing no change in LAD structure in Kdm4d MUT or WT injected embryos. **d)** Chromosome plot of the paternal pronucleus showing no change in LAD structure in Kdm4d MUT or WT injected embryos.

Genome wide mapping of LADs pre-fertilization

DamID in fully grown oocytes reveals the lack of conventional LAD structure

In order to address if a pre-existing LAD pattern is inherited from the germline upon fertilization we aimed to map LADs in gametes. Sperm cells are devoid of lamin proteins, therefore performing DamID with Dam-lamin B1 fusions in sperm is not feasible. Moreover, the introduction of Dam-nuclear periphery fusion proteins is not possible through microinjection into sperm, instead it would require the generation of a transgenic mouse line. Therefore, we focused on female gametes to map LADs before fertilization.

We injected fully grown mouse oocytes with the AID-Dam-lamin B1 and the control Dam-only mRNA. Imaging the ^{m6}A-Tracer in oocytes surprisingly revealed no clear peripheral ring of methylation but an unconventional pattern of one or two patches of ^{m6}A-Tracer signal at the periphery (**Figure 31**). This methylated patch of the genome showed a higher DAPI intensity suggesting that more compact or more AT rich genomic regions are methylated. Also, when co-injected with a fluorescent fused histone, we detected a higher signal of H2B-mRFP at the sites of methylation (**Figure 31b**).

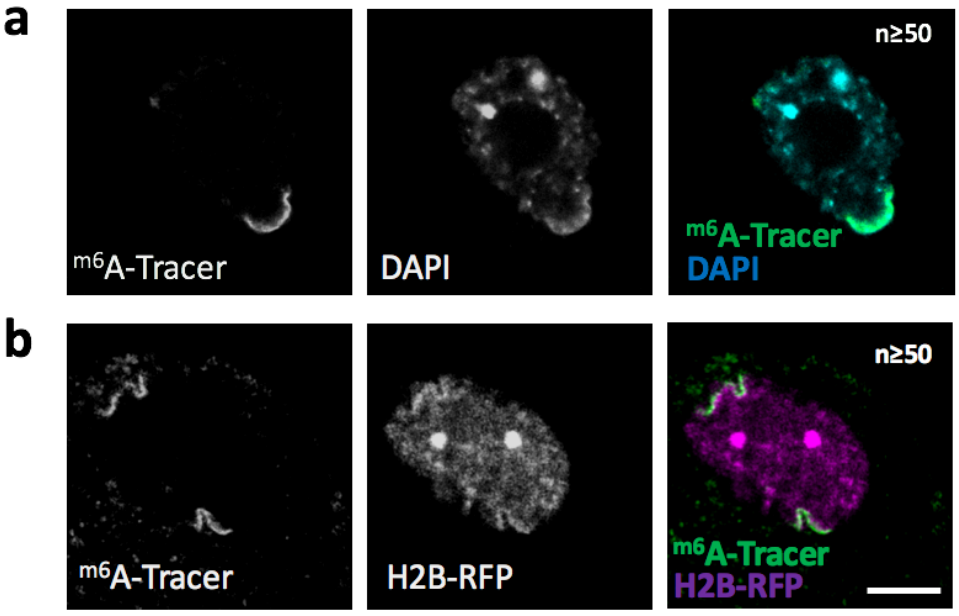

Figure 31. Dam-lamin B1 methylate only a fraction of the nuclear periphery in oocytes

The ^{m6}A-Tracer signal is enriched in one or two distinct "patches" at the nuclear periphery of oocytes. The methylated regions show a higher DAPI intensity **(a)** and a higher incorporation of H2B-mRFP **(b)**. Scale bar represents 10 µm.

Furthermore, the methylated patch is present in a “bulging” region of the nucleus surrounded by invaginations (**Figure 31**).

Next, we aimed to cytologically test if only a few distinct or several different chromosomes localize to the peripheral patch in oocytes. Therefore, we designed an experiment to methylate the peripheral genome in interphase oocytes followed by inducing their resumption to meiotic division and perform chromosome spreading to detect the ^{m6}A-Tracer on chromosomes (**Figure 33a**). In order not to introduce promiscuous methylation of DNA during prophase and metaphase, we had to degrade the AID-Dam-lamin B1 protein before nuclear envelope breakdown. Therefore, first we

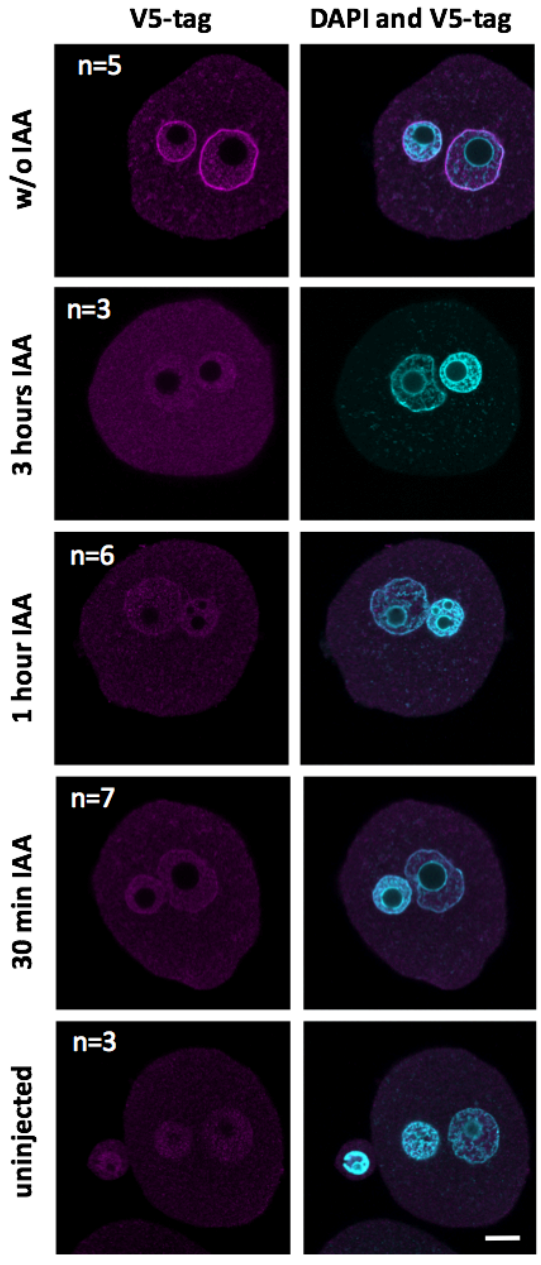

Figure 32. The AID degron system efficiently depletes AID-Dam-lamin B1 within 30 minutes.

Zygotes were injected with 50 ng/ µl AID-Dam-lamin B1 mRNA (10x higher concentration compared to that used in DamID sequencing experiments) and protein production was allowed for 6-8 hours. Subsequently to test the robustness of protein degradation, the embryos were transferred into IAA containing medium. The embryos were fixed 3 hours, 1 hour and 30 minutes after the administration of IAA. Immunofluorescent staining of the V5-tag in the AID-Dam-lamin B1 construct was performed. Control zygotes are either untreated with IAA (degradation not induced, therefore strong peripheral protein signal present) or non-injected embryos to assess the background of the antibody staining. Scale bar represents 10 µm.

tested the rapidity of protein degradation after auxin administration. To this end, we used zygotes due to their easier availability. After 6-8 hours expression of AID-Dam-lamin B1 we transferred zygotes into auxin for 3, 1, 0.5 hours and detected the presence of the AID-Dam-lamin B1 protein by V5-tag staining. Importantly, we observed the complete degradation of our protein within 30 minutes after the addition of auxin (**Figure 32**).

We performed the oocyte chromosome spreading experiment (**Figure 33a**) and surprisingly observed that only one or two chromosomes showed a strong ^{m6}A-tracer signal (**Figure 33b**). Co-staining with centromeric (CREST) and telomeric (TRF1)

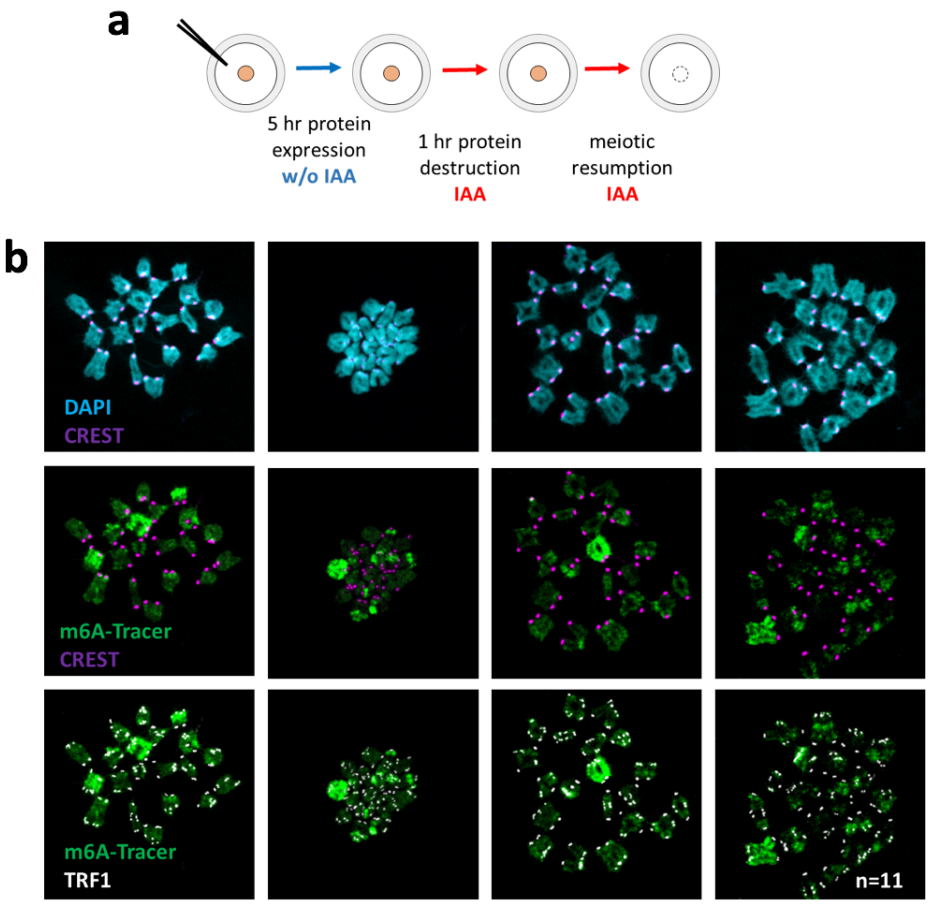

Figure 33. Chromosome spreads reveal ^{m6}A-methylation only on one-two chromosomes in oocytes.

a) Experimental scheme to perform chromosome spreads and detect ^{m6}A methylation that occurred only in interphase in oocytes. 5-8 hours after injection with AID-Dam-lamin B1 and the ^{m6}A-Tracer the oocytes are washed into IAA containing medium to degrade the AID-Dam-lamin B1 protein. Subsequently, the oocytes are released from IBMX to resume meiosis and the chromosomes are spread and co-stained with centromere and telomere markers. **(b)** The ^{m6}A-Tracer signal is enriched at only one or two distinct chromosomes and does not show a preferred colocalization with either centromeres (CREST) or telomeres (TRF1). Spreads from four distinct oocytes are depicted.

markers did not reveal a particular enrichment of methylation at these regions but methylation was present on one to two entire chromosomes.

We aimed to decipher whether it is always the same chromosome(s) that are localizing to the peripheral patch in oocytes or whether these are random chromosomes. Therefore, we performed single cell DamID sequencing on oocytes. Our data revealed that all autosomes apart from chromosome 14 exhibit the same pattern of methylation both in Dam-only and Dam-lamin B1 samples (**Figure 34a**) as illustrated by single-cell DamID profiles on chromosome 10. Chromosome 14 in the Dam-lamin B1 condition, however showed a distinct enrichment of methylation on its right arm when compared to Dam-only. Most strikingly, chromosome X showed a clear accumulation of methylation only in the Dam-lamin B1 condition (**Figure 34a**). This enrichment is further illustrated by the total number of reads per chromosome obtained from DamID sequencing. Clearly it is only chromosome 14 and mainly the X chromosome that shows the most contact with Dam-lamin B1 in oocytes (**Figure 34b**).

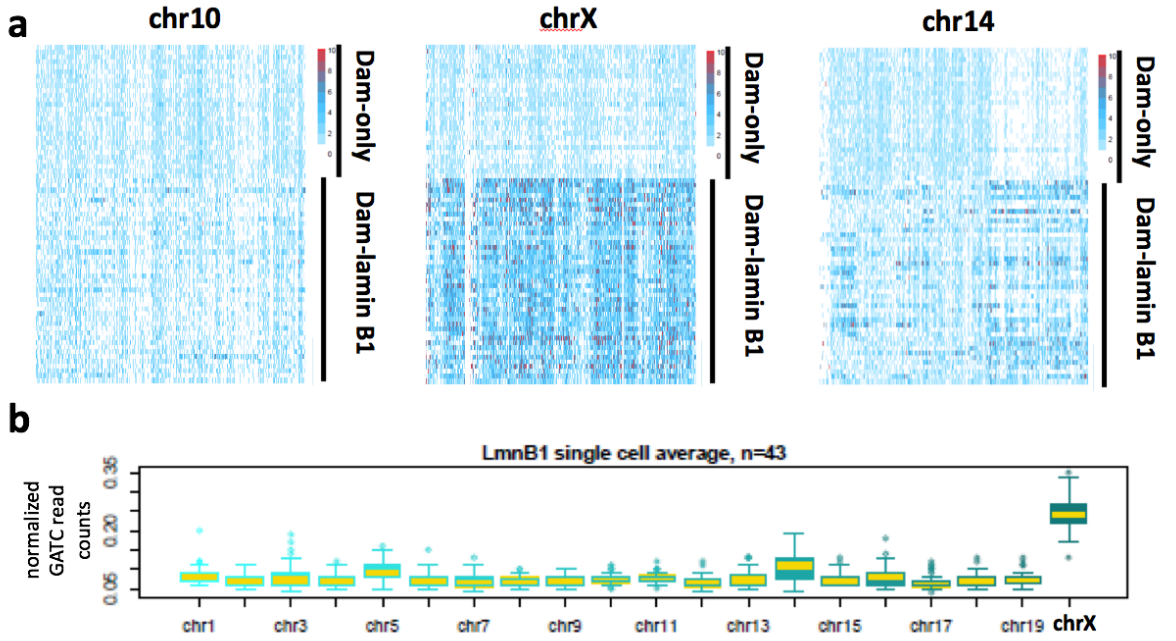

Figure 34. Single-cell DamID sequencing of oocytes reveals an X chromosome specific m6A-methylation.

a) Each row represents data from a single oocyte injected either with Dam-only (top rows) or Dam-lamin B1 (bottom rows). The x axis represents the entire length of the indicated chromosomes. The darker colours indicated higher levels of methylation in calculated in every 100kb bin over the chromosome axis. **b)** Quantification of total number of GATC reads illustrates that chromosome 14 and chromosome X show the highest levels of contact with the nuclear lamina compared to all other autosomes.

Next, we performed DamID on pools of oocytes similar to the conditions employed for the post-fertilization embryos. The sequencing data of pooled oocytes further confirmed that the autosomes show an identical pattern of ^{m6}A-methylation in Dam-lamin B1 samples as in Dam-only samples. This is illustrated both by chromosome plots (**Figure 35a**) and by genome wide positive correlation of OE values from all autosomes in Dam-only versus Dam-lamin B1 samples (**Figure 35b**). Contrarily, in all other post-fertilization stages the Dam-only and Dam-lamin B1 OE values show a clear negative correlation (**Figure 13 and Figure 35b**). These results suggest that oocytes lack a clear LAD patterning on their autosomes, the X chromosome, however is tightly associated with the nuclear periphery.

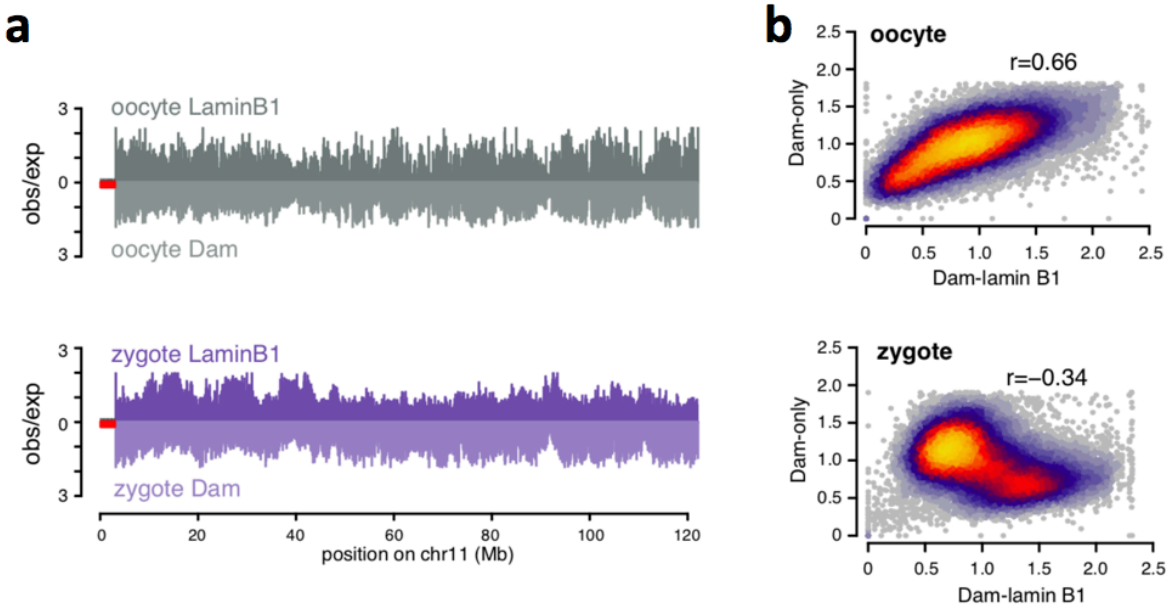

Figure 35. Pooled DamID of oocytes shows an identical methylation pattern in Dam-only and Dam-lamin B1 on autosomes – contrary to zygotes.

a) Each row represents data from a single oocyte injected either with Dam-only (top rows) or Dam-lamin B1 (bottom rows). The x axis represents the entire length of the indicated chromosomes. The darker colours indicated higher levels of methylation in calculated in every 100kb bin over the chromosome axis. **b)** Quantification of total number of GATC reads illustrates that chromosome 14 and chromosome X show the highest levels of contact with the nuclear lamina compared to all other autosomes.

Given the specific, local interaction of the X chromosome with the NL, we aimed to investigate if there are NL components that are specifically enriched at the “patch” identified by the ^{m6}A-Tracer. To this end, we performed immunofluorescent staining of known NL component proteins. Both lamin B1 and lamin A/C showed a uniformly

distributed peripheral staining in oocytes (**Figure 36a**). Surprisingly, the staining with an anti-LBR antibody revealed a specific localization of LBR in a similar patch as observed in the ^{m6}A-Tracer stainings (**Figure 36b**). When we performed LBR staining on oocytes that were previously inected with Dam-lamin B1 and the ^{m6}A-Tracer mRNA, we observed a clear overlap of the ^{m6}A-Tracer patch and the LBR patch (**Figure 36b**).

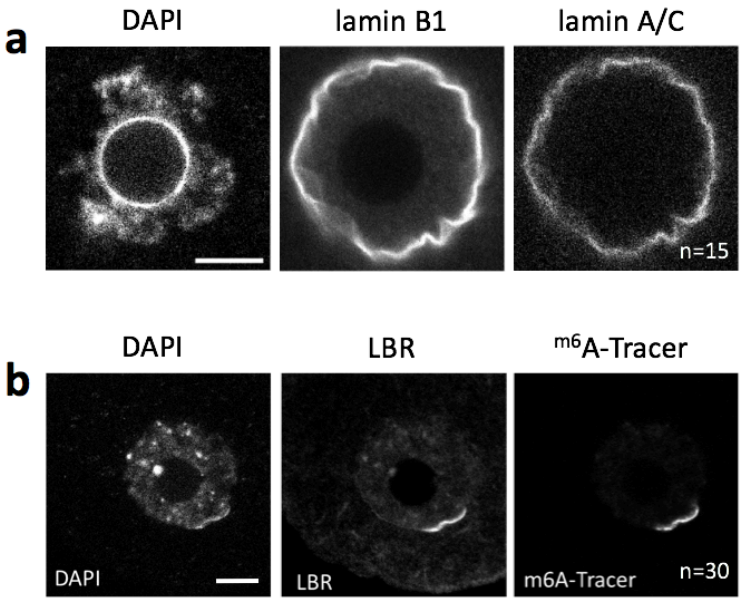

Figure 36. LBR localizes in a patch at the nuclear periphery overlapping the m6A-Tracer signal in oocytes.

a) Immunofluorescent staining of endogenous lamin B1 and lamin A/C shows a clear peripheral localization of both proteins in oocytes. **b)** Immunofluorescent staining of LBR shows a distinct patch at the nuclear periphery overlapping with the m6A-Tracer signal in oocytes. Scale bar represents 10 µm.

Given the particular localization of LBR in mouse oocytes, we aimed to investigate if this pattern is also present in oocytes of other species. We obtained fully grown oocytes from pigs (*Sus scrofa domesticus*), cows (*Bos taurus*) and rats (*Rattus norvegicus*). We performed immunostaining with the same LBR antibody used for mouse oocytes given the high conservation of the protein among species. LBR localized to a similar patch in rat oocytes as observed in the mouse; the bovine and pig oocytes, however did not show this particular staining patter (**Figure 37**). Given the largely weak, background like staining in these species either LBR might not be expressed in bovine and pig oocytes at all or the antibody used might not recognize LBR in these species. Nevertheless, our data suggests that the patchy localization of LBR is potentially specific to rodents.

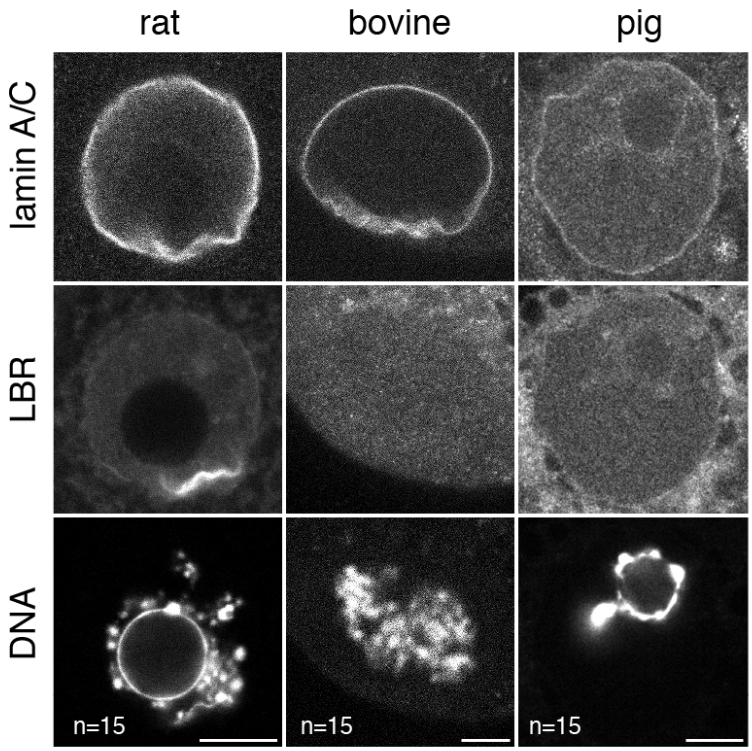

Figure 37. LBR staining in rat, bovine and pig oocytes.

Immunofluorescent detection of lamin A/C reveals uniform peripheral localization in all species tested. LBR staining however is present in a patch only in rats but not in bovine and pigs. Scale bar represents 10 µm.

Discussion

During my PhD work in a collaborative effort with Jop Kind's laboratory we have created genome-wide maps of LADs in early mouse embryos. We have identified LADs in zygotes, 2-cell and 8-cell embryos as well as in ES cells that correspond to the ICM of the blastocyst. Moreover, we have generated these maps in a hybrid background thus we were able to decipher the differences in LAD organization between the two parental alleles. Also, we have confirmed our sequencing data with the orthogonal method of DNA-FISH.

Additionally, we have compared our LAD domains with several genetic and epigenetic features such as chromatin marks and TAD information from HiC data. We have found that LAD formation precedes TAD maturation independently of DNA replication. Moreover, we have uncovered a potential mechanism of allele specific LAD formation in the zygote that depends on the epigenetic mark, H3K4 methylation. Below, I discuss on these findings in detail and highlight potential implications and further directions of research that arise from our study.

LADs are present throughout preimplantation development and are dynamic

Our DamID mapping with Dam-lamin B1 revealed a clear LAD patterning already in zygotes and also in 2-cell and 8-cell embryos (**Figure 12**). This is not necessary expected since up to date, LADs have been found to be always a heterochromatic and repressive environment. However, electron microscopy studies especially in the zygote and also in the 2-cell embryo have observed the absence of canonical electron dense heterochromatin at the nuclear periphery (Ahmed et al., 2010). Also, the mobility of histones in these early stages is higher than 8-cell or ES cell histone mobility suggesting that chromatin movements are possibly also higher in zygotes and 2-cell embryos compared to other cells (Boskovic et al., 2014; Ooga et al., 2016; Ooga and Wakayama, 2017). Based on these results it would have been reasonable to observe undefined LAD patterns in zygotes or 2-cell embryos. Nevertheless, it seems that in early embryos the clear LAD structure does not depend on the heterochromatic nature of LADs and also LADs can be present in cells with higher histone mobility.

Even though, the electron microscopy studies have reported the lack of peripheral heterochromatin, the mirroring pattern between Dam-lamin B1 and Dam-only (which marks accessible regions) suggest that LADs are composed of a less accessible chromatin compared to iLADs already in the early embryo (**Figure 13**). This enrichment of closed chromatin in LADs is less obvious in the zygote (**Figure 16**) – due to allelic differences discussed in the next chapter – and becomes increasingly clear as development progresses.

The number, genomic coverage and size of LADs are stable across stages with one notable exception of the 2-cell stage which contains more and smaller sized LADs (**Figure 15**). Furthermore, these small 2-cell stage LADs exhibit the most atypical genomic features of all stages examined (**Figure 16**). Zygotes, 2-cell embryos and ES cell controls show the canonical A/T richness and CpG sparsity. The 2-cell stage, however, shows the least contrast between iLADs and LADs in these genomic features. The 2-cell stage is particular in the mouse embryo since ZGA occurs at this time. It is possible that the more fragmented, non-canonical LAD patterning of 2-cell embryos is due to the high transcription from both genic and intergenic regions.

We observed that about half of the genome is stably maintained either in the interior or at the nuclear periphery across preimplantation development (**Figure 15**). The other half, however, exhibits a dynamic re-localization from one stage to another. Interestingly the majority of zygotic LADs return to the periphery by the ES cell stage which is also reflected in the highest similarity of LAD organization between zygotes and ES cells (**Figure 12**). This is intriguing, since it suggests that the zygote has a more differentiated-like nuclear organization which is then remodelled into small fragmented LADs at the 2-cell stage coinciding with ZGA and epigenetic reprogramming. Eventually going through the 8-cell stage, the genome reorganizes into a more canonical LAD structure. These results suggest that the reorganization of LADs might be part of the epigenetic reprogramming program of the embryo, however whether this is a side effect or it drives other epigenetic changes like remodelling of histone marks remains to be determined. Addressing this question would be particularly hard because to date there is no known perturbation that would only affect genome organization without interfering with other processes like gene expression of chromatin modifications.

Lower transcription correlates with embryonic LADs – cause or consequence?

In terms of gene expression, we have not analyzed the zygotic LADs because *de novo* transcription is hard to define at this stage due to the carryover of maternal transcripts from the oocyte. In 2-cell and 8-cell embryos, however, genes within LADs showed the tendency to be lower transcribed compared to genes within iLADs (**Figure 16**). In the 2-cell stage this difference in expression between peripheral and internal regions is lower than in the 8-cell stage which again could be a consequence of widespread transcription occurring during ZGA in 2-cell embryos. Also, it is possible that LADs gradually become more strictly repressive as development progresses. The lower transcription from LADs in 2-cell and 8-cell stages is similar to what have been observed in somatic cells. This suggests that LADs of the early embryo already represent a repressive environment or that lowly transcribed genes are already preferentially stored at the periphery in embryos.

In vitro differentiation systems have shown that changes in transcription between cell states can be accompanied by changes in peripheral positioning (Peric-Hupkes et al., 2010). This study of ES cell to astrocyte differentiation revealed that several genes that turn on upon the transition from ES to astrocyte also relocate towards the nuclear interior. Contrarily, a handful of genes that cease transcription during this transition relocate towards the NL. Whether the repositioning and the change in transcription are functionally related to each other is not known. The preimplantation embryo provides a clear step-wise system in which these questions could be studied. It will be of great interest to check the expression dynamics of genes located in regions with different localization dynamics (e.g. different ribbons of the alluvial plot in **Figure 15**). Such analysis would reveal if the relocation and the change in transcription are in functional relation to each other and whether they occur concomitantly or one precedes the other.

Whether LAD patterning depends on transcription in the embryo is an intriguing question which could be effectively answered with our experimental setup. The treatment of embryos with alpha-amanitin or 5,6-Dichloro-1-β-D-ribofuranosylbenzimidazole (DRB) results in an efficient inhibition of global Pol II transcription (Abe et al., 2015; Abe et al., 2018; Schultz, 2002). Also, Pol III specific inhibitors have been successfully used in zygotes (Lin et al., 2014). Performing lamin B1 DamID in Pol II or Pol III inhibitor treated zygotes or 2-cell stage embryos would answer these questions. Moreover, taking advantage of the reversible nature of DRB,

well-designed experiments could dissect the contribution of zygotic transcription to LAD formation both at the zygote and 2-cell stages. Because, blocking transcription arrests embryos at the 2-cell stage, only the contribution of 8-cell transcription and not of previous stages may be assessed on LAD maintenance at the 8-cell stage.

However, there are caveats to the perturbation of global transcription with inhibitors. In case changes in nuclear organization are observed, it will be hard to conclude whether this is due to the lack of transcription itself or whether this is due to the lack of production of certain proteins that are essential for maintaining nuclear organization. One way to tackle this problem would be to perform similar DamID experiments in cycloheximide (CHX) treated embryos which lack active translation. An even more precise way of dissecting the contribution of transcription to genome organization would be to affect transcription only locally in defined LADs.

Fortunately, the tools to locally affect gene expression are rapidly evolving. Both TALEs (Transcription activator-like effectors) and the Cas9 protein of CRISPR (Clustered Regularly Interspaced Short Palindromic Repeats) system have been successfully used to modulate the expression of mainly repetitive elements but also single genes (Amabile et al., 2016; Bintu et al., 2016; Fuentes et al., 2018; Jachowicz et al., 2017). One could envision injecting embryos with selected LAD specific a TALE/Cas9 fused to activator or repressor domains and performing lamin B1 DamID in these embryos to map LADs. Alternatively, the positioning of the activated/repressed regions could be assessed by DNA-FISH. Those LADs that naturally change positioning concomitant with changing gene expression would be of particular interest to activate/repress. For example, regions that are at the periphery in zygotes and relocate to the interior at the 2-cell stage (concomitantly increasing gene expression) could be kept silent in the 2-cell embryos and one could unravel if the naturally increased transcription activity is necessary for relocation or not.

Based on data from somatic cells, several research groups have suggested that peripheral localization induces gene silencing (Finlan et al., 2008; Kumaran and Spector, 2008; Therizols et al., 2014). Therefore, it would also be critical to perturb the localization of defined LADs in embryos and see if this change in organization leads to a change in expression. To do so, one could take advantage of the above mentioned TALE and CRISPR systems or zinc finger proteins (ZFs) which can be fused with components of the NL thereby tethering specific regions to the nuclear periphery (Jachowicz et al., 2013). In order to keep regions in the nuclear interior one would need

to fuse these sequence specific DNA binding proteins to architectural proteins of the interior. These are harder to identify but one candidate is Npm2, a component of the nucleolar precursor body present in embryos. However, such experiments are harder to conclude from, since it is possible that proximity to the NPB in itself might perturb transcription.

LADs exhibit low heterogeneity in single cells

In addition to using populations of around twenty cells per replicate, we also performed DamID on single cells from embryos. Importantly, our single cell data shows almost identical patterning to DamID data from pools of embryos (**Figure 17**). Moreover, comparison of DNA-FISH distances with CF scores from single cell DamID also shows a high correlation between these orthogonal methods further confirming the validity of our findings (**Figure 18**).

We were particularly interested in the heterogeneity of genome organization during preimplantation since this is the developmental time window when the very first cell fate decisions arise. Epigenetic and gene expression differences between lineages that will contribute to the ICM or the TE are observable already from the 4-cell stage but become clearest by the compact 16-cell stage morula or rather the 36-cell blastocyst. Whether there is heterogeneity in nuclear organization reflecting cell fate is unknown, since all HiC studies beyond the zygote stage (Du et al., 2017; Ke et al., 2017) were performed on pools of several embryos, not single cells.

Unfortunately, our DamID experiments were not robust enough to profile all of the cells from the same 8-cell embryo. This was due to the approximately 50 percent efficiency in PCR amplification of our single cell samples. Nevertheless, if there were significant differences between two populations of cells at the 8-cell stage we would have expected to detect these when sampling the 114 cells we obtained from multiple 8-cell embryos. However, we did not observe higher variability or two distinct populations between single cells at the 8-cell stage compared to other stages (**Figure 17**). This suggests that LAD patterning is not yet cell lineage specific in these early embryos. Alternatively, our DamID sequencing with the 100 kb resolution and with the high sample drop-out rate might not be sensitive enough to acknowledge these differences.

One important control would be to perform DamID on the blastocyst stage which clearly consists of two distinct cell lineages. Based on lamin B1 DamID of *in vitro*

cultures ES cells and trophoectoderm stem cells (TS cells) significant differences in LAD patterning have been reported (Kim et al., 2011). These changes were mainly detected on genes which are differentially expressed between ES and TS cells. These expression differences are similar to those in the ICM and the TE, therefore it is likely that single cell DamID on *in vivo* blastocyst would reveal two distinct populations.

The paternal and maternal LADs differ early in development

We used hybrid crosses between mice (CAST and CBAxC57Bl6 – shortly F1) that significantly differ in their genome sequence at known sites (SNPs) to distinguish the alleles in DamID sequencing. However, a potential caveat of using hybrid embryos is the alternative explanation to why differences in LADs might be present in data from hybrids. It is plausible, that not the developmental history of the alleles (whether they went through oogenesis or spermatogenesis) but the sequence composition accounts for the differences in localization. For example, this could be due to essential positioning factors binding to regions that have SNPs between the two strains and therefore the effect of such peripheral tethering factors could be seen only on alleles from one of the strains. Such differences would be “strain specific”.

To test if allelic differences are strain or parent of origin specific we employed two independent approaches. First, we performed DamID on 2-cell embryos from reciprocal crosses in which we inverted the sex of the two strains (originally CAST males mated with F1 females – in reciprocal crosses F1 males mated with CAST females). Second, we took advantage of the zygote in which the two alleles reside in distinct pronuclei. Using non-hybrid embryos, the paternal and maternal genomes can be physically separated by micromanipulation. Comparison of OE values from both reciprocal crosses and mechanically separated non-hybrid pronuclei revealed that the differences in LADs between alleles are likely parent of origin and not strain specific (**Figure 20, 22).**

The differences between alleles were pronounced at the zygote stage. The maternal pronucleus showed a more uncanonical, fragmented LAD patterning reminiscent of the 2-cell stage on both alleles. Also, maternal LADs seem to be in an open state as judged by the DHS signal (**Figure 20**). The paternal pronucleus, however, exhibited a clear, canonical domain patterning with large, continuous stretches of lamina association depleted of accessible chromatin. This asymmetry of the paternal genome being more defined in terms of structure has also been observed

in HiC and DNA-FISH studies of A/B compartments in the zygote (Flyamer et al., 2017). The causes behind this asymmetry remain to be determined, however it is plausible that the different germline history contributes to the paternal genome bearing more structured chromatin. Also, it might simply be a consequence of the paternal genome entering the egg in a more “interphase” state from the sperm head. The maternal genome is in a meiotic condensed chromosomal configuration upon fertilization from which an interphase pronucleus has to be assembled. This could be a cause of the more fragmented LAD structure and weaker compartmentalization.

Allelic differences are still observable during the 2-cell and 8-cell stages which might still be a result of the differences carried over from the zygote. However, concluding this requires further analysis. Nevertheless, by the ES cell stage the allelic differences are almost fully diminished. Our data suggests that there is a gradual consolidation of allelic differences in LAD organization taking place during preimplantation development.

The relationship between LADs, TADs and compartments in the embryo

One of the big questions in the field of nuclear organization is whether the different levels of organization depend on each other and whether they are set up simultaneously or in a step-wise manner. To address this questions, systems in which nuclear organization is set up *de novo* are needed, since cell culture cells show a clear organization which nuclear structure is maintained throughout cell divisions.

LADs precede TAD maturation

In the embryo, the TAD structure must establish gradually since TADs before the 8-cell stage cannot be identified; only a slight decrease in TAD insulation can be seen at the boundaries of TAD domains that were originally identified in ES cells (Du et al., 2017; Flyamer et al., 2017; Ke et al., 2017). There are arguments whether this is true *de novo* establishment or just gradual maturation of TADs with gradually increasing insulation at their boundaries. Nevertheless, there is definitely less TAD structure present immediately after fertilization than from the 8-cell stage onwards.

Our data clearly shows, that LADs are present immediately after fertilization in the late-zygote stage, preceding the presence of mature TADs (**Figure 12, 23**). Whether LAD formation helps priming TADs or whether the presence of LADs is

necessary to mature TADs by the 8-cell stage is an intriguing questions. To address this, one would need a system in which LAD formation can be prevented.

Fortunately, our observation that experimental reduction of H3K4me3 results in loss of LAD patterning of the paternal pronucleus might provide a system to decipher the LAD-TAD or LAD-compartment dependency. Experimentally, one could perform HiC in WT or MUT Kdm5b injected zygotes derived from a hybrid background. This experiments would reveal – at least in case of the paternal allele – whether the absence of LAD patterning results in less insulation at TAD boundaries or whether compartment formation is perturbed. One caveat of this experiment is that whether H3K4me3 itself (independently of affecting LADs) plays a role in TAD formation or compartmentalization could not be distinguished.

LADs can overlap A compartment in the embryo

Canonical LADs overlap with B compartments in all cell types examined up to date. This is indeed the case also in zygotes, 8-cell embryos and ES cells (**Figure 23**). Intriguingly, almost 40 percent of the 2-cell stage LADs, however, have an A compartments status (**Figure 23**). Given the non-canonical genomic features of 2-cell LADs (**Figure 16**) and the widespread transcription occurring at this stage, this might not be surprising. To our knowledge the 2-cell embryo represents the only cell type in which almost half of the peripheral genomic regions reside in A compartments. This data suggests that the compartment status might not be a driver of LAD positioning – at least in 2-cell embryos.

When we compared the temporal compartment dynamics with the peripheral positioning of regions, we found that about quarter of the genome that is stably at the periphery across all stages keeps its B compartment status. Also, another quarter of the genome which is stably in the nuclear interior remains to be in the A compartment in all stages. In other cases, when a region is originally in the interior and then relocates to the periphery as development progresses (*de novo* forming LADs), several scenarios can occur. The relocation to the periphery can be accompanied by a simultaneous shift in the compartment status from A to B. Also, a change in A to B compartmentalization can precede or follow one stage later the relocation of a region to the NL. These results suggest that there is no clear explanation whether compartmentalization helps to drive relocation or the other way around. All scenarios exist and one would need to experimentally perturb one of these processes to gain

more insight. Also, results are likely to be locus specific and not general. Nevertheless, the H3K4me3 depletion induced paternal LAD loss in Kdm5b injected zygotes could be a model system to test whether this dependency exists.

LADs and B compartments are independent of S phase progression

Going through DNA replication has been shown to be important for peripheral positioning of genes in somatic cells (Shachar et al., 2015). Furthermore, HiC experiments in 2-cell stage mouse embryos have shown that TAD maturation depends on DNA replications but not on transcription (Du et al., 2017; Ke et al., 2017). Therefore, we were interested to check if LAD maintenance depends on the progression through S-phase.

First, after reanalysing published HiC data of control and DNA polymerase inhibitor treated 2-cell stage embryos (Ke et al., 2017), we found that compartmentalization is stably maintained even in the absence of DNA replication (**Figure 25**). Given the uncanonically large overlap of 2-cell LADs with A compartments we wondered if even though compartments are stable without replication, whether LAD maintenance is perturbed. One could imagine that those LADs that overlap B compartments are not affected by replication but those overlapping A compartments might be. Interestingly, we found that 2-cell embryos treated with aphidicolin to inhibit S-phase do not show significant changes in their LAD patterning. This result suggests that contrarily to somatic cells, peripheral locus positioning can occur without replication in 2-cell embryos.

H3K4me3 regulates paternal LAD formation in the zygote

Studies from *C. elegans* have demonstrated that peripheral chromatin organization is dependent on the repressive heterochromatic marks H3K9me2 and H3K9me3 (Gonzalez-Sandoval et al., 2015; Towbin et al., 2012). The enzymes responsible for the deposition of these chromatin marks in worms are MET-2 (a mammalian Setdb1 homolog) and SET-25, a previously uncharacterized histone methyltransferase (HMT). When MET-2 and SET-25 are knocked out, the heterochromatic array that the authors use for assessing positioning is relocated to the nuclear interior and also becomes derepressed. These results suggest that methylation on H3K9 is necessary for peripheral positioning. In the mouse early embryo, H3K9me levels are low and asymmetric showing higher levels in the maternal

genome. We tested whether the removal of H3K9me3 in zygotes perturbs LAD formation by the overexpression of the Kdm4d demethylase followed by DamID. However, we found that neither the maternal nor the paternal LADs are affected by reduced H3K9me3 levels (**Figure 30**). This data suggests that the heterochromatic mark H3K9me3 typically enriched in LADs in other cell types is not essential for zygotic LAD formation. Therefore, we turned to assessing other histone marks in relation to LADs.

Currently there is a limited number of studies that reported genome wide positioning of histone marks in the mouse preimplantation embryo. Only H3K4me3, H3K27me3 and recently H3K9me3 have been assessed by ChIP-seq systematically in all stages of preimplantation (Dahl et al., 2016; Liu et al., 2016; Wang et al., 2018; Zhang et al., 2016; Zheng et al., 2016). Also, H3K27ac have been interrogated but only at the 2-cell stage (Wu et al., 2016a).

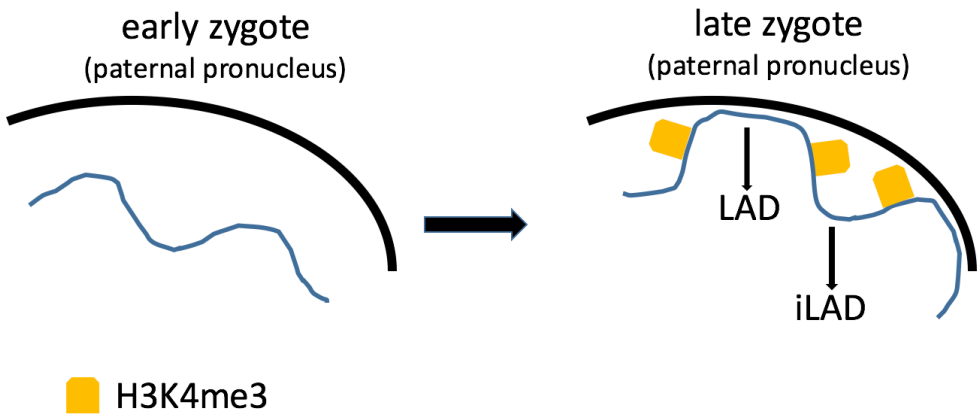

Figure 38. Proposed model of paternal LAD formation in the zygote

The sperm derived H3K4me3 is likely removed from the paternal pronucleus in early zygotes. *De novo* methylation of H3K4 occurs outside of (or on the border) of LADs during the zygotic cell cycle. The LAD pattern of nuclear organization is set up in an iLAD localized H3K4me3 dependent manner.

The alignment of the ChIP-seq data with LAD coordinates revealed no clear correlation between LADs and H3K27me3 (data not shown). However, we observed a striking asymmetric depletion versus enrichment of H3K4me3 on the paternal and maternal LADs in zygotes, respectively (**Figure 26**). In later stages, H3K4me3 became progressively excluded from LADs on both alleles. The asymmetry of H3K4me3 on LADs is likely a consequence of the very different nature of H3K4me3 peaks between the two alleles (Dahl et al., 2016; Liu et al., 2016; Zhang et al., 2016; Zheng et al.,

2016). The oocyte carries non-canonical, broad domains of H3K4me3 whereas the sperm contributes very little of this mark since its genome is mainly packaged around protamines and not histones. However, upon fertilization the paternal chromatin rapidly acquires H3K4me3 *de novo* with more canonical promoter peaks contrary to the broad domains that the maternal pronucleus inherited from the oocyte (Xu and Xie, 2018).

This striking asymmetric correlation and anti-correlation of H3K4me3 in the zygote male and female LADs prompted us to investigate its potential contribution to LAD formation. We experimentally reduced the levels of H3K4me3 by overexpressing a demethylase and found that while the maternal genome structure remains unaffected, the paternal pronucleus loses LAD patterning (**Figure 26**). The demethylation is specific to H3K4 and does not affect H3K9 methylation. Also, the nuclear lamina does not show observable changes by immunofluorescent staining, therefore likely this effect is due to the reduction in true H3K4 methylation. To exclude the possibility that our overexpressed demethylase (Kdm5b) does not exert its effect by demethylating other for example non histone targets we could overexpress a K4M mutated histone 3 (Aoshima et al., 2015). Another way to specify if it is the histone methylation causes the phenotype would be to remove the endogenous HMT either by siRNA or by using a degron system. The most likely candidate for this approach is Lysine Methyltransferase 2D (Kmt2d) which is inherited from the oocyte (Andreu-Vieyra et al., 2010).

What exactly the “flat” DamID signal means in the paternal pronucleus upon Kdm5b overexpression could be explained in different ways. In our experiments, the Dam-lamin B1 protein is expressed over the course of eight hours. It could be that during this time the entire genome makes contacts with the NL, thereby yielding a uniform distribution of OE values over all chromosomes. This could be due to an increased mobility of chromatin in the absence of H3K4me3, however, why this would occur is of question. Alternatively, one could argue that no genomic regions come into contact with the NL upon H3K4me3 reduction, however this is unlikely since in this case we would expect to recover no sequencing fragments from the paternal genome.

There are several possibilities how mechanistically H3K4me3 could mediate LAD patterning in the paternal pronucleus:

1) One could imagine that other epigenetic marks downstream of H3K4me3 are responsible for LAD patterning, and in the H3K4me3 depleted condition these other marks might be mislocalized. For example, DNA methylation has been shown to be

reduced in regions where H3K4me3 is present (Morselli et al., 2015). In the H3K4me3 reduced condition 5mC might be spread all over the genome and if LAD patterning is dependent on 5mC (which have not been previously investigated) this could explain the loss of LAD structure.

2) Another possible mechanism could be that upon H3K4me3 depletion chromatin binding proteins important for LAD structure might be mislocalized on the genome. For example, LAD formation might depend on components of the NL which act as hinges to tether LADs to the periphery. If these peripheral anchoring proteins distinguish LADs based on the lack of H3K4me3, it could occur that when the genome is globally devoid of H3K4me3 these anchors might sequester loci aspecifically to the NL.

3) Alternatively, H3K4me3 might create a local chromatin environment that favours interactions with similar active chromatin in the interior of the nucleus. Possibly, this clustering of active chromatin in the nuclear interior could be a driver of LAD formation leaving non-H3K4me3 bearing chromatin to be passively positioned to the NL. In the H3K4me3 depleted condition this distinction between internal and peripheral clustering might be lost resulting in the absence of LAD patterning.

Potentially, several other mechanisms might be in play behind the LAD formation of the paternal pronucleus which need to be experimentally tested.

Potential mechanisms controlling maternal LAD structure

Our experiments with Kdm5b overexpression have clearly reduced the levels of H3K4me3 in both pronuclei (**Figure 26e and 26f**). Why the LADs of the maternal pronucleus remains largely unaffected while the paternal genome loses LAD patterning is an intriguing question.

One obvious difference between the two pronuclei is the nature of H3K4me3. The maternal pronucleus inherits the broad, uncanonical H3K4me3 domains whereas the paternal pronucleus *de novo* acquires a more canonical promoter peak like H3K4me3 pattern. Since the reduction of H3K4me3 by Kdm5b is not complete (**Figure 26e**), it is plausible that there is a different threshold of sensitivity at which different types of H3K4me3 (broad domains vs. promoter peaks) exert their effect on nuclear organization. Alternatively, broad domains might have no role at all in directing LAD formation and the maternal LAD establishment could be completely H3K4me3 independent. Another possibility is that H3K4me3 binding factors or yet unidentified

components of the NL might localize asymmetrically between the maternal and the paternal pronucleus could might explain the asymmetric effect of the Kdm5b experiments.

The canonical heterochromatin mark H3K9me3 shows an asymmetric localization in the zygote with high enrichment on the maternal genome and barely detectable levels on the paternal genome (Puschendorf et al., 2008). Even though, our preliminary analysis of the published H3K9me3 ChIP-seq data did not show a clear relationship between H3K9me3 and LADs neither in the maternal nor in the paternal pronucleus, it is possible that the high levels of H3K9me3 specifically in the maternal pronucleus could contribute to LAD patterning.

This question could be efficiently addressed in a similar way as of the H3K4me3 reducing Kdm5b experiments. The Kdm4d demethylase is known to specifically remove the H3K9me3 mark from chromatin (Krishnan and Trievel, 2013). The overexpression of this enzyme and its catalytically inactive form has already been tested in mouse preimplantation embryos resulting in the removal of virtually all detectable H3K9me3 as judged by IF staining (Matoba et al., 2014). Therefore, performing lamin B1 DamID on Kdm4d injected embryos would answer if H3K9me3 plays a role in LAD patterning.

Regardless, whether one of the above mentioned possibilities or other mechanisms are in place for maternal LAD formation, it is likely that the maternal LAD establishment occurs through different processes compared to paternal LAD formation. Therefore, the setting up of LAD patterning post fertilization contributes one more example to the list of epigenetic asymmetries identified to date in the mammalian zygote.

Oocytes likely lack LADs genome wide

Our DamID sequencing data from oocytes suggests the lack of LAD structure on autosomes. Only in oocytes do we observe a positive correlation between the negative control Dam-only signal and the Dam-lamin B1 signal, suggesting that there are no specific genome-NL contacts of the autosomal genome in oocytes. One potential explanation to this result might be a failed DamID experiment, however we do observe methylation on chromosome 14 and the X chromosome suggesting that methylation indeed occurred in oocytes.

The potential caveat to this experiment is that if the AID-Dam-lamin B1 construct is not incorporated uniformly into the NL – but only at a specific region – it might yield this peculiar X chromosome specific LAD pattern. In order to test this, we will have to perform more control experiments. One way will be the overexpression EGFP-lamin B1 at similar concentrations to AID-Dam-lamin B1 to see if a uniform peripheral signal is detected. Ideally, an immunofluorescent staining of the AID-Dam-lamin would also prove or disprove these results, however at such low concentrations of mRNA injection as 5 ng/µl the detection of the resulting proteins by immunofluorescent staining is not possible. Other experiments to dis/prove the non-uniform localization of the DamID construct will be essential to strengthen or question these findings.

Nevertheless, if oocytes truly lack LADs it implies that there are no peripheral genome contacts in the female germline which might be passed on to the next generation. This possibility presents a scenario in which the genome-NL contacts must establish *de novo* upon fertilization. Therefore, epigenetic information in nuclear organization likely is not inherited.

The potential roles of the LBR-X chromosome interaction in oocytes

The specific ^{m6}A-Tracer accumulation on one or two chromosomes and the sequencing results indicate that in oocytes only chromosome 14 and chromosome X are in molecular contact with the NL under our experimental conditions. These results raise several questions: 1) how are these two chromosomes specifically selected to contact the NL, 2) is there a role of these specific chromosome contacts during oocyte development, 3) are these contacts important (i.e. represent an inheritable mark) after fertilization.

Why chromosome 14 is the only autosome that contacts the periphery is an intriguing and difficult to answer question. In the future, we will have to compare the genetic composition, sequence conservation and epigenetic features of chromosome 14 with other autosomes. Such analysis might provide insights into why only this autosome contacts the nuclear periphery in oocytes.

An important developmental event that occurs to the X chromosome during the first days after fertilization is that in female embryos specifically the paternal X chromosome stays inactive (Harper et al., 1982; Okamoto et al., 2004). This process is called paternal specific imprinted X inactivation. In the extraembryonic tissues the paternal X chromosome stays inactivated. In the ICM, however, both maternal and

paternal X chromosomes are reactivated and random X inactivation occurs (Kay et al., 1993; Lyon, 1961). Imprinted X inactivation is a prime example of epigenetic regulation; however, its exact mechanism is elusive. It is, however, clear that both imprinted and random X inactivation involves the expression of a long noncoding RNA – Xist – that coats the inactive chromosome and is essential for its silencing (Avner and Heard, 2001; Borensztein et al., 2017). The first possible mechanism – of how only the paternal X chromosome becomes inactivated – is that the paternal X chromosome could carry an imprint from the sperm that would regulate this chromosome to stay inactive. The other scenario is that the maternal X chromosome harbours an activating imprint acquired in the oocyte, keeping it active during the first cleavage divisions and in extraembryonic tissues. In mouse, likely this second possibility takes place.

It has been previously shown, that an imprinted mark is still absent 5 days after birth in oocytes and is built up on the X chromosome during oocytes growth (Tada et al., 2000). Recently, it has been demonstrated through ChIP-seq from different stages of mouse oocytes that it is the H3K27me3 histone modification that is gradually acquired over the Xist promoter during oocyte growth (Inoue et al., 2017b; Zheng et al., 2016). If H3K27me3 is experimentally removed upon fertilization, both paternal and maternal X chromosomes upregulate Xist expression and become inactivated (Inoue et al., 2017b). These results identify H3K27me3 as an imprinted mark in oocytes responsible for keeping the maternal X chromosome active in the first cleavage stages and in extraembryonic tissues.

The LBR protein has been recently identified as a factor interacting with the Xist long noncoding RNA and proved to be essential for the establishment of X inactivation in ES cell cultures that represent a model for random X inactivation (Chen et al., 2016; Chen et al., 2017). Interestingly, our findings show that LBR localizes to a specific region of the NL contacting either the X chromosome or chromosome 14 or both (**Figure 34 and 36**). This observation raises the possibility that LBR might play a role in imprinted X inactivation in the mouse. Also, the observation that LBR localizes to a specific patch in mouse and rats but not in bovine and pigs (**Figure 37**), suggests that LBR might be linked to imprinted X inactivation. This hypothesis requires mechanistic testing which could be achieved through an oocyte specific deletion of the LBR gene. The oocyte specific knock-out strategy will be essential since the constitutive knock-out LBR mice die shortly after birth (Cohen et al., 2008; Shultz et al., 2003). Experiments with LBR depleted oocytes fertilized by wild-type sperm could assess

whether the maternal LBR protein is required for imprinted X inactivation. RNA-FISH of Xist or RNA-seq of 8-cell embryos from these crosses would formally answer if without maternal LBR both X chromosomes become inactivated in female embryos.

Mechanistically, it would be intriguing to decipher if there is a link between the H3K27me3 mark and LBR. Since the H3K27me3 is acquired over the Xist promoter only during oocyte growth, it will be essential to determine at what stage of oocyte development does the LBR patch form. This could be achieved by histological staining of mouse ovaries at different stages of development and would answer if LBR becomes accumulated at the peripheral patch prior to the Xist H3K27me3 acquisition. Using the LBR knock-out mouse, one could determine by ChIP-seq whether H3K27me3 is dependent on LBR. Similarly, using the already existing oocyte specific knock-out of the polycomb protein Eed (embryonic ectoderm development protein) one could determine if in H3K27me3 depleted oocytes the LBR patch is still formed or if it is built up independently of H3K27me3.

The potential role of oocyte LBR in imprinted X inactivation is purely hypothetic, thus requires experimental testing.

List of contributions

All embryo work, DNA-FISH and HiC data analysis was done by Máté Borsos. The DamID amplification, library preparation and sequencing was done by Jop Kind. The DamID data was analyzed by Sara Perricone. Techniques performed by our collaborator Jop Kind are indicated in *italics* in the materials and methods section.

Materials and Methods

Embryo collection and manipulation. Experiments with animals were carried out according to valid legislation in France and under the authorization of the Com'eth Institute of Genetics, Molecular and Cellular Biology ethical committee and in compliance with the local government (Government of Upper Bavaria). GV oocytes were collected 44-48 hours after PMSG injection. Oocytes were cultured in IBMX containing M16 while embryos were cultured in KSOM drops under paraffin oil (Sigma). Preimplantation embryos were collected from 5-8 weeks old F1 (CBAxC57BL/6J) females mated with CAST/EiJ males for hybrid crosses and with F1 males for non-hybrid crosses. Ovulation was induced by injecting 10 IU PMSG (IDT Biologika Gmbh) and then hCG (MSD Animal Health) 46-48 hours later. Reciprocal crosses (CAST/EiJ females mated with F1 males) were performed without inducing ovulation. For DamID, an mRNA mixture containing 250 ng/µl TIR1, 50 ng/µl membrane-EGFP and embryonic stage dependent concentrations of AID-Dam-LaminB1 or AID-Dam-only were injected into the cytoplasm of embryos. To methylate LADs only at the stages of interest we washed the embryos into auxin-free media for 6-8 hours at the late-S, G2 phases of the cell cycle. Zygotes (21 hours post hCG) were isolated and injected with 5 ng/µl AID-Dam-LaminB1 or 20 ng/µl AID-Dam-only and kept in auxin free KSOM for 6-8 hours to methylate LADs or accessible regions, respectively. For DamID at 2-cell stage late-zygotes (27-28 hours post hCG) were isolated and injected with 10 ng/µl AID-Dam-LaminB1 or 40 ng/µl AID-Dam-only in auxin (500µM) containing media. Auxin was removed at 2-cell stage for 6-8 hours (from 42 to 48-50 hours post hCG). For DamID at 8-cell stage late-2-cell embryos (46-48 hours post hCG) were isolated and injected with 20 ng/µl AID-Dam-LaminB1 or 40 ng/µl AID-Dam-only in auxin containing media. Auxin was removed at 8-cell stage for 6-8 hours (from 66 to 72-74 hours post hCG). Afterwards, the zona pellucida was removed by treatment with 0.5%

pronase in M2 at 37 °C and the polar bodies were mechanically separated from the embryos and discarded. Either pools of 20 blastomeres or single blastomeres were placed into 2 µl of DamID buffer (10mM TRIS acetate pH 7.5, 10mM magnesium acetate, 50mM potassium acetate) and stored at -80 °C until downstream processing.

For DamID in Kdm5b overexpressing embryos, early zygotes from non-hybrid crosses (18 hours post hCG) were injected with 2 µg/µl wild-type or mutant Kdm5B, 5 ng/µl AID-Dam-LaminB1, 250 ng/µl TIR1 and 50 ng/µl membrane-EGFP coding mRNA. Zygotes were kept in auxin containing KSOM for 3 hours to prevent adenine methylation during pronucleus formation. At 21 hours post hCG auxin was removed for 6-8 hours to allow methylation. To separate pronuclei, the PN5 zygotes were transferred to M2 media containing 10 µg/ml cytochalasin B (Sigma-Aldrich). The zona pellucida was cut with a Piezo driven micromanipulator and one of the pronuclei was isolated into M2 drops. The pronuclei were distinguished based on their size and their relative position to the second polar body. The remaining embryos containing a single pronucleus were treated with pronase to remove the zona pellucida and the polar bodies were discarded. The karyoplasts and the single pronuclei containing embryos were frozen in DamID buffer as above. For DamID in replication inhibited 2-cell embryos, late zygotes (26-28 hours post hCG) from hybrid crosses (CBAxC57BL/6J females mated with CAST/EiJ males) were injected with 10 ng/µl AID-Dam-LaminB1, 250 ng/µl TIR1 and 50 ng/µl membrane-EGFP coding mRNA and kept in auxin containing media to prevent Dam activity in the zygote. Embryos were washed into aphidicoline (3 µg/ml) containing media when reaching the first metaphase. Auxin was removed from 42 to 48-50 hours post hCG to allow methylation of LADs in the late 2-cell stage.

Bovine and pig oocytes were kindly provided by Prof. Dr. Eckhard Wolf and Mayuko Kurome. Rat oocytes were kindly provided by Andrew Flatley.

Plasmid construction and mRNA production. The in vitro transcription plasmids containing the wild-type Kdm5b was obtained from Addgene (86398) (Zhang et al., 2016). To generate a catalytically inactive version of Kdm5b the H499A mutation was introduced by site directed mutagenesis. The in vitro transcription plasmids containing the wild-type and mutant Kdm4d were obtained from Addgene (61553, 61554) (Matoba et al., 2014). mRNA was in vitro transcribed with T7 or T3 mMESSAGE mMACHINE kits (Ambion) and purified by LiCl precipitation. All plasmids generated in this study are available at Addgene under “Torres-Padilla lab plasmids”.

Immunofluorescence. Embryos were treated with 0.5% pronase in M2 to remove zona pellucida at 37 °C, washed in PBS and fixed in 4% PFA for 15 minutes at room temperature. After permeabilizing in 0.5% Triton-X 100 in PBS for 20 minutes, embryos were kept in blocking buffer (3% BSA in PBS) from one hour to overnight. Embryos were incubated overnight in primary antibody mixes (Supplementary Table 1) diluted in blocking buffer, washed three-times in PBS and stained with secondary antibodies conjugated with (Alexa 488, Alexa 568, Alexa 594 or Alexa 647) in blocking buffer for one hour. After washing three-times in PBS embryos were mounted in Vectashield containing DAPI. For visualising global transcription, zygotes were pulsed with 50 μM EU for one hour (26-27 hours post hCG) and visualised with the Click-iT RNA Alexa Fluor 594 Imaging Kit according to the manufacturer's instructions (Thermo Fischer).

Chromosome spreads. Fully grown oocytes cultured in IBMX were injected with an mRNA mixture containing 250 ng/μl TIR1, 50 ng/μl membrane-EGFP and 5 ng/μl AID-Dam-lamin B1. After 6-8 hours post injection, the oocytes were washed into IAA containing medium and 2 hours later were washed into IBMX free medium to allow meiotic resumption. 4 hours after nuclear envelope breakdown, the zona pellucida was removed by pronase treatment and the oocytes were treated in 1:1 mixture of FBS and water for 15 minutes. Oocytes were placed into 2 μl drops of 2 % PFA containing 0.5 % TritonX-100 and 0.1M DTT on glass slides and incubated overnight at room temperature in a humidified chamber. The slides were air dried and washed in

Slides were blocked in 3 % BSA containing 0.1% TritonX-100 for 1 hour at room temperature and incubated with anti-EGFP antibody (ab13970) 1:1000 dilution, CREST antibody (FZ90C-CS1058) 1:2500 dilution and anti-TRF1 antibody (in house) 1:50 dilution overnight at room temperature. Slides were washed three-times in 0.1 % TritonX-100 containing PBS and incubated with secondary antibodies conjugated with (Alexa 488, Alexa 594 and Alexa 647) for 1 hour at room temperature followed by three-times washes in PBS and mounted in Vectashield containing DAPI.

DNA-FISH. DNA-FISH was performed as described previously, using a protocol that preserves 3D information (Miyanari and Torres-Padilla, 2012). BACs were ordered from BACPAC or RIKEN DNABank (Supplementary Table 1) and purified with NucleoBond® Xtra Midi Plus kit (Macherey-Nagel). BACs were nick translated with 5-TAMRA, Atto594, Atto647N conjugated dUTPs according to the manufacturer's instructions (Roche). To combine nuclear envelope staining with DNA-FISH,

immunostaining was performed with mAb414 (1:1000) as described above, followed by postfixation in 2% PFA for 10 minutes. Next, embryos were washed in 0.5% Triton-X 100 for 10 minutes and treated with HCl solution (0.1N HCl, 0.5 Triton-X 100, and 1 mg/ml PVP in water) for 90 seconds, washed into prehybridization buffer (50 % formamide, 1 mg/ml PVP, 0.05% TritonX, 0.5 mg/ml BSA) and incubated in it at 37 °C for one hour. Embryos were transferred into drops of 0.2 µl hybridization buffer (prehybridization buffer containing 1 µg/µl mouse Cot-1 DNA) under mineral oil, denatured at 80 °C for 10 minutes and incubated at 37 °C for one hour. Embryos were transferred into drops of 0.2 µl hybridization buffer containing a mixture of three probes, each at 5 ng/µl which were previously denatured at 80 °C for 10 minutes under oil. After overnight hybridization at 37 °C, embryos were washed twice in 2x SSC, 0.05 Triton-X 100, 1 mg/ml PVP at RT followed by washing three times 10 minutes in in 0.2x SSC, 0.05 Triton-X 100, 1 mg/ml PVP at 55 °C and mounted in Vectashield containing DAPI on slides with spacers (Grace Bio-Labs SecureSeal) to preserve 3D structure.

Table 2. DNA-FISH probes

name	ID	location	provider
iLAD1	RP23-278K6	chr4:154166444-154351367	BACPAC
iLAD2	RP23-214P21	chr8:121014748-121211934	BACPAC
iLAD3	RP23-299E16	chr5:136856848-137055210	BACPAC
LAD1	B6Ng01-224G13	chr13:118649277-118793034	RIKEN
LAD2	RP23-300N5	chr12:117475115-117666869	BACPAC
LAD3	RP23-73M19	chr11:108987725-109107402	BACPAC
LAD4	RP23-248A14	chr3:109703354-109905959	BACPAC
LAD5	RP24-245M16	chr9:94493947-94654374	BACPAC
LAD6	RP23-447L6	chr12:77637724-77818978	BACPAC
newLAD1	RP23-53G23	chr5:145946121-146115870	BACPAC
newLAD2	RP23-152H19	chr11:73182054-73393482	BACPAC
disLAD1	RP24-289K11	chr13:23892535-24061885	BACPAC
disLAD2	RP23-294E8	chr14:23338458-23517984	BACPAC

Imaging and analysis. Microscopy images were acquired on a Leica SP8 confocal microscope equipped with a Plan Apochromat 63x/1.4 oil objective at 1.5 micron z steps for immunofluorescence and at 0.3 micron z steps for DNA FISH. H3K4me3, LaminB1 and EU intensity was quantified in the nuclei defined by creating masks on the DAPI staining using a custom made Icy protocol. DNA FISH spots were

identified and their distance was measured relative to the DAPI mask periphery using another custom made Icy protocol. The centre of the DAPI mask was defined as 0 and the FISH spots location along the vector from the centre to the periphery defined as 1 was determined. Immunofluorescence signal intensities of all experimental groups were normalized to the median of the control group's (Kdm5b mutant) intensity separately for each biological replicate. The differences in signal intensity and FISH spot distance were subjected to Wilcoxon signed-rank test between groups or stages of development. For each stage between 71 to 220 FISH spots were analysed.

Hi-C data analysis. Hi-C data analysis. Data for untreated embryos were used from GSE82185, for the aphidicolin treated and their control 2-cell embryos from PRJCA000241. Raw files from all biological replicates were pooled and analyzed with HiC-Pro (version 2.10.0) as described in (Du et al., 2017) but aligning to the mm10 mouse reference genome. Compartments were called using the HiTC package (Servant et al., 2015). ICE normalized 100-kb interaction matrices were binned with a bin size of 500 kb and a step size of 100 kb. Observed/expected matrices were used to generate correlation matrices and perform principal component analysis. A/B compartments were defined by the first principal component and gene density. TADs and insulation scores were calculated as described (Du et al., 2017).

Cell culture. *F1 hybrid 129/Sv:Cast/Eij mouse embryonic stem cells (Monkhorst et al., 2008) were cultured at 37°C, 5% CO2 on primary mouse embryonic fibroblasts (MEFs), in Glasgows minimum essential medium (G-MEM; Gibco #21710025) supplemented with 10% fetal bovine serum (FBS; Sigma #F7524), 1% PEN/STREP (Gibco #15140122), 1% GlutaMAX (Gibco #35050038), 1% non-essential amino acids (Gibco #11140035), 1% sodium pyruvate (Gibco #11360039), 143 µM β-mercaptoethanol (Sigma #M6250) and 1:1000 human leukemia inhibitor factor (LIF; in-house production).*

Generating cell lines. *Stable clonal Dam and Dam-lamin B1 lines were created by transfection of EF1alpha-Tir1-neo with hPGK-AID-Dam-lamin B1 or hPGK-AID-Dam plasmids in a ratio of 1:5 plasmids with Effectene (Qiagen #301427). Clones were selected with 250 µg/ml G418 (Thermofisher #10131035) and selection of the clones was based on methylation levels as determined by DpnII-qPCR. To reduce the background methylation levels in the presence of 1.0 mM indole-3-acetic acid (IAA; Sigma #I5148), we transduced the selected clones of both AID-Dam-lamin B1 and Dam with extra hPGK-Tir1-puro followed by selection with 0.8 µg/ml puromycin (Sigma*

#P8833-10mg). Positive clones were screened for IAA induction by DpnII-qPCR assays and DamID PCR products (Vogel et al., 2007).

DamID induction and harvesting. *Expression of AID-Dam and AID-Dam-lamin B1 was suppressed by culturing the cells in the presence of 1.0 mM IAA for 48 hours. DamID was induced by IAA washout 12 hours prior to harvesting. 12 hours after IAA washout, cells were collected in G-MEM supplemented with 10% FBS and 1% PEN/STREP and stained with 10ug/ml Hoechst 34580 (Sigma #911004450) for 45 minutes at 37 °C. Single cell or 20-cell populations were sorted in 96-well plates at G2/M phase of the cell cycle based on the DNA content histogram.*

Single cell DamID. *Single cells or populations of cells were manually sorted in 8-well PCR strips in 2 µl of DamID buffer (10mM TRIS acetate pH 7.5 (Sigma #T1258); 10mM magnesium acetate (Sigma #63052); 50mM potassium acetate (Sigma #95843); 2.01% Tween-20 (Sigma #P2287). 1 µl of lysis buffer with proteinase K (10mM TRIS acetate pH 7.5 (Sigma #T1258); 10mM magnesium acetate (Sigma #63052); 50mM potassium acetate (Sigma #95843); 2.01% Tween-20 (Sigma #P2287); 2.01% Igepal (Sigma #I8896) and 2.01mg/ml proteinase K (Roche #03115828001) was added to the samples, followed by proteinase K digestion at 42 °C for 12 hours in a thermoblock with heated lid. Proteinase K was inactivated by heating the samples for 20 minutes at 80 °C. In the following steps, reagents were added with an Eppendorf Multipipette Plus mounted with a 0.1 ml Combitip (Eppendorf #0030089405). The surface of the reaction volume was never touched by the pipette tip. Genomic DNA (gDNA) was digested for 8 hours by the addition of 7 µl of DpnI reaction mix (0.1 µl DpnI (10U/µl, New England Biolabs #R0176L); 0.7 µl 10x One-Phor-all-buffer plus (100mM TRIS acetate pH7.5; 100mM magnesium acetate; 500mM potassium acetate) and 6.2 µl nuclease free H2O) and incubation at 37 °C in a PCR machine, followed by heat inactivation at 80 °C for 20 minutes. Adaptor ligation was performed by the addition of 10 µl ligation mix (2 µl 2x T4 ligation buffer; 0.5 µl T4 ligase (5U/ul, Roche #10799009001); 0.05 µl 50µM double-stranded DamID adapter [27] and 7.3 µl nuclease free H_2O) and incubation in a PCR machine at 16 °C overnight. Heat inactivation at 65 °C for 10 minutes the next day was followed by PCR amplification by the addition of 30 µl PCR mix (10 µl 5x MyTaq Red reaction buffer (Bioline #25043), 1.25 µl PCR barcoded primer (50 µM) NNNNNNBARCODGTGGTCGCGGCCGAGGATC (Supplementary Table 2), 0.5 µl MyTaq DNA polymerase (Bioline #25043) and 18.25 µl nuclease free H_2O). The PCR*

primer carries 6 random nucleotides at the 5' end to meet the Illumina software requirements of generating reads with diverse starting sequences and a 6 nucleotides sample barcode (Supplementary Table 2). The thermal cycling scheme is as follows:

Step	*Denature*	*Anneal*	*Extend*
1		*72 0C for 10 min*	
2	*94 0C for 1 min*	*65 0C for 5 min*	*72 0C for 15 min*
3-6	*94 0C for 1 min*	*65 0C for 1 min*	*72 0C for 10 min*
*7-35**	*94 0C for 1 min*	*65 0C for 1 min*	*72 0C for 2 min*

**33 for the population samples*

Of the resulting PCR product 8 µl was used for standard 1% agarose gel electrophoresis for analytical purpose and estimation of DNA concentration. All samples were pooled and prepared for Illumina sequencing.

Single-cell DamID Illumina library preparation and sequencing. *Of 300 ng purified PCR product the 3' or 5' overhanging ends were blunted in a 50 µl reaction following the manufacturer's instructions (End-It DNA End-Repair Kit, Epicentre #ER81050). The blunted DNA samples were again purified using the PCR purification colomns of Qiagen and eluted with 26 µl nuclease free H2O. Next, a 3' adenine was added by incubation for 30 minutes at 37 °C in a 50 µL reaction mix (1x New Engeland Biolabs restriction buffer 2, 200 µM dATP (Roche #11051440001) and 25 units of Klenow 3' → 5' exo– (New Engeland Biolabs #M0212M). After heat inactivation at 75 °C for 20 minutes, the DNA was purified with Agencourt AMPure XP beads (Beckman Coulter #A63881). A 1.8 x volume of beads over DNA sample was used, manufacturer's instructions were followed and the DNA was eluted with 20 µl of nuclease free H_2O. To the purified DNA the Illumina indexed Y-shaped adapters (TruSeq Nano DNA LT Library Prep Kit #FC-121-4402) were then ligated for two hours at room temperature in a 40 µl reaction mix (4µl 10x T4 ligation buffer, 0.5 µl T4 ligase (5U/ul) Roche #10799009001, 2.5 µl Illumina adapter, with nuclease-free H2O added to 40 µl final volume). Next, the T4 ligase reaction was heat inactivated at 65 °C for 10 minutes followed by 2 times DNA purification with 1.8 x volume followed by 1.2 x volume AMPure beads as described for the previous step. For the addition of the Illumina index primers a PCR reaction was performed with the DNA from the previous step in a 20 µl MyTaq red DNA polymerase PCR reaction mixture (10 µl 2x MyTaq reaction mixture (Bioline #BIO21110), 1 µl 2.5 µM Illumina oligo mix, nuclease-free H2O till a final volume of 20 µl). The DNA was amplified for 6-8 PCR amplification*

cycles (94 °C 1 minute; 94 °C 30 seconds, 58 °C 30 seconds and 72 °C for 30 seconds for 9 cycles and 72 °C for 2 minutes) after which 5 µl of each sample was analyzed by agarose gel electrophoresis. For Illumina multiplex sequencing typically 4 to 10 separate libraries of each 20-50 single cells were mixed in approximate equimolar ratios as judged from the agarose gel image. The pooled sample was subjected to a Qiagen PCR column purification and subsequent AMPure bead purification with 1.6 x volume of beads over DNA sample before it was used for sequencing.

Processing of single-cell DamID sequencing reads. *Total number of raw and final GATC reads are shown in Supplementary Table 3. Basecalling and filtering were performed using standard software of the Illumina HiSeq 2500. Sequenced 151 reads were parsed in order to obtain the gDNA for downstream analysis. When present, the first 6 random bases were discarded; subsequently the reads were demultiplexed and the 15 bp of adapter trimmed using custom scripts and cutadapt. The pre-processed reads were then mapped to the mm10 (or alternative genome assemblies) using bwa (version bwa-0.7.12) aln with default parameters. Reads aligning to the genome with quality score below 25 were discarded. The computation of Observed over Expected (OE) value per bin was carried out as described (Kind et al., 2015). Briefly, reads that precisely flanked an annotated GATC site were associated with GATC-fragments and kept for downstream analysis. In order to compare population samples to single cell samples, multiple reads aligning to the same position were counted as one and subsequently aggregated in genomic segments of 100kb in order to determine the experimentally Observed value. This was then divided by the Expected value per 100kb bin. The expected value was generated by in-silico determining potential DamID-seq reads of the same length as the experimental data (~131 bp), aligning them to the mm10 genome assembly and selecting them based on the same filtering applied to the experimental data and aligned to GATC-fragments (see above). The final OE value per 100 kb bins was computed by dividing the ratio of the two counts (Observed, Expected) by the total number of observed reads per bin. LAD domain calling was performed on the average population replicates for each stage in (parental or non-allelic) OE values calculated using a two-state hidden Markov model (HMM) (Filion et al., 2010), which allows the classification of each 100kb segment as LAD or iLADs.The computation of CF scores was carried out as described in (Kind et al., 2015), by binarization of the OE values and subsequent summation of the CF score across the single cell samples per 100kb bin.*

Identification of parental-specific reads. *For hybrid samples C57BL/6 x CAST/EiJ or 129/Sv x CAST/EiJ, CAST/EiJ and 129/Sv genomes were de novo compiled by nucleotide substitution of strain specific SNPs using the SNPsplit_genome_preparation tool (version SNPsplit_v0.3.0/) (http://www.bioinformatics.babraham.ac.uk/projects/SNPsplit/) in the original mm10 genome assembly. The database of annotated SNPs between different mouse strains was obtained from ftp://ftp-mouse.sanger.ac.uk/current_snps/strain_specific_vcfs/. The reads were separately aligned to the parental (mm10 or hybrid) genomes using the above described parameters. The edit distance of the alignments of pre-filtered reads (quality score >= 25) was compared to the two genomes. The reads aligning with the lowest edit distance were assigned to the appropriate parental genome. The reads aligning with equal edit distance between the parental genomes were not assigned to the parental genomes but were kept for "non-allelic" profiles.*

Comparative genomics to published datasets. *Low-input ChIP data for H3K4me3 and DNA-hypersensitivity data were respectively obtained from Gene Expression Omnibus (GEO) accession numbers GSE71434 and GSE76642. Alignment was carried out as described for the DamID sequencing reads. Picard tools (version picard-tools-1.130) (http://picard.sourceforge.net) was used to remove PCR duplicates. Additionally, as the H3K4me3 arises from a mouse mixed genetic background C57BL/6N x PWK, the assignment of reads belonging to parental genomes was carried out as described for the DamID libraries. Normalisation in read per million (RPM) was then carried out in fixed genomic windows of 5kb or 100kb to allow direct comparison with DamID data. Gene expression data was obtained from GEO accession GSE71434. The samples were aligned to the mm10 genome assembly using hisat2 (version hisat2-2.0.3-beta) with default parameters. Reads mapping with quality score lower than 200 were discarded. htseq-count (version 0.6.0) was then used to assign the mapped reads to a transcriptional model file (gencode.vM9.annotation.gtf) obtained from (https://www.gencodegenes.org). Only genes annotated in the refFlat (http://hgdownload.soe.ucsc.edu/goldenPath/mm10/database/) database were considered for downstream analysis. The reads per kilobase per million (RPKM) were calculated for each gene by normalising the total number of mapped reads per gene by the gene length in kb and sample size. A gene TSS was considered to be located*

within a LAD when the region surrounding its TSS (+/- 250 bp) was located within a LAD.

Statistical testing. Statistical tests were computed in order to test the correlation between datasets and/or the significance of specific features. The R programming language (versions R-3.1.2 and R-3.4.0) was widely used with this purpose. In general, before applying any test, the normality of the distributions was tested by the Anderson-Darling Normality test (R Package nortest). In our study, due to the non-normal distribution of the data analysed, non-parametrical tests such as the Wilcoxon rank-sum test (two-sided, unless otherwise specified) and Spearman correlation coefficient were chosen.

List of chemicals

3-Indoleacetic acid (IAA)	(Sigma, I3750-25G)
5-TAMRA NHS ester	(Sigma, 53048)
Alexa Fluor 488 Goat Anti-Mouse IgG	(Thermo Fischer, A11001)
Alexa Fluor 488 Goat Anti-Rabbit IgG	(Thermo Fischer, A11034)
Alexa Fluor 594 Goat anti-Mouse IgG	(Thermo Fischer, R37121)
Alexa Fluor 594 Goat anti-Rabbit IgG	(Thermo Fischer, A11037)
Aminoallyl-dUTP sodium salt	(Sigma, A0410)
Ampicillin	(Fischer Scientific, 10193433)
anti-EGFP antibody	(Abcam, ab13970)
anti-TRF1 antibody	(in house)
Aphidicolin	(Sigma, A0781)
Atto 594 NHS ester	(Sigma, 08741)
Atto 647N NHS ester	(Sigma, 18373)
Bovine Serum Albumin	(Sigma, A2153)
Click-it DNA imaging kit	(Thermofischer, C10337)
Click-it RNA imaging kit	(Thermofischer, C10330)
CREST antibody	(Europa Bioproducts, FZ90C-CS1058)
cytochalasin B	(Sigma, C6762)
Dextran	(Sigma, 1179708)
DTT	(Sigma, D9779)
EDTA 0.5M pH8.0	(Invitrogen, 15575-020)
Ethanol	(HMGU, 5000003)
Formaldehyde	(Sigma, 8.18708)
Formamide	(Sigma, F9037)
Glycerol	(Fischer Scientific, 10021083)
Glycogen	(Thermo Fischer, R0561)
hCG	(MSD Animal Health)
Hydrochloric acid	(Sigma, H1758)
IBMX	(Sigma, I5879)
LB Agar	(Fischer Scientific, L1515.500)
LB Broth	(Fischer Scientific, L1520.500)
mAb414 antibody	(Abcam, ab24609)

NICK TRANSLATION MIX	(Roche, 11745808910)
NucleoBond® Xtra Midi Plus kit	(Macherey-Nagel, 740410.10)
NucleoSpin® Gel and PCR Clean-up	(Machery-Nagel, 740609.10)
NucleoSpin® Miniprep Kit	(Macherey-Nagel, 5000814)
Paraffin oil	(Sigma, 18512)
Phusion High-Fidelity DNA Polymerase	(Invitrogen, F530S)
PMSG	(IDT Biologika Gmbh)
Pronase	(Roche, 000000010165921001)
PVP	(Sigma, PVP40)
RNase-Free Water	(Quiagen, 129112)
SecureSeal™ imaging spacer	(Sigma, GBL654008)
SOC Broth	(Fischer Scientific, S1030.500)
SSC buffer	(Sigma, 93017)
T3 mMESSAGE mMACHINE kit	(Ambion, AM1348)
T5 Exonuclease	(NEB, M0363S)
T7 mMESSAGE mMACHINE kit	(Ambion, AM1344)
Taq DNA ligase	(NEB, M0208S)
TRIS acetate	(Sigma, 93295)
magnesium acetate solution	(Sigma, 63052)
potassium acetate solution	(Sigma, 95843)
Triton X-100	(Sigma, T9284)
Vectashield with DAPI	(Vectorlabs, H-1200)

References

Abe, K., Yamamoto, R., Franke, V., Cao, M., Suzuki, Y., Suzuki, M.G., Vlahovicek, K., Svoboda, P., Schultz, R.M., and Aoki, F. (2015). The first murine zygotic transcription is promiscuous and uncoupled from splicing and 3' processing. EMBO J *34*, 1523-1537.

Abe, K.I., Funaya, S., Tsukioka, D., Kawamura, M., Suzuki, Y., Suzuki, M.G., Schultz, R.M., and Aoki, F. (2018). Minor zygotic gene activation is essential for mouse preimplantation development. Proc Natl Acad Sci U S A.

Adenot, P.G., Mercier, Y., Renard, J.P., and Thompson, E.M. (1997). Differential H4 acetylation of paternal and maternal chromatin precedes DNA replication and differential transcriptional activity in pronuclei of 1-cell mouse embryos. Development *124*, 4615-4625.

Ahmed, K., Dehghani, H., Rugg-Gunn, P., Fussner, E., Rossant, J., and Bazett-Jones, D.P. (2010). Global chromatin architecture reflects pluripotency and lineage commitment in the early mouse embryo. PLoS One *5*, e10531.

Amabile, A., Migliara, A., Capasso, P., Biffi, M., Cittaro, D., Naldini, L., and Lombardo, A. (2016). Inheritable Silencing of Endogenous Genes by Hit-and-Run Targeted Epigenetic Editing. Cell *167*, 219-232 e214.

Amendola, M., and van Steensel, B. (2015). Nuclear lamins are not required for lamina-associated domain organization in mouse embryonic stem cells. Embo Rep *16*, 610-617.

Amouroux, R., Nashun, B., Shirane, K., Nakagawa, S., Hill, P.W.S., D'Souza, Z., Nakayama, M., Matsuda, M., Turp, A., Ndjetehe, E.*, et al.* (2016). De novo DNA methylation drives 5hmC accumulation in mouse zygotes. Nature Cell Biology *18*, 225-+.

Andreu-Vieyra, C.V., Chen, R., Agno, J.E., Glaser, S., Anastassiadis, K., Stewart, A.F., and Matzuk, M.M. (2010). MLL2 is required in oocytes for bulk histone 3 lysine 4 trimethylation and transcriptional silencing. Plos Biol *8*.

Aoshima, K., Inoue, E., Sawa, H., and Okada, Y. (2015). Paternal H3K4 methylation is required for minor zygotic gene activation and early mouse embryonic development. Embo Rep *16*, 803-812.

Avner, P., and Heard, E. (2001). X-chromosome inactivation: counting, choice and initiation. Nat Rev Genet *2*, 59-67.

Banaszynski, L.A., Chen, L.C., Maynard-Smith, L.A., Ooi, A.G., and Wandless, T.J. (2006). A rapid, reversible, and tunable method to regulate protein function in living cells using synthetic small molecules. Cell *126*, 995-1004.

Bedzhov, I., Leung, C.Y., Bialecka, M., and Zernicka-Goetz, M. (2014). In vitro culture of mouse blastocysts beyond the implantation stages. Nat Protoc *9*, 2732-2739.

Bedzhov, I., and Zernicka-Goetz, M. (2014). Self-organizing properties of mouse pluripotent cells initiate morphogenesis upon implantation. Cell *156*, 1032-1044.

Bickmore, W.A., and van Steensel, B. (2013). Genome architecture: domain organization of interphase chromosomes. Cell *152*, 1270-1284.

Bintu, L., Yong, J., Antebi, Y.E., McCue, K., Kazuki, Y., Uno, N., Oshimura, M., and Elowitz, M.B. (2016). Dynamics of epigenetic regulation at the single-cell level. Science *351*, 720-724.

Bolzer, A., Kreth, G., Solovei, I., Koehler, D., Saracoglu, K., Fauth, C., Muller, S., Eils, R., Cremer, C., Speicher, M.R*., et al.* (2005). Three-dimensional maps of all chromosomes in human male fibroblast nuclei and prometaphase rosettes. Plos Biol *3*, 826-842.

Bonev, B., Mendelson Cohen, N., Szabo, Q., Fritsch, L., Papadopoulos, G.L., Lubling, Y., Xu, X., Lv, X., Hugnot, J.P., Tanay, A*., et al.* (2017). Multiscale 3D Genome Rewiring during Mouse Neural Development. Cell *171*, 557-572 e524.

Borensztein, M., Syx, L., Ancelin, K., Diabangouaya, P., Picard, C., Liu, T., Liang, J.B., Vassilev, I., Galupa, R., Servant, N*., et al.* (2017). Xist-dependent imprinted X inactivation and the early developmental consequences of its failure. Nat Struct Mol Biol *24*, 226-233.

Borsos, M., and Torres-Padilla, M.E. (2016). Building up the nucleus: nuclear organization in the establishment of totipotency and pluripotency during mammalian development. Genes Dev *30*, 611-621.

Boskovic, A., Eid, A., Pontabry, J., Ishiuchi, T., Spiegelhalter, C., Raghu Ram, E.V., Meshorer, E., and Torres-Padilla, M.E. (2014). Higher chromatin mobility supports totipotency and precedes pluripotency in vivo. Genes Dev *28*, 1042-1047.

Boyle, A.P., Davis, S., Shulha, H.P., Meltzer, P., Margulies, E.H., Weng, Z., Furey, T.S., and Crawford, G.E. (2008). High-resolution mapping and characterization of open chromatin across the genome. Cell *132*, 311-322.

Boyle, S., Rodesch, M.J., Halvensleben, H.A., Jeddeloh, J.A., and Bickmore, W.A. (2011). Fluorescence in situ hybridization with high-complexity repeat-free oligonucleotide probes generated by massively parallel synthesis. Chromosome Res *19*, 901-909.

Brinster, R.L. (1963). A Method for in Vitro Cultivation of Mouse Ova from Two-Cell to Blastocyst. Exp Cell Res *32*, 205-208.

Buenrostro, J.D., Giresi, P.G., Zaba, L.C., Chang, H.Y., and Greenleaf, W.J. (2013). Transposition of native chromatin for fast and sensitive epigenomic profiling of open chromatin, DNA-binding proteins and nucleosome position. Nat Methods *10*, 1213-1218.

Buenrostro, J.D., Wu, B., Litzenburger, U.M., Ruff, D., Gonzales, M.L., Snyder, M.P., Chang, H.Y., and Greenleaf, W.J. (2015). Single-cell chromatin accessibility reveals principles of regulatory variation. Nature *523*, 486-490.

Burns, K.H., Viveiros, M.M., Ren, Y., Wang, P., DeMayo, F.J., Frail, D.E., Eppig, J.J., and Matzuk, M.M. (2003). Roles of NPM2 in chromatin and nucleolar organization in oocytes and embryos. Science *300*, 633-636.

Burton, A., Muller, J., Tu, S., Padilla-Longoria, P., Guccione, E., and Torres-Padilla, M.E. (2013). Single-cell profiling of epigenetic modifiers identifies PRDM14 as an inducer of cell fate in the mammalian embryo. Cell Rep *5*, 687-701.

Burton, A., and Torres-Padilla, M.E. (2010). Epigenetic reprogramming and development: a unique heterochromatin organization in the preimplantation mouse embryo. Brief Funct Genomics *9*, 444-454.

Burton, A., and Torres-Padilla, M.E. (2014). Chromatin dynamics in the regulation of cell fate allocation during early embryogenesis. Nat Rev Mol Cell Biol *15*, 723-734.

Casanova, M., Pasternak, M., El Marjou, F., Le Baccon, P., Probst, A.V., and Almouzni, G. (2013). Heterochromatin reorganization during early mouse development requires a single-stranded noncoding transcript. Cell Rep *4*, 1156-1167.

Chambeyron, S., and Bickmore, W.A. (2004). Chromatin decondensation and nuclear reorganization of the HoxB locus upon induction of transcription. Gene Dev *18*, 1119-1130.

Chambeyron, S., Da Silva, N.R., Lawson, K.A., and Bickmore, W.A. (2005). Nuclear re-organisation of the Hoxb complex during mouse embryonic development. Development *132*, 2215-2223.

Chen, C.K., Blanco, M., Jackson, C., Aznauryan, E., Ollikainen, N., Surka, C., Chow, A., Cerase, A., McDonel, P., and Guttman, M. (2016). Xist recruits the X chromosome to the nuclear lamina to enable chromosome-wide silencing. Science *354*, 468-472.

Chen, C.K., Chow, A., Lai, M., and Guttman, M. (2017). Response to Comment on "Xist recruits the X chromosome to the nuclear lamina to enable chromosome-wide silencing". Science *356*.

Cohen, T.V., Klarmann, K.D., Sakchaisri, K., Cooper, J.P., Kuhns, D., Anver, M., Johnson, P.F., Williams, S.C., Keller, J.R., and Stewart, C.L. (2008). The lamin B receptor under transcriptional control of C/EBPepsilon is required for morphological but not functional maturation of neutrophils. Hum Mol Genet *17*, 2921-2933.

Constantinescu, D., Gray, H.L., Sammak, P.J., Schatten, G.P., and Csoka, A.B. (2006). Lamin A/C expression is a marker of mouse and human embryonic stem cell differentiation. Stem Cells *24*, 177-185.

Crane, E., Bian, Q., McCord, R.P., Lajoie, B.R., Wheeler, B.S., Ralston, E.J., Uzawa, S., Dekker, J., and Meyer, B.J. (2015). Condensin-driven remodelling of X chromosome topology during dosage compensation. Nature *523*, 240-244.

Cremer, M., von Hase, J., Volm, T., Brero, A., Kreth, G., Walter, J., Fischer, C., Solovei, I., Cremer, C., and Cremer, T. (2001). Non-random radial higher-order chromatin arrangements in nuclei of diploid human cells. Chromosome Res *9*, 541-567.

Dahl, J.A., Jung, I., Aanes, H., Greggains, G.D., Manaf, A., Lerdrup, M., Li, G., Kuan, S., Li, B., Lee, A.Y.*, et al.* (2016). Broad histone H3K4me3 domains in mouse oocytes modulate maternal-to-zygotic transition. Nature *537*, 548-552.

De Iaco, A., Planet, E., Coluccio, A., Verp, S., Duc, J., and Trono, D. (2017). DUX-family transcription factors regulate zygotic genome activation in placental mammals. Nat Genet *49*, 941-945.

Dechat, T., Adam, S.A., Taimen, P., Shimi, T., and Goldman, R.D. (2010). Nuclear lamins. Cold Spring Harb Perspect Biol *2*, a000547.

Deglincerti, A., Croft, G.F., Pietila, L.N., Zernicka-Goetz, M., Siggia, E.D., and Brivanlou, A.H. (2016). Self-organization of the in vitro attached human embryo. Nature *533*, 251-254.

Deng, Q., Ramskold, D., Reinius, B., and Sandberg, R. (2014). Single-cell RNA-seq reveals dynamic, random monoallelic gene expression in mammalian cells. Science *343*, 193-196.

Dixon, J.R., Selvaraj, S., Yue, F., Kim, A., Li, Y., Shen, Y., Hu, M., Liu, J.S., and Ren, B. (2012). Topological domains in mammalian genomes identified by analysis of chromatin interactions. Nature *485*, 376-380.

Du, Z., Zheng, H., Huang, B., Ma, R., Wu, J., Zhang, X., He, J., Xiang, Y., Wang, Q., Li, Y.*, et al.* (2017). Allelic reprogramming of 3D chromatin architecture during early mammalian development. Nature *547*, 232-235.

Eckersley-Maslin, M.A., Bergmann, J.H., Lazar, Z., and Spector, D.L. (2013). Lamin A/C is expressed in pluripotent mouse embryonic stem cells. Nucleus *4*, 53-60.

Eddy, C.A., and Pauerstein, C.J. (1980). Anatomy and physiology of the fallopian tube. Clin Obstet Gynecol *23*, 1177-1193.

Eskeland, R., Leeb, M., Grimes, G.R., Kress, C., Boyle, S., Sproul, D., Gilbert, N., Fan, Y., Skoultchi, A.I., Wutz, A.*, et al.* (2010). Ring1B compacts chromatin structure and represses gene expression independent of histone ubiquitination. Mol Cell *38*, 452-464.

Evans, M.J., and Kaufman, M.H. (1981). Establishment in culture of pluripotential cells from mouse embryos. Nature *292*, 154-156.

Fadloun, A., Le Gras, S., Jost, B., Ziegler-Birling, C., Takahashi, H., Gorab, E., Carninci, P., and Torres-Padilla, M.E. (2013). Chromatin signatures and retrotransposon profiling in mouse embryos reveal regulation of LINE-1 by RNA. Nat Struct Mol Biol *20*, 332-338.

Filion, G.J., van Bemmel, J.G., Braunschweig, U., Talhout, W., Kind, J., Ward, L.D., Brugman, W., de Castro, I.J., Kerkhoven, R.M., Bussemaker, H.J.*, et al.* (2010). Systematic protein location mapping reveals five principal chromatin types in Drosophila cells. Cell *143*, 212-224.

Finlan, L.E., Sproul, D., Thomson, I., Boyle, S., Kerr, E., Perry, P., Ylstra, B., Chubb, J.R., and Bickmore, W.A. (2008). Recruitment to the nuclear periphery can alter expression of genes in human cells. PLoS Genet *4*, e1000039.

Flyamer, I.M., Gassler, J., Imakaev, M., Brandao, H.B., Ulianov, S.V., Abdennur, N., Razin, S.V., Mirny, L.A., and Tachibana-Konwalski, K. (2017). Single-nucleus Hi-C reveals unique chromatin reorganization at oocyte-to-zygote transition. Nature *544*, 110-114.

Fuentes, D.R., Swigut, T., and Wysocka, J. (2018). Systematic perturbation of retroviral LTRs reveals widespread long-range effects on human gene regulation. Elife *7*.

Gassler, J., Brandao, H.B., Imakaev, M., Flyamer, I.M., Ladstatter, S., Bickmore, W.A., Peters, J.M., Mirny, L.A., and Tachibana, K. (2017). A mechanism of cohesin-dependent loop extrusion organizes zygotic genome architecture. EMBO J *36*, 3600-3618.

Gomez-Diaz, E., and Corces, V.G. (2014). Architectural proteins: regulators of 3D genome organization in cell fate. Trends Cell Biol *24*, 703-711.

Gonzalez-Sandoval, A., Towbin, B.D., Kalck, V., Cabianca, D.S., Gaidatzis, D., Hauer, M.H., Geng, L., Wang, L., Yang, T., Wang, X.*, et al.* (2015). Perinuclear Anchoring of H3K9-Methylated Chromatin Stabilizes Induced Cell Fate in C. elegans Embryos. Cell *163*, 1333-1347.

Guelen, L., Pagie, L., Brasset, E., Meuleman, W., Faza, M.B., Talhout, W., Eussen, B.H., de Klein, A., Wessels, L., de Laat, W.*, et al.* (2008). Domain organization of human chromosomes revealed by mapping of nuclear lamina interactions. Nature *453*, 948-951.

Hajkova, P., Jeffries, S.J., Lee, C., Miller, N., Jackson, S.P., and Surani, M.A. (2010). Genome-wide reprogramming in the mouse germ line entails the base excision repair pathway. Science *329*, 78-82.

Handoko, L., Xu, H., Li, G., Ngan, C.Y., Chew, E., Schnapp, M., Lee, C.W., Ye, C., Ping, J.L., Mulawadi, F.*, et al.* (2011). CTCF-mediated functional chromatin interactome in pluripotent cells. Nat Genet *43*, 630-638.

Harper, M.I., Fosten, M., and Monk, M. (1982). Preferential paternal X inactivation in extraembryonic tissues of early mouse embryos. J Embryol Exp Morphol *67*, 127-135.

Harr, J.C., Luperchio, T.R., Wong, X., Cohen, E., Wheelan, S.J., and Reddy, K.L. (2015). Directed targeting of chromatin to the nuclear lamina is mediated by chromatin state and A-type lamins. J Cell Biol *208*, 33-52.

Hendrickson, P.G., Dorais, J.A., Grow, E.J., Whiddon, J.L., Lim, J.W., Wike, C.L., Weaver, B.D., Pflueger, C., Emery, B.R., Wilcox, A.L.*, et al.* (2017). Conserved roles of mouse DUX and human DUX4 in activating cleavage-stage genes and MERVL/HERVL retrotransposons. Nat Genet *49*, 925-934.

Hirano, Y., Hizume, K., Kimura, H., Takeyasu, K., Haraguchi, T., and Hiraoka, Y. (2012). Lamin B receptor recognizes specific modifications of histone H4 in heterochromatin formation. J Biol Chem *287*, 42654-42663.

Holland, A.J., Fachinetti, D., Han, J.S., and Cleveland, D.W. (2012). Inducible, reversible system for the rapid and complete degradation of proteins in mammalian cells. Proc Natl Acad Sci U S A *109*, E3350-3357.

Inoue, A., Jiang, L., Lu, F., Suzuki, T., and Zhang, Y. (2017a). Maternal H3K27me3 controls DNA methylation-independent imprinting. Nature *547*, 419-424.

Inoue, A., Jiang, L., Lu, F., and Zhang, Y. (2017b). Genomic imprinting of Xist by maternal H3K27me3. Genes Dev *31*, 1927-1932.

Inoue, A., and Zhang, Y. (2011). Replication-dependent loss of 5-hydroxymethylcytosine in mouse preimplantation embryos. Science *334*, 194.

Ishiuchi, T., Enriquez-Gasca, R., Mizutani, E., Boskovic, A., Ziegler-Birling, C., Rodriguez-Terrones, D., Wakayama, T., Vaquerizas, J.M., and Torres-Padilla, M.E. (2015). Early embryonic-like cells are induced by downregulating replication-dependent chromatin assembly. Nat Struct Mol Biol *22*, 662-671.

Jachowicz, J.W., Bing, X., Pontabry, J., Boskovic, A., Rando, O.J., and Torres-Padilla, M.E. (2017). LINE-1 activation after fertilization regulates global chromatin accessibility in the early mouse embryo. Nat Genet *49*, 1502-1510.

Jachowicz, J.W., Santenard, A., Bender, A., Muller, J., and Torres-Padilla, M.E. (2013). Heterochromatin establishment at pericentromeres depends on nuclear position. Gene Dev *27*, 2427-2432.

Kay, G.F., Penny, G.D., Patel, D., Ashworth, A., Brockdorff, N., and Rastan, S. (1993). Expression of Xist during mouse development suggests a role in the initiation of X chromosome inactivation. Cell *72*, 171-182.

Ke, Y., Xu, Y., Chen, X., Feng, S., Liu, Z., Sun, Y., Yao, X., Li, F., Zhu, W., Gao, L.*, et al.* (2017). 3D Chromatin Structures of Mature Gametes and Structural Reprogramming during Mammalian Embryogenesis. Cell *170*, 367-381 e320.

Kim, Y., Sharov, A.A., McDole, K., Cheng, M., Hao, H., Fan, C.M., Gaiano, N., Ko, M.S., and Zheng, Y. (2011). Mouse B-type lamins are required for proper organogenesis but not by embryonic stem cells. Science *334*, 1706-1710.

Kim, Y., Zheng, X., and Zheng, Y. (2013). Proliferation and differentiation of mouse embryonic stem cells lacking all lamins. Cell Res *23*, 1420-1423.

Kim, Y., and Zheng, Y. (2013). Generation and characterization of a conditional deletion allele for Lmna in mice. Biochem Biophys Res Commun *440*, 8-13.

Kind, J., Pagie, L., de Vries, S.S., Nahidiazar, L., Dey, S.S., Bienko, M., Zhan, Y., Lajoie, B., de Graaf, C.A., Amendola, M.*, et al.* (2015). Genome-wide maps of nuclear lamina interactions in single human cells. Cell *163*, 134-147.

Kind, J., Pagie, L., Ortabozkoyun, H., Boyle, S., de Vries, S.S., Janssen, H., Amendola, M., Nolen, L.D., Bickmore, W.A., and van Steensel, B. (2013). Single-cell dynamics of genome-nuclear lamina interactions. Cell *153*, 178-192.

Krishnan, S., and Trievel, R.C. (2013). Structural and functional analysis of JMJD2D reveals molecular basis for site-specific demethylation among JMJD2 demethylases. Structure *21*, 98-108.

Kumaran, R.I., and Spector, D.L. (2008). A genetic locus targeted to the nuclear periphery in living cells maintains its transcriptional competence. J Cell Biol *180*, 51-65.

Ladstatter, S., and Tachibana-Konwalski, K. (2016). A Surveillance Mechanism Ensures Repair of DNA Lesions during Zygotic Reprogramming. Cell *167*, 1774-1787 e1713.

Legartova, S., Stixova, L., Laur, O., Kozubek, S., Sehnalova, P., and Bartova, E. (2014). Nuclear structures surrounding internal lamin invaginations. J Cell Biochem *115*, 476-487.

Li, R., and Albertini, D.F. (2013). The road to maturation: somatic cell interaction and self-organization of the mammalian oocyte. Nat Rev Mol Cell Biol *14*, 141-152.

Lieberman-Aiden, E., van Berkum, N.L., Williams, L., Imakaev, M., Ragoczy, T., Telling, A., Amit, I., Lajoie, B.R., Sabo, P.J., Dorschner, M.O.*, et al.* (2009). Comprehensive mapping of long-range interactions reveals folding principles of the human genome. Science *326*, 289-293.

Lin, C.J., Koh, F.M., Wong, P., Conti, M., and Ramalho-Santos, M. (2014). Hira-mediated H3.3 incorporation is required for DNA replication and ribosomal RNA transcription in the mouse zygote. Dev Cell *30*, 268-279.

Lin, Y.C., Benner, C., Mansson, R., Heinz, S., Miyazaki, K., Miyazaki, M., Chandra, V., Bossen, C., Glass, C.K., and Murre, C. (2012). Global changes in the nuclear positioning of genes and intra- and interdomain genomic interactions that orchestrate B cell fate. Nat Immunol *13*, 1196-1204.

Liu, X., Wang, C., Liu, W., Li, J., Li, C., Kou, X., Chen, J., Zhao, Y., Gao, H., Wang, H.*, et al.* (2016). Distinct features of H3K4me3 and H3K27me3 chromatin domains in pre-implantation embryos. Nature *537*, 558-562.

Lu, F., Liu, Y., Inoue, A., Suzuki, T., Zhao, K., and Zhang, Y. (2016). Establishing Chromatin Regulatory Landscape during Mouse Preimplantation Development. Cell *165*, 1375-1388.

Lyon, M.F. (1961). Gene action in the X-chromosome of the mouse (Mus musculus L.). Nature *190*, 372-373.

Macfarlan, T.S., Gifford, W.D., Driscoll, S., Lettieri, K., Rowe, H.M., Bonanomi, D., Firth, A., Singer, O., Trono, D., and Pfaff, S.L. (2012). Embryonic stem cell potency fluctuates with endogenous retrovirus activity. Nature *487*, 57-63.

Martin, C., Brochard, V., Migne, C., Zink, D., Debey, P., and Beaujean, N. (2006). Architectural reorganization of the nuclei upon transfer into oocytes accompanies genome reprogramming. Mol Reprod Dev *73*, 1102-1111.

Matoba, S., Liu, Y., Lu, F., Iwabuchi, K.A., Shen, L., Inoue, A., and Zhang, Y. (2014). Embryonic development following somatic cell nuclear transfer impeded by persisting histone methylation. Cell *159*, 884-895.

Meuleman, W., Peric-Hupkes, D., Kind, J., Beaudry, J.B., Pagie, L., Kellis, M., Reinders, M., Wessels, L., and van Steensel, B. (2013). Constitutive nuclear lamina-genome interactions are highly conserved and associated with A/T-rich sequence. Genome Res *23*, 270-280.

Miyanari, Y., and Torres-Padilla, M.E. (2012). Control of ground-state pluripotency by allelic regulation of Nanog. Nature *483*, 470-473.

Miyazaki, S., and Ito, M. (2006). Calcium signals for egg activation in mammals. J Pharmacol Sci *100*, 545-552.

Monkhorst, K., Jonkers, I., Rentmeester, E., Grosveld, F., and Gribnau, J. (2008). X inactivation counting and choice is a stochastic process: evidence for involvement of an X-linked activator. Cell *132*, 410-421.

Morselli, M., Pastor, W.A., Montanini, B., Nee, K., Ferrari, R., Fu, K., Bonora, G., Rubbi, L., Clark, A.T., Ottonello, S.*, et al.* (2015). In vivo targeting of de novo DNA methylation by histone modifications in yeast and mouse. Elife *4*, e06205.

Mulnard, J. (1965). [Cytochemical aspects of the regulation in vitro of the mouse ovum after destruction of one of the blastomeres of stage II. 1. Acid phosphomonoesterase]. Mem Acad R Med Belg *5*, 31-67.

Nagano, T., Lubling, Y., Varnai, C., Dudley, C., Leung, W., Baran, Y., Mendelson Cohen, N., Wingett, S., Fraser, P., and Tanay, A. (2017). Cell-cycle dynamics of chromosomal organization at single-cell resolution. Nature *547*, 61-67.

Nakamura, T., Arai, Y., Umehara, H., Masuhara, M., Kimura, T., Taniguchi, H., Sekimoto, T., Ikawa, M., Yoneda, Y., Okabe, M.*, et al.* (2007). PGC7/Stella protects against DNA demethylation in early embryogenesis. Nat Cell Biol *9*, 64-71.

Nishimura, K., Fukagawa, T., Takisawa, H., Kakimoto, T., and Kanemaki, M. (2009). An auxin-based degron system for the rapid depletion of proteins in nonplant cells. Nat Methods *6*, 917-922.

Nora, E.P., Goloborodko, A., Valton, A.L., Gibcus, J.H., Uebersohn, A., Abdennur, N., Dekker, J., Mirny, L.A., and Bruneau, B.G. (2017). Targeted Degradation of CTCF Decouples Local Insulation of Chromosome Domains from Genomic Compartmentalization. Cell *169*, 930-944 e922.

Nora, E.P., Lajoie, B.R., Schulz, E.G., Giorgetti, L., Okamoto, I., Servant, N., Piolot, T., van Berkum, N.L., Meisig, J., Sedat, J.*, et al.* (2012). Spatial partitioning of the regulatory landscape of the X-inactivation centre. Nature *485*, 381-385.

Okamoto, I., Otte, A.P., Allis, C.D., Reinberg, D., and Heard, E. (2004). Epigenetic dynamics of imprinted X inactivation during early mouse development. Science *303*, 644-649.

Ooga, M., Fulka, H., Hashimoto, S., Suzuki, M.G., and Aoki, F. (2016). Analysis of chromatin structure in mouse preimplantation embryos by fluorescent recovery after photobleaching. Epigenetics *11*, 85-94.

Ooga, M., and Wakayama, T. (2017). FRAP analysis of chromatin looseness in mouse zygotes that allows full-term development. PLoS One *12*, e0178255.

Peaston, A.E., Evsikov, A.V., Graber, J.H., de Vries, W.N., Holbrook, A.E., Solter, D., and Knowles, B.B. (2004). Retrotransposons regulate host genes in mouse oocytes and preimplantation embryos. Dev Cell *7*, 597-606.

Peric-Hupkes, D., Meuleman, W., Pagie, L., Bruggeman, S.W., Solovei, I., Brugman, W., Graf, S., Flicek, P., Kerkhoven, R.M., van Lohuizen, M.*, et al.* (2010). Molecular maps of the reorganization of genome-nuclear lamina interactions during differentiation. Mol Cell *38*, 603-613.

Petropoulos, S., Edsgard, D., Reinius, B., Deng, Q., Panula, S.P., Codeluppi, S., Reyes, A.P., Linnarsson, S., Sandberg, R., and Lanner, F. (2016). Single-Cell RNA-Seq Reveals Lineage and X Chromosome Dynamics in Human Preimplantation Embryos. Cell *167*, 285.

Phillips-Cremins, J.E., Sauria, M.E., Sanyal, A., Gerasimova, T.I., Lajoie, B.R., Bell, J.S., Ong, C.T., Hookway, T.A., Guo, C., Sun, Y.*, et al.* (2013). Architectural protein subclasses shape 3D organization of genomes during lineage commitment. Cell *153*, 1281-1295.

Plachta, N., Bollenbach, T., Pease, S., Fraser, S.E., and Pantazis, P. (2011). Oct4 kinetics predict cell lineage patterning in the early mammalian embryo. Nat Cell Biol *13*, 117-123.

Pratt, H.P. (1989). Marking time and making space: chronology and topography in the early mouse embryo. Int Rev Cytol *117*, 99-130.

Probst, A.V., Okamoto, I., Casanova, M., El Marjou, F., Le Baccon, P., and Almouzni, G. (2010). A Strand-Specific Burst in Transcription of Pericentric Satellites Is Required for Chromocenter Formation and Early Mouse Development. Dev Cell *19*, 625-638.

Puschendorf, M., Terranova, R., Boutsma, E., Mao, X., Isono, K., Brykczynska, U., Kolb, C., Otte, A.P., Koseki, H., Orkin, S.H.*, et al.* (2008). PRC1 and Suv39h specify parental asymmetry at constitutive heterochromatin in early mouse embryos. Nat Genet *40*, 411-420.

Quinodoz, S.A., Ollikainen, N., Tabak, B., Palla, A., Schmidt, J.M., Detmar, E., Lai, M.M., Shishkin, A.A., Bhat, P., Takei, Y.*, et al.* (2018). Higher-Order Inter-chromosomal Hubs Shape 3D Genome Organization in the Nucleus. Cell.

Rao, S.S., Huntley, M.H., Durand, N.C., Stamenova, E.K., Bochkov, I.D., Robinson, J.T., Sanborn, A.L., Machol, I., Omer, A.D., Lander, E.S.*, et al.* (2014). A 3D map of the human genome at kilobase resolution reveals principles of chromatin looping. Cell *159*, 1665-1680.

Rao, S.S.P., Huang, S.C., Glenn St Hilaire, B., Engreitz, J.M., Perez, E.M., Kieffer-Kwon, K.R., Sanborn, A.L., Johnstone, S.E., Bascom, G.D., Bochkov, I.D.*, et al.* (2017). Cohesin Loss Eliminates All Loop Domains. Cell *171*, 305-320 e324.

Reddy, K.L., Zullo, J.M., Bertolino, E., and Singh, H. (2008). Transcriptional repression mediated by repositioning of genes to the nuclear lamina. Nature *452*, 243-247.

Rodman, T.C., Pruslin, F.H., and Allfrey, V.G. (1984). Protamine-DNA association in mammalian spermatozoa. Exp Cell Res *150*, 269-281.

Rodriguez-Terrones, D., and Torres-Padilla, M.E. (2018). Nimble and Ready to Mingle: Transposon Outbursts of Early Development. Trends Genet.

Schultz, R.M. (2002). The molecular foundations of the maternal to zygotic transition in the preimplantation embryo. Hum Reprod Update *8*, 323-331.

Schwarzer, W., Abdennur, N., Goloborodko, A., Pekowska, A., Fudenberg, G., Loe-Mie, Y., Fonseca, N.A., Huber, W., C, H.H., Mirny, L.*, et al.* (2017). Two independent modes of chromatin organization revealed by cohesin removal. Nature *551*, 51-56.

Servant, N., Varoquaux, N., Lajoie, B.R., Viara, E., Chen, C.J., Vert, J.P., Heard, E., Dekker, J., and Barillot, E. (2015). HiC-Pro: an optimized and flexible pipeline for Hi-C data processing. Genome Biol *16*, 259.

Sexton, T., Yaffe, E., Kenigsberg, E., Bantignies, F., Leblanc, B., Hoichman, M., Parrinello, H., Tanay, A., and Cavalli, G. (2012). Three-dimensional folding and functional organization principles of the Drosophila genome. Cell *148*, 458-472.

Shachar, S., Voss, T.C., Pegoraro, G., Sciascia, N., and Misteli, T. (2015). Identification of Gene Positioning Factors Using High-Throughput Imaging Mapping. Cell *162*, 911-923.

Shultz, L.D., Lyons, B.L., Burzenski, L.M., Gott, B., Samuels, R., Schweitzer, P.A., Dreger, C., Herrmann, H., Kalscheuer, V., Olins, A.L.*, et al.* (2003). Mutations at the mouse ichthyosis locus are within the lamin B receptor gene: a single gene model for human Pelger-Huet anomaly. Hum Mol Genet *12*, 61-69.

Smallwood, S.A., Lee, H.J., Angermueller, C., Krueger, F., Saadeh, H., Peat, J., Andrews, S.R., Stegle, O., Reik, W., and Kelsey, G. (2014). Single-cell genome-wide bisulfite sequencing for assessing epigenetic heterogeneity. Nat Methods *11*, 817-820.

Smith, Z.D., Chan, M.M., Humm, K.C., Karnik, R., Mekhoubad, S., Regev, A., Eggan, K., and Meissner, A. (2014). DNA methylation dynamics of the human preimplantation embryo. Nature *511*, 611-615.

Smith, Z.D., Chan, M.M., Mikkelsen, T.S., Gu, H., Gnirke, A., Regev, A., and Meissner, A. (2012). A unique regulatory phase of DNA methylation in the early mammalian embryo. Nature *484*, 339-344.

Solovei, I., Wang, A.S., Thanisch, K., Schmidt, C.S., Krebs, S., Zwerger, M., Cohen, T.V., Devys, D., Foisner, R., Peichl, L.*, et al.* (2013). LBR and lamin A/C sequentially tether peripheral heterochromatin and inversely regulate differentiation. Cell *152*, 584-598.

Stevens, T.J., Lando, D., Basu, S., Atkinson, L.P., Cao, Y., Lee, S.F., Leeb, M., Wohlfahrt, K.J., Boucher, W., O'Shaughnessy-Kirwan, A.*, et al.* (2017). 3D structures of individual mammalian genomes studied by single-cell Hi-C. Nature *544*, 59-64.

Sullivan, T., Escalante-Alcalde, D., Bhatt, H., Anver, M., Bhat, N., Nagashima, K., Stewart, C.L., and Burke, B. (1999). Loss of A-type lamin expression compromises nuclear envelope integrity leading to muscular dystrophy. J Cell Biol *147*, 913-920.

Susor, A., Jansova, D., Anger, M., and Kubelka, M. (2016). Translation in the mammalian oocyte in space and time. Cell Tissue Res *363*, 69-84.

Tachibana-Konwalski, K., Godwin, J., van der Weyden, L., Champion, L., Kudo, N.R., Adams, D.J., and Nasmyth, K. (2010). Rec8-containing cohesin maintains bivalents without turnover during the growing phase of mouse oocytes. Genes Dev *24*, 2505-2516.

Tada, T., Obata, Y., Tada, M., Goto, Y., Nakatsuji, N., Tan, S., Kono, T., and Takagi, N. (2000). Imprint switching for non-random X-chromosome inactivation during mouse oocyte growth. Development *127*, 3101-3105.

Tang, F., Barbacioru, C., Nordman, E., Li, B., Xu, N., Bashkirov, V.I., Lao, K., and Surani, M.A. (2010). RNA-Seq analysis to capture the transcriptome landscape of a single cell. Nat Protoc *5*, 516-535.

Tarkowski, A.K. (1959). Experiments on the development of isolated blastomers of mouse eggs. Nature *184*, 1286-1287.

Tarkowski, A.K., and Wroblewska, J. (1967). Development of blastomeres of mouse eggs isolated at the 4- and 8-cell stage. J Embryol Exp Morphol *18*, 155-180.

Therizols, P., Illingworth, R.S., Courilleau, C., Boyle, S., Wood, A.J., and Bickmore, W.A. (2014). Chromatin decondensation is sufficient to alter nuclear organization in embryonic stem cells. Science *346*, 1238-1242.

Torres-Padilla, M.E., Parfitt, D.E., Kouzarides, T., and Zernicka-Goetz, M. (2007). Histone arginine methylation regulates pluripotency in the early mouse embryo. Nature *445*, 214-218.

Towbin, B.D., Gonzalez-Aguilera, C., Sack, R., Gaidatzis, D., Kalck, V., Meister, P., Askjaer, P., and Gasser, S.M. (2012). Step-wise methylation of histone H3K9 positions heterochromatin at the nuclear periphery. Cell *150*, 934-947.

Towbin, B.D., Gonzalez-Sandoval, A., and Gasser, S.M. (2013). Mechanisms of heterochromatin subnuclear localization. Trends Biochem Sci *38*, 356-363.

van Steensel, B., and Henikoff, S. (2000). Identification of in vivo DNA targets of chromatin proteins using tethered Dam methyltransferase. Nat Biotechnol *18*, 424-428.

Vogel, M.J., Peric-Hupkes, D., and van Steensel, B. (2007). Detection of in vivo protein-DNA interactions using DamID in mammalian cells. Nat Protoc *2*, 1467-1478.

Wang, C., Liu, X., Gao, Y., Yang, L., Li, C., Liu, W., Chen, C., Kou, X., Zhao, Y., Chen, J.*, et al.* (2018). Reprogramming of H3K9me3-dependent heterochromatin during mammalian embryo development. Nat Cell Biol *20*, 620-631.

Wen, B., Wu, H., Shinkai, Y., Irizarry, R.A., and Feinberg, A.P. (2009). Large histone H3 lysine 9 dimethylated chromatin blocks distinguish differentiated from embryonic stem cells. Nat Genet *41*, 246-250.

Whiddon, J.L., Langford, A.T., Wong, C.J., Zhong, J.W., and Tapscott, S.J. (2017). Conservation and innovation in the DUX4-family gene network. Nat Genet *49*, 935-940.

White, M.D., Angiolini, J.F., Alvarez, Y.D., Kaur, G., Zhao, Z.W., Mocskos, E., Bruno, L., Bissiere, S., Levi, V., and Plachta, N. (2016). Long-Lived Binding of Sox2 to DNA Predicts Cell Fate in the Four-Cell Mouse Embryo. Cell *165*, 75-87.

Wianny, F., and Zernicka-Goetz, M. (2000). Specific interference with gene function by double-stranded RNA in early mouse development. Nat Cell Biol *2*, 70-75.

Wilson, K.L., and Foisner, R. (2010). Lamin-binding Proteins. Cold Spring Harb Perspect Biol *2*, a000554.

Wu, J., Huang, B., Chen, H., Yin, Q., Liu, Y., Xiang, Y., Zhang, B., Liu, B., Wang, Q., Xia, W.*, et al.* (2016a). The landscape of accessible chromatin in mammalian preimplantation embryos. Nature *534*, 652-657.

Wu, T.P., Wang, T., Seetin, M.G., Lai, Y., Zhu, S., Lin, K., Liu, Y., Byrum, S.D., Mackintosh, S.G., Zhong, M.*, et al.* (2016b). DNA methylation on N(6)-adenine in mammalian embryonic stem cells. Nature *532*, 329-333.

Xu, Q., and Xie, W. (2018). Epigenome in Early Mammalian Development: Inheritance, Reprogramming and Establishment. Trends Cell Biol *28*, 237-253.

Ye, Q., and Worman, H.J. (1996). Interaction between an integral protein of the nuclear envelope inner membrane and human chromodomain proteins homologous to Drosophila HP1. J Biol Chem *271*, 14653-14656.

Zernicka-Goetz, M., Morris, S.A., and Bruce, A.W. (2009). Making a firm decision: multifaceted regulation of cell fate in the early mouse embryo. Nat Rev Genet *10*, 467-477.

Zhang, B., Zheng, H., Huang, B., Li, W., Xiang, Y., Peng, X., Ming, J., Wu, X., Zhang, Y., Xu, Q.*, et al.* (2016). Allelic reprogramming of the histone modification H3K4me3 in early mammalian development. Nature *537*, 553-557.

Zheng, H., Huang, B., Zhang, B., Xiang, Y., Du, Z., Xu, Q., Li, Y., Wang, Q., Ma, J., Peng, X.*, et al.* (2016). Resetting Epigenetic Memory by Reprogramming of Histone Modifications in Mammals. Mol Cell *63*, 1066-1079.

Zuccotti, M., Garagna, S., Merico, V., Monti, M., and Alberto Redi, C. (2005). Chromatin organisation and nuclear architecture in growing mouse oocytes. Mol Cell Endocrinol *234*, 11-17.